PROPOSAL OF AN OVERALL CONTROL ARCHITECTURE FOR THE MELISSA LOOP

Carles Ciurans Molist

PROPOSAL OF AN OVERALL CONTROL ARCHITECTURE FOR THE MELISSA LOOP

PhD Thesis, by Carles Ciurans Molist

UAB, 2023

TABLE OF CONTENTS

Acknowledgments 4
Resum 6
Résumé 7
Summary 8
Resumen 9
1. INTRODUCTION 10
1.1. State of the art of Space Exploration 11
1.2. Life Support Systems 12
1.2.1. Regenerative Life Support Systems 13
1.2.2. Bioregenerative Life Support Systems 15
1.2.3. State-of-the-art of Bioregenerative Life Support Systems Projects 16
1.3. The MELiSSA Project 19
1.3.1. Modelling and controlling the MELiSSA Loop 21
2. OBJECTIVES 23
2.1. Scope of this Project 24
2.2. Outline and contribution to the MELiSSA Project 24
3. DESIGN OF A HIERARCHICAL CONTROL STRUCTURE 27
Nomenclature 28
3.1. Introduction 29
3.2. Controllability of BLSSs 29
3.3. From MGs to BLSSs 30
3.4. Control and Operation Managements of BLSSs 33
3.5. Simulation Analysis 38
3.6. Conclusions 40
4. IMPLEMENTING A HIERARCHICAL CONTROL STRUCTURE TO INTEGRATE A NITRIFICATION REACTOR, A PHOTOSYNTHETIC BIOREACTOR AND A CREW COMPARTMENT 42
Nomenclature 43
4.1. Introduction 47
4.2. Modelling the Compartments 47
4.2.1. C3 Compartment Model 49
4.2.2. C4a Compartment Model 51
4.2.3. C5 Compartment Model 52
4.2.4. Membrane Separation 52
4.2.5. Storage Gas Tanks 53

4.3. Method: HCS of the MELiSSA Pilot Plant 53
4.3.1. Level 3: Tertiary Controller 56
4.3.2. Level 2: Secondary Controller 57
4.3.3. Level 1: Local Controllers 60
4.4. Simulation Results 60
4.4.1. Simulation Plan 60
4.5. Results 63
4.5.1. Main Outcome 63
4.5.2. Level 3 of the HCS 64
4.5.3. Level 2 of the HCS 65
4.5.4. Local Controllers and Process Performance 65
4.6. Conclusions 69
5. MULTILEVEL MECHANISTIC MODEL OF A HIGHER PLANTS CHAMBER 70
Nomenclature 71
5.1. State of the art of modelling higher plants 74
5.2. Model Proposal 76
5.2.1. Multilevel Mechanistic Model 76
5.3. Integration of the Multilevel Mechanistic Model with Advanced Control Architectures 84
5.4. Simulation Scenarios 87
5.4.1. Simulation conditions for Multilevel Model Validation 87
5.4.2. Advanced Control Architecture Configuration 88
5.5. Results 89
5.5.1. Validating Photosynthesis Rates 89
5.5.2. Distribution of Metabolic Fluxes using a Metabolic Diel Model 90
5.5.3. Sensitivity Analysis 94
5.5.4. Testing the integration of Multilevel Model Approach to Advanced Control Architectures in Dynamic Simulations 96
5.6. Conclusions 98
5.7. Appendixes 100
5.7.1. Appendix 1: Boundary Layer Model 100
5.7.2. Appendix 2: Summary of metabolic reactions 103
6. CONTROL-BASED OPTIMIZATION OF OXYGEN AND CARBON DIOXIDE DISTRIBUTION IN A BIOREGENERATIVE LIFE SUPPORT SYSTEM 105
Nomenclature 106
6.1. Introduction 109
6.1.1. Main Contribution 110

6.2. The MELiSSA Loop and the MELiSSA Pilot Plant integration phase 110
6.2.1. The MELiSSA Pilot Plant..... 110
6.2.2. Integration Scenarios..... 111
6.2.3. C3: Nitrification compartment 114
6.2.4. C4a: Cyanobacteria Photobioreactor 114
6.2.5. Higher Plants Compartment..... 114
6.2.6. C5: Crew compartment 117
6.2.7. Gas Management and Storage System..... 117
6.3. Hierarchical Control of the MPP..... 118
6.3.1. Tertiary control level..... 118
6.3.2. Secondary Control Level..... 120
6.3.3. Predictive Functional Controllers 130
6.3.4. Simulation conditions and controllers' specifications..... 132
6.4. Results 134
6.4.1. Comparison of controllers..... 134
6.5. Conclusions 146
6.6. Appendix 147
6.6.1. Appendix 1: Validation of the photosynthesis model based on light color ratio 147
7. CONCLUSIONS AND FUTURE WORK..... 149
8. REFERENCES 154

Acknowledgments

Considero la finalització d'aquesta tesis doctoral el punt culminant de la meva etapa de formació en el camp de la biotecnologia. És clar que el procés formatiu no acaba d'acabar mai, sobretot si et mantens actiu en entorns de recerca i innovació. Però el fet de doctorar-se no pot quedar ni diluït per aquesta obvietat ni menystingut, ja que representa la màxima fita en l'educació superior. El doctorat representa una culminació d'un procés molt més llarg i complex que el que comprèn l'elaboració d'una tesis doctoral. De fet, aquest procés comença a casa, sent l'entorn familiar, en el meu cas, determinant. Per tant, vull començar els agraïments pels precursors: els meus avis. L'avi **Josep** i **Joan**, que malauradament han marxat durant el transcurs del doctorat. Amb ells va marxar, també, la meva àvia **Nuri**, que juntament amb la iaia **Palmira** m'han arrencat l'amor més sincer. El meu agraïment etern a tot el que m'heu ensenyat. També vull agrair als meus pares **Ramon** i **Rosa,** i al meu germà **Jordi**, l'educació, l'amor, el carinyo i haver-me donat un entorn ideal per poder acabar fent el que m'agrada. De me mare, ningú més lluny del món acadèmic n'he obtingut el millor dels talents, les *soft-skills*, el saber-se espavilar. Del meu pare, telecos, amant de l'electrònica i el control, i del meu germà, neuròleg, n'havia de sortir una tesis de control aplicat als sistemes de suport de vida. I a tota la meva família amb qui he crescut, **Jordi**, **Conxi**, **Marc**, **Guillem**, **Magda** i **Felipe**, **Cristina**, i la part política, **Rosa** i **Pol**, moltes gràcies!

Un agraïment també als meus dos directors de tesis: **Claude-Gilles Dussap** i en **Francesc Gòdia**. **Gilles** made me discover a whole way of thinking, the french school. It is talking to Professors like Gilles when you realize you are in front of a wise man, with a deep knowledge on process and chemical engineering. I am also thankful to have had the possibilitty to live and enjoy the Auvergne, a gorgeous place in France. I d'en **Quico,** per descomptat, en vull agrair l'ambició de voler iniciar una tesis gens fàcil, amb molt poca literatura però amb la convicció de que es podia fer i que es faria bé. També et vull agrair la sort que tenim els que formem part del teu equip de poder aprendre de la teva manera de gestionar la gent i el projecte, amb confiança i fe cega en nosaltres. Moltes gràcies també per haver-me fet confiança donant-me l'oportunitat de seguir vinculat al MELiSSA després de la tesis. Of course, thank you ESA and MELiSSA Foundation for funding my project and for believing in the investment on young scientists as a driving-force for progress and innovation. També és de rebut agrair a la Universitat Autònoma de Barcelona i al DEQBA oferir un entorn i unes condicions fantàstiques per fer recerca.

Thanks also **Josep Maria Guerrero**, **Najmeh Bazmohammadi** and the colleagues from CROM in Denmark for opening the doors of control theory to me and welcoming me so kindly every time I have visited Aalborg. I believe the MPP-CROM collaboration has just started! També, gràcies a

l'Igor per l'ajuda i l'empenta per poder publicar l'estudi del metabolisme de plantes, que tant ens va fer suar. Als companys de la MELiSSA Pilot Plant: **Vane**, **Carol**, **Marcel**, **Cynthia**, **Arnau**, **Cristian**, **Santi**, **Guillaume**, **Bea**, **Daniella**, **Enrique**, **David**; treballar amb vosaltres és extremadament fàcil i divertit. Som els millors fent el que fem! I mirant enrere no em puc oblidar dels aprenentatges a Corbion, vull agrair especialment a la **Margarita**, en **Joan Miquel** i l'**Elisenda** posar-me davant d'un reactor de 250 m^3 a les 4 AM a ple Desembre... crec honestament que així es fan els passos més importants.

Als meus amics de biotecnologia: **Martí** (i al seu germà petit en Nasi per deixar-me utilitzar una de les seves peces de la col·lecció *Lonely Astronaut* a la portada), **Audald**, **Pau**, **Javi**, **Queralt**, **Anna**, **Mireia**, **Ana** i **Laura**, sense vosaltres la vida seria coixa. I als **Renegats**, una llista tant llarga de gent i tant important que no acabaria mai els agraïments. I perquè tant si les coses van bé, com si van mal dades, sempre torno a La Garriga.

Finalment, el més sentit agraïment a tu **Alba**, per aguantar tants anys de tesis sense queixar-te de tenir al costat un ordinador enganxat a un home. Sense dubte, has sigut el millor dels sistemes de suport de vida (amb el permís del MELiSSA). Prometo que a partir d'ara podrem dormir més tranquils. Et passo la pilota, la propera ets tu!

Resum

L'objectiu d'aquesta tesis és proposar una estratègia de control pel sistema MELiSSA, que és una xarxa de compartiments interconnectats pensada per treballar en un entorn aïllat. De tots els reptes relacionats amb el disseny I l'operació del sistema MELiSSA, utilitzat en aquest estudi com un cas d'estudi d'un sistema de suport de vida bio-regeneratiu, l'estratègia de control destaca per ésser alhora remarcablement complexa però necessària. Els requeriments associats a l'operació d'un sistema de suport de vida pensat per allotjar una missió tripulada són certament exigents: Un alt grau de reciclatge, eficiència, autonomia, resiliència, fiabilitat i robustesa són algunes de les característiques assumides en el procés de disseny d'un sistema de suport de vida. Davant del repte de dissenyar un sistema que satisfaci aquests requeriments, l'estratègia de control sobresurt com un actor amb molt de pes. En l'estudi presentat, s'ha dissenyat una arquitectura de control amb una organització jeràrquica organitzada en diferents nivells: El Nivell 3 (control terciari) representa un element de supervisió que genera referències (*setpoints*) basats en criteris d'operació generals; El Nivell 2 (control secundari) representa un nivell corrector que adapta les referències rebudes des de control terciari d'acord amb l'estat del procés (procés entès com el conjunt de compartiments que conformen el sistema MELiSSA); El Nivell 1 (controlador primari) genera una acció de control per a ésser enviada als elements de control de cada compartiment. L'exercici de disseny d'aquesta arquitectura de control requereix de la disponibilitat de models matemàtics del sistema d'interès, que en aquest cas són els compartiments del MELiSSA, per a poder ajustar la configuració dels diferents controladors i per avaluar el comportament de l'estructura de control jeràrquic abans de la seva implementació en un sistema real. Davant d'aquesta necessitat de disponibilitat de models, s'han dedicat esforços importants en generar models matemàtics de plantes, basats en primers principis amb informació dels fluxos metabòlics i escalable a la cambra de plantes superiors de la Planta Pilot del MELiSSA. Aquest estudi proporciona una eina de simulació dinàmica i també intenta generar i transmetre el coneixement adquirit sobre les dinàmiques i el comportament d'un sistema complex com és el MELiSSA.

Résumé

Une stratégie de contrôle global pour la boucle MELiSSA est développée. MELiSSA est une boucle de compartiments interconnectés, conçue pour fournir un système de support vie aux humains dans le cadre d'une mission d'exploration de long terme dans l'espace. La boucle MELiSSA est un cas exemplaire de système biorégénératif, comprenant des fonctions de recyclage de l'eau et de l'oxygène ainsi que de production de nourriture. Parmi tous les aspects complexes liés à la conception et au fonctionnement de la boucle MELiSSA, la stratégie de contrôle est cruciale. Le système de support vie destiné à accueillir une mission avec équipage doit répondre à plusieurs exigences : un degré élevé de circularité, une efficacité maximale, une autonomie importante, une forte résilience, la fiabilité et la robustesse, tout ceci devant être des propriétés acquises pour le fonctionnement du système. Afin de répondre au défi de concevoir un système répondant à l'ensemble de ces exigences, l'approche contrôle est une problématique clé. Dans ce travail, une architecture de contrôle a été conçue en prenant en compte les contraintes liées au système. Une structure hiérarchique a été configurée. Elle est composée de plusieurs niveaux de contrôle : le niveau 3 (contrôleur tertiaire) représente la couche de supervision qui génère des points de consigne basés sur des critères de fonctionnement généraux ; le niveau 2 (contrôleur secondaire) est une couche corrective adaptant les consignes reçues du contrôleur tertiaire et l'état du procédé dans son ensemble, c'est-à-dire la boucle des compartiments ; le niveau 1 (contrôleur principal) génère les commandes de contrôle à envoyer aux compartiments, sous-systèmes et interfaces entre les compartiments pour suivre les consignes générées dans les couches supérieures du contrôle hiérarchique. Cette stratégie de contrôle nécessite d'avoir des modèles mathématiques et une représentation des systèmes d'intérêt, en l'occurrence des compartiments MELiSSA, pour pouvoir régler les contrôleurs et tester les performances globales de la structure de contrôle hiérarchique avant de l'implémenter dans un environnement physique. Un effort important a été fait pour générer un modèle mathématique du compartiment plantes supérieures. Ce modèle est basé sur les principes fondamentaux, intégrant des informations métaboliques et sur les transferts physiques. Il est adapté à la chambre de culture de plantes supérieures de la boucle MELiSSA. Cette étude contribue à générer un outil pour le contrôle de la boucle MELiSSA. Cet outil peut être utilisé pour effectuer des simulations dynamiques sur le long terme de la boucle et pour générer des connaissances sur la dynamique et le comportement d'un système aussi complexe et interconnecté que la boucle MELiSSA.

Summary

An overall control strategy for the MELiSSA loop is developed. MELiSSA is a loop of interconnected compartments conceived to provide life support to humans in long-term exploration mission in Space. Out of all the challenging aspects related to the design and operation of the MELiSSA loop, used in this study as an exemplary case of a bioregenerative life support system, the control strategy stands out for being strikingly complex, but crucial. The requirements of a life support system to host a crewed mission are certainly very demanding. A high degree of circularity, efficiency, autonomy, resilience, reliability, and robustness are characteristics taken for granted in the operation of a life support system. In order to respond to the challenge of designing an engineering system to satisfy all these requirements, the control approach arises as a major key player. Here, a control architecture has been designed considering the requirements and a hierarchical structure has been configured consisting on several control levels: Level 3 (tertiary controller) represents a supervisory layer that generates setpoints based on general operation criteria; Level 2 (secondary controller) represents a corrective layer adapting the references received from the tertiary controller and the status of the process (understood as the loop of compartments); Level 1 (primary controller) that generates control commands to send to the compartments, subsystems and interfaces between compartments to track the setpoints generated in the higher layers in the hierarchy. This exercise requires the availability of mathematical models of the system of interest, in this case the MELiSSA compartments, to be able to tune the controllers and to test the overall performance of the hierarchical control structure before implementing it in a physical environment. Consequently, important efforts have been done in generating a mathematical model of higher plants, based on first-principles, embedding metabolic information and adaptable to the higher plants chamber of the MELiSSA loop. Overall, this study contributes to generate a tool for the control of the MELiSSA loop, but also with applications to perform dynamic long-term simulations of the loop, and to the knowledge generation on the dynamics and behavior of a complex system like MELiSSA.

Resumen

El objetivo de esta tesis es proponer una estrategia de control para el sistema MELiSSA, que es una red de compartimentos interconectados pensada para trabajar en un entorno aislado. De todos los retos relacionados con el diseño i la operación del sistema MELiSSA, utilizado en éste estudio como un caso de estudio de un sistema de soporte de vida bio-regenerativo, la estrategia de control destaca por ser a la vez remarcablemente compleja y necesaria. Los requisitos asociados a la operación de un sistema de soporte de vida pensado para alojar una misión tripulada son ciertamente exigentes: Un alto grado de reciclaje, eficiencia, autonomía, resiliencia, fiabilidad y robustez son algunas de las características a tener en cuenta en el proceso de diseño de un sistema de soporte de vida. Delante del reto de diseñar un sistema que pueda satisfacer estos requisitos, la estrategia de control destaca como un actor con mucha relevancia. En el estudio presentado, se ha diseñado una arquitectura de control con una organización jerárquica organizada en diferentes niveles: El nivel 3 (control terciario) representa un elemento de supervisión que genera referencias (*setpoints*) basados en criterios de operación generales; El nivel 2 (control secundario) representa un nivel corrector que adapta las referencia recibidas des del control terciario de acuerdo con el estado del proceso (proceso entendido como el conjunto de compartimentos que conforman el sistema MELiSSA); El nivel 1 (controlador primario) genera una acción de control para ser enviada a los elementos de control de cada compartimento. El ejercicio de diseño de esta arquitectura de control requiere de la disponibilidad de modelos matemáticos del sistema de interés, que en este caso son los compartimentos del MELiSSA, para poder ajustar la configuración de los diferentes controladores y evaluar el compartimento de la estructura de control jerárquico antes de su implementación en un sistema real. Delante de esta necesidad de disponibilidad de modelos, se han dedicado esfuerzos importantes en generar modelos matemáticos del crecimiento de plantas, basados en primeros principios con información de los flujos metabólicos i escalable a la cámara de plantas superiores de la Planta Piloto del MELiSSA. Este estudio proporciona una herramienta de simulación dinámica y también intenta generar y transmitir el conocimiento adquirido sobre las dinámicas y el comportamiento de un sistema complejo como es el MELiSSA.

1. INTRODUCTION

1.1. State of the art of Space Exploration

Space exploration has recently attracted the attention of private companies and renewed the interest of the general public encouraged by both new economic opportunities and the exciting human milestones depicted in the horizon. Space agencies have continuously worked breaking new barriers in space research involving many disciplines: space exploration, Earth observation, communication, or planetary sciences among many others. The current space exploration activities include probably the most exciting endeavor for humankind in the near future, which is its presence on Mars by early 2040s. The steps before reaching Mars are long and complex. The European Space Agency (ESA) plans this roadmap towards Mars in a stepwise approach with three main blocks before human landing (ESA, 2022):

1. Ensuring and strengthening the current presence of technology in the Low Earth Orbit (LEO).
2. Returning humankind to the lunar surface for developing scientific and infrastructure assets and walking towards the construction of a lunar permanent habitat.
3. Mastering the logistics between the Earth and Mars first with robots and later with a progressively increased cargo load to acquire knowledge for a potential human settlement in Mars.

The activities beyond LEO will require much more information and technical advances in many areas: radiation and its effects on materials and on biological life and strategies to cope with it, new communication technologies, impact of long-term missions on human physiology going from cognitive capacity, neural disorders to nutrition diet, metabolism and psychology, new propulsion engines and rockets, landing and propulsion techniques and novel architectural concepts to be tested in outer space to host humans to mention some.

The future of space exploration can be divided in two main categories: crewed and non-crewed missions. Recently, several non-crewed missions successfully achieved their purpose including the ESA probe Rosetta landing on the comet 67P and representing the first successful landing on a comet (Bibring et al., 2007); the NASA probes Curiosity and Perseverance which are currently exploring the Martian soil and atmosphere, the second including a drone vehicle which achieved the first successful drone flight out of Earth (Siebach, 2021). Mars exploration is currently a hot topic with other agencies apart from ESA and NASA undertaking missions like the Chinese Tianwen-1 and the Emirates Mars Missions (Zheng, 2020). Other relevant space probes are Voyager 1 and 2 which have both explored Jupiter, Venus and Saturn and are currently in the interstellar space, being the Voyager 1 the farthest human-made object.

Crewed missions are another type of exploration activities whose requirements are more demanding than the probe-based missions mainly associated to guaranteeing the safety of the crew. The history of human presence in Outer Space is also full of success such as the first orbital flight by Yuri Gagarin, the crewed space station Salyut, under operation for 20 years, the joint USA-USSR space station Mir, the currently under operation International Space Station (ISS) and the Apollo missions that sent a total of 12 astronauts to the Moon during the 60s and early 70s. One of the things all these crewed missions had in common was the presence of a life support system (LSS) ranging from a very primitive design in Yuri Gagarin flight consisting on an air conditioning system and mainly open loop support with enough supplies to sustain life during the 108 minutes flight (Diamant & Humphries, 1990) to the more sophisticated technology in the ISS.

1.2. Life Support Systems

LSSs have been essential for the success of past and currently under operation crewed missions and will play a crucial role in the futur. LSSs are the set of strategies and technologies to sustain life in a human crewed mission and their scope can vary substantially. Life in outer space has typically been bounded to Earth but has evolved in complexity over time together with the technical progress and the distance of missions from Earth. One of the first crewed missions was carried within the Apollo program, whose LSS was designed so astronauts carried all oxygen needed during the flight, with carbon dioxide removal through molecular sieves and thermal control on board. Water was partially recovered from the atmospheric humidity control as well as from the fuel cell powering the spaceship (Ellis & Willis, 1968). Mir space station in operation from 1986 to 1996 had a thermal control and a LSSs aimed at regenerating air through the so-called Vozdukh module, a regenerable gas absorber module, still used in the ISS (Law et al., 2010). The ISS itself, a part of absorbing CO_2 with the Vozdukh module and the Carbon Dioxide Removal Assembly (CDRA), also obtains water from both a Sabatier reactor and from the condensation of air humidity (Pütz et al., 2016). Oxygen is produced through the so-called Oxygen Generation Assembly (OGA) that electrolyzes water, producing hydrogen that is recirculated to the Sabatier reactor (Bowman et al., 2017). Urine is also processed in a Vapor Compression Distillation (VPA), which generates an efflux of water that requires pretreatment in a Water Processor Assembly (WPA) consisting in a set of filters and a catalytic oxidation module (Volpin et al., 2020).

All these technologies that have been used to support the human presence in LEO and lunar missions are based on physicochemical processes. However, not all conversions are possible through these technologies. For example, edible food cannot be chemically synthesized without

biological processes taking place either naturally (i.e. crop production, livestock) or synthetically (i.e. cultured meat). On the one hand, the main disadvantage related to the use of physicochemical reactions is that the operational conditions for them to happen tend to be more extreme. For example, the Sabatier reaction takes place at around 400 ºC and 2 MPa, conditions that are much more extreme than the equivalent biological methanation reaction that can operate at around 40 – 70ºC (Junaedi et al., 2011; Vogt et al., 2019). Such conditions may also spoil hardware as it has already been observed in the Urine Processing Unit (UPA) in the ISS, whose use of very low pH has been reported to hamper the distillation columns (Kayatin et al., 2016). On the other hand, the main advantage of physicochemical processes is that hardware that carry physicochemical reactions is very compact, reliable and proven in long-term missions. Finally, current technologies used in space applications, because of the nature of the missions tightly bound to the Earth, assume a low degree of circularity: The constant food refilling in the ISS or the methane release as a by-product of the Sabatier reactions, are two examples of such non-circularity. This is an approach no longer valid for future crewed missions of long duration in Space.

1.2.1. Regenerative Life Support Systems

When space missions aim at travelling to Mars or expect to stay orbiting in the Cislunar Space like in the NASA's newly announced Lunar Orbital Platform Gateway (Crusan, 2017), circularity and regenerative technologies will be crucial to sustain life since Earth support will be more limited. It has already been announced by NASA that the transit to Mars will last between 420 days outbound and return to 620 days and the stay in Mars soil is expected to last around 30 days all depending on the logistics and the final aim of the mission (Dunbar, 2021). Such long missions involve huge amounts of consumables required by the crew. It is considered that, on average, a 82-kg astronaut consumes 0.83 kg O_2, 3.9 kg potable H_2O and 0.62 kg fresh food on a daily basis. In turn, 0.99 Kg CO_2, 0.11 kg of waste solids (in urine and feces) and a range of waste water is generated including that recovered from hygiene tasks (Ewert & Stromgren, 2019; Grigoriev et al., 2011). See Fig 1. 1 for a summary of a human metabolic balance

Fig 1. 1. Human consumables and throughput values in kg/crewmember/day.

It is possible to calculate the amount of cargo needed if the current technologies of resource recovery on board the ISS are used. Considering the average expected duration of the transit to Mars, that would last 520 days, in terms of edible biomass, a cargo load of 1450 Kg of fresh food would be needed per astronaut. For a crew of 4 people, the amount of mass required would be around 5800 Kg. In terms of water, some regeneration is achieved mainly by the following units: The Water Processor Assembly (WPA) and the Urine Processor Assembly (UPA) which collect water from urine, the atmosphere and from the Sabatier reactor. Overall, 75% of water is recovered (Pruitt et al., 2015). Considering the 3.9 kg potable H_2O needed per crew member, it results in a total need of 2028 Kg Water in a mission like the Mars transit. Finally, O_2 is mainly generated in the Oxygen Generation System (OGS), which is an electrolysis unit that consume water and produce H_2 as a by-product. This strategy regenerates 80% of the oxygen needs, being the 20% left provided in the form of pressurized oxygen. The non-recycled oxygen would account for 370 Kg in a Mars Transit mission. Considering only the re-supply of consumables representing the metabolite needs of a 4-crewed Mars Transit mission, the amount of initial load to guarantee life approximates to around 4 tons of mass. The current hardware to facilitate the regeneration of oxygen, water, and the removal of CO_2 weights 6.249 Kg (see Grigoriev et al., 2011 for a full list of equipment load, spare parts, and payback ratio analysis) taking into account also the required spare parts given failure probabilities in a Mars transit mission. Overall, more than 10 tons of payload are required considering only the life support system. The Chinese Tianzhou, designed to resupply Tiangong-1, is the only vehicle capable of carrying such payload (SpaceX Dragon 2 can re-supply up to 6000 kg of cargo). Therefore, in terms of logistics and cargo capabilities, current technology is far away from assuming the payload associated to a Mars Transit mission using Life Support Systems as designed for LEO missions. It is thus recognized by the different space agencies and actors that regenerative life support systems are mandatory for future Mars missions.

Summarizing, physicochemical processes are the current players that provide life support systems in LEO missions. These processes are proven to be long-term efficient, compact (and thus with a low equivalent mass) and reliable, but they lack the capacity to generate food, which is crucial for missions that will not be bond to Earth re-supply. Bio-based conversions are the only mean to tackle with edible biomass. These bio-based conversion processes must be interfaced with physicochemical processes in long-term space missions since they have the following notable capabilities: The capacity to produce edible food onboard, a high degree of circularity and mass recycling, the capacity to manage waste matter and the use of mild

conditions in the reactions contributing to the minimization of risks for the crew, to mention a few. technologies.

1.2.2. Bioregenerative Life Support Systems

The research on BLSSs has always been coupled with ecology studies since it is unavoidable to conceive the BLSSs in a space habitat as an artificial ecosystem analog to the Biosphere with limited mass exchange and open energy exchange. However, even though the comparison between BLSSs and the Biosphere is conceptually obvious, differences are huge, starting by the scale. The history of BLSSs dates to the early 20th century with the first studies on closed ecological systems done in the Soviet Union, where the concept of Biosphere was first described by V. Vernadski (1926). Life was described at that time as a geological force and it is curious to see how futuristic projects like the Mars Terraformation, which proposes the possibility to turn uninhabitable planets into habitable ones assume the same principle of life as a driving force (Conde-Pueyo et al., 2020). V. Vernadski conceptualization of the principles governing natural and artificial ecosystems was picked up by another soviet scientist, K. Tsiolkovsky, who depicted the possibility to apply those principles to astronautics and first proposed the co-existence of humans and plants in a spaceship (Tsiolkovsky, 1926; Wheeler, 2010). The growth of plants has captured most of the attention of scientists since Vernadski and Tsiolkovsky studies given the multifunctional capabilities of plants including the regeneration of air by the CO_2 capture, and the O_2 production both through the photosynthesis process, the partial wastewater treatment mainly by removing impurities through the transpiration or the potential psychological benefit for crew members (Massa et al., 2016). Between the Salyut and the ISS, dozens of plant growth chambers have been tested in space shuttles and space stations using several crops (lettuce, onion, kale, cauliflower, soybean, potato, rice, tomato, Chinese cabbage, turnip, Swiss chard, radish, strawberry, carrot, spinach, pepper, cucumber, pea, wheat, and beet among others) with an increasing surface area and control capacities over the years (Zabel et al., 2016). However, all these tests have never been integrated in the life support system of a spaceship but have always been operated stand-alone for scientific data collection. Though a crucial and essential element for BLSSs, plants are not the only biological agents assessed, since algae and cyanobacteria have also been considered and experimentally tested for such purpose. In fact, similarities between plants, algae and cyanobacteria are striking specially regarding their underlying biochemistry, but of course completely different in terms of culture techniques. By 2018, a total of 51 experiments were run in space, the vast majority involving *Chlorella* genus, and four of them using cyanobacteria (*Nostoc, Gloeocapsa, Anabaena*) in different space stations mainly to study the impact of space conditions on microbial physiology (Niederwieser

et al., 2018). Among many interesting observations, an experiment carried in 2008 stands out: In this experiment, *Chlorella, Rosenvingiella* and *Gloeocapsa* cultures were exposed to the outside ISS conditions including extreme temperatures and vacuum. All microorganisms survived but showing some carotenoid damage (Cockell et al., 2011). Aligned with these observations, genome mutations were detected in *Nostoc* sp. CCCryo 231-06 cultures exposed to extreme temperatures and radiation affecting biofilm synthesis and photosystem pathways in an almost 2-year long experiment in the EXPOSE-R2 platform outside the ISS (Y. Liu et al., 2022). All the experiments reported for plants, algae and cyanobacteria were done on standalone mode of operation to study which of those biological systems tested could potentially be integrated in a partially or fully closed ecosystem to support crews' life.

In parallel, a lot of progress has been made over the last decades on studying the integration of stand-alone life support technologies into crewed habitats. Doing that directly in Space can be difficult, so most of the agencies develop ground demonstrations before launching BLSSs technologies to Space to test and tune the different candidate technologies.

1.2.3. State-of-the-art of Bioregenerative Life Support Systems Projects.

Different space agencies have programs aimed at developing technologies for future long-term crewed missions less dependent on Earth support. Though some consensuses exist, and common technologies are being developed by space agencies in parallel, like the need for reliable Space farming capabilities, there exist conceptual differences worth mentioning:

- NASA's advanced life support system (ALS) program is characterized by developing a combined physicochemical/biological life support system, being the biological compartment centered on developing higher plant chamber cultures integrated with environmental control technologies to monitor and control temperature, humidity and contaminants and integrate carbon capture units to trap carbon dioxide in case it is accumulated due to plants and crew metabolic activities. However, plenty of experiments have been done related to plant growth (see the review by Johson et al. (2021) for a full list of NASA's plant-related research activities), being Veggie, the most productive project in terms of quantity of experiments and scientific contribution in the field of space agriculture, in operation in the ISS since 2014 (G. Massa et al., 2021). In the near future, the project Ohalo III is aimed at recycling transpired water in the ISS to grow crops (Johnson et al., 2021)

- The Japanese Aerospace Exploration Agency (JAXA) has also investigated higher plants and physicochemical technologies and integrated both in the Closed Ecology Experiment Facilitie which run from 2005 to 2007. CEEF had an increased complexity compared to NASA's Lunar-Mars Life Support Test Project, with both capture of carbon dioxide and oxygen to improve the gas management, a water and a waste processing unit. The waste processing unit involved pyrolysis and incinerations steps to generate carbon dioxide and monoxide as gas effluents that were then used in the higher plants compartment. In those tests closure of food reached 80% of the edible food needs, but there was a surplus of oxygen and shortage of carbon dioxide (Tako et al. 2010). Looking to the future, JAXA has been assigned the development of the LSS for the Gateway which will involve the design of the crew habitat, the thermal and environmental control and the batteries among others (Fuller et al., 2022)
- Russian space programs stand out in LSS-related activities in the 70s and 80s with the BIOS program, the first artificial life support system tested in a crewed experiment. BIOs programs shaped the way for others to come like the American Biosphere and introduced the culture of green algae (Chlorella in BIOS-3) as a robust and easy to recover unit that can complement a diet based on higher plants (Salisbury et al., 1997).
- ESA's life support system program is quite unique in its approach because it was initially conceived as fully bioregenerative, meaning based on biological compartments. The inspiration on the fundamental reactions found on Earth to sustain life for humankind lies behind this bio-based approach, as stated in Hendrickx et al. (2006). Thus, the requirement of producing O_2, removing CO_2 and providing edible food in a reduced space can be satisfied with cyanobacteria culture, specifically *Limnospira indica*. Then, a healthy diet is achieved by the culture of a combination of higher crops which provides also certain degrees of freedom to achieve the desired supply of nutrients. Next challenge is the processing of wastes, which on Earth is typically done by a pool of bacteria that, through anaerobic digestion involving several reactions, produce gas outflows of carbon dioxide and methane and a liquid outflow rich in volatile fatty acids. These volatile fatty acids were originally expected to be converted to carbon dioxide by the photoautotroph bacteria *Rhodospirillum rubrum*, but intense investigation has been recently placed on using microbial fuel cells to carry this reaction, which is demonstrated to be very efficient in the production of CO_2. Finally, photosynthetic compartments require nitrogen in the form of nitrate preferably, but usually nitrogen-compounds from human wastes are found in reduced forms, like the case of urea in the urine. Thus, urine must be converted to nitrate prior to its use to feed photosynthetic compartments

through an oxidation step, which is usually referred as nitrification. See Fig 1. 2 for a graphical description of the MELiSSA loop.

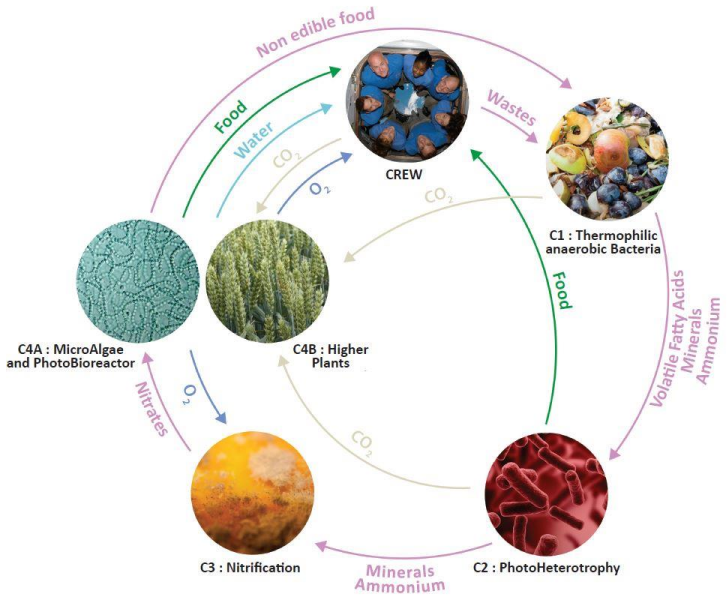

Fig 1. 2. Graphical representation of the MELiSSA Loop

The Micro-Ecological Life Support System Alternative (MELiSSA), which is how ESA's life support system program is known, has been developing research and technologies for future space missions for the last 35 years. The MELiSSA loop is inspired by the phenomena that takes place in many ecosystems on Earth with full energy exchange in different forms (sun radiation, heat transfer, etc.), but with a constrained mass exchange. More specifically, the MELiSSA loop was inspired by lake ecosystems where a consortium of bacteria, algae, higher plants, and animals cohabit in natural hysteresis.

- One of the latest powerful players to join the research in BLSS is China, with the so-called Lunar Palace as the main and one of the most advanced human rated habitat located in Beijing where it is possible to grow different types of crops with a food processing unit and a waste management unit. Unlike the other projects mentioned above from different agencies, the crew habitat is more advanced in the Lunar Palace with different rooms aimed at the crew wellbeing and health monitoring (Dong et al., 2017b).

A summary of the most relevant BLSSs test-beds based on their main technologies and developing institution is represented in Table 1. 1.

Table 1. 1. Summary of past and current life support system test beds

Project	Waste Management	Photosynthesis	Developer	Reference
BIOS-3	Incineration	Microalgae and plant crops	Institute of Biophysics, Russia	(Salisbury et al., 1997)
Biosphere 2	Biological conversion	Microorganisms' consortium, coral reef, tropical rainforest	University of Arizona	(Nelson, Burgess, et al., 1993; Severinghaus et al., 1994)
CEEF	Incineration	Plant crops	Institute for Environmental Sciences, Japan	(Tako et al., 2010)
ALSSTB	RLSS Test Bed	Plant crops	NASA	(Barta & Henninger, 1996)
MELiSSA	Biological conversion	Cyanobacteria and plant crops	ESA	(Gòdia et al., 2004a)
Lunar Palace	Biological conversion	Plant crops	China Manned Space Engineering Office	(Dong et al., 2017a)

1.3. The MELiSSA Project

The MELiSSA research activities are carried by a MELiSSA consortium made up by scientists and engineers from different fields, companies and universities working towards the same objective. The MELiSSA project has many branches all of them contributing to the core objective of the program which is to develop a bioregenerative life support system for space missions. The following list summarizes the main activities gathered by the MELiSSA consortium:

- Space experiments: among several in-flight experiments, two projects capitalizing ESA's intention to assess the viability of biological organisms in orbital flights should be highlighted. The first one is the Arthrospira-B of the ARTEMISS project (Poughon et al., 2020) that studied the growth of *L. indica* on board the ISS with successful results in

batch mode, which will be complemented by ARTEMISS-C with a continuous growth of *L. indica* with online monitoring (Fahrion et al., 2021). The second one is the Urinis-A project, which aims at studying the impact of space conditions on a nitrification culture in terms of activity rates, transcriptome, proteome, and metabolome analysis, among others (Verbeelen et al., 2021).

- The MELiSSA Pilot Plant (MPP): since 2009 the MELiSSA Project is testing the different technologies that have been and are being developed in a ground demonstrator, the MELiSSA Pilot Plant. Its objective is to integrate the different technologies and compartments that configurate the final MELiSSA loop in a single platform to carry experiments in stand-alone and in integrated mode of operation. Several topics are studied including the study of the dynamics of the compartments in their different modes of operation, the implementation of model-based predictive control strategies, the microbial growth inside the different compartments or the energy and mass transfer to mention a few (Gòdia et al., 2004b). The MELiSSA Pilot Plant has an intensive experimental schedule and constant communication with the MELiSSA consortium that allows to assess new technologies in a unique integration facility. Among the different achievements of the MPP, it is worth mentioning the recent integration in the liquid phase of a nitrification bioreactor providing nitrate to a photobioreactor, and in the gas phase the integration of a photobioreactor to a crew compartment exchanging carbon dioxide and oxygen and to the nitrification bioreactor (Garcia-Gragera et al., 2021).
- Higher Plants Characterization: research on space farming is crucial for the MELiSSA project. This is performed at the recently inaugurated PaCMAN Unit Laboratory in the University of Naples Federico II, for studying plants growth, biometry, and physiology with very fine capacity to carry those analysis discriminating for both shoots and roots. Also the Higher Plants Culture in the MPP has been very productive in terms of knowledge generation, being more focused on integrating plants to the rest of the MELiSSA loop (Peiro et al., 2020).
- Systems-based Modelling and Control

  From a system engineering point of view, the MELiSSA loop represents a complex system. The phenomena that take place naturally on Earth, when simplified and brought into a controlled engineered environment, gets strikingly hard to characterize and control. The main difference lies on the scale, the dynamics of the evolution of the involved states (compound concentration, pressure, temperature, etc.) and the impact of disturbances over time. Basically, Earth massive volume and complex geological and biological interactions provide a natural hysteresis on Earth considered undisturbed for

some, like in the case of James Lovelock Gaia's hypothesis (Lovelock, 1990) or tending to an unbalance like John Krichner's amendment of the "natural balance" concept.(Kricher, 2009). In any case, differences in scale, storing capacity and thermodynamics makes Earth and small-scale artificial ecosystems difficult to compare (Nelson, Alling, et al., 1993).

Each of the selected functional subsystems identified and selected to be part of the MELiSSA loop are experimentally characterized, mathematically modelled and optimized individually but also analyzed in an integrated mode (Fulget et al., 1999). A thorough understanding of the MELiSSA compartments operating in standalone and integrated to each other is important given the demanding requirements associated to crewed missions involving mass, energy, safety, efficiency, crew time, reliability, and sustainability aspects (list obtained from the Advanced Life Support System Evaluator – ALISSE(Brunet et al., 2010)).

- Terrestrial Applications

  One of the aims of the MELiSSA loop, beyond its core Space application, is to impact the society with contributions on circularity. The MELiSSA loop, as several projects and businesses on Earth, works towards minimizing the expenditure and maximizing the re-utilization of wastes. Thus, it is possible to find nowadays MELiSSA derived technology in a wide range of sites and applications around the world: One of the first ones was the installation in 2005 of a water recycling unit in the Concordia Station in Antarctica with the capacity to re-use 80% of the grey water for the demand of a population of 25 people (Lasseur & Mergeay, 2021). Similarly, the Roland Garros tennis tournament since the 2020th edition is using such grey water recycling technology. Also in 2020, the spinoff *Hydrohm* was funded, with a technology going one step further and recovering phosphorus, nitrogen and salts from urine and re-using urine for toilet flushing. The full list of terrestrial applications derived from MELiSSA activities can be found in the MELiSSA Foundation website: www.melissafoundation.com.

1.3.1. Modelling and controlling the MELiSSA Loop

Modelling both the complete MELiSSA loop as well as its compartments in standalone mode of operation is demanding due to the nature of the systems under study, which are biological reactions. The enzyme kinetics, the energy and mass transfer in bioreactors or the equilibrium of carbon species in aqueous media are a few examples of the behavior of biological compartments. These phenomena are described and their corresponding models are used to predict the evolution of the system under study over time, which can eventually lead to the

development of predictive maintenance tasks of hardware, to support operation and research activities, to optimize the process designs or to define predictive controllers among others. In fact, one of the technologies currently in the spotlight of many technology companies, the Digital Twins (Singh et al., 2021), is based on the idea of having a cybernetic replica of a physical system aimed at providing monitoring, optimization of the physical device, predicting issues or scheduling maintenance and was firstly described by NASA to support space missions remotely (Shafto et al., 2010). NASA considered in 2000 that computer science had the capacity to increase the robustness of aerospace systems and would become crucial to recover long-term human exploration missions halted since the Apollo program (Glaessgen & Stargel, 2012). ESA Agenda 2025, which represents the European space roadmap states the need to contribute to the digitalization of the organization by fully deploying model-based systems engineering affecting not only engineering but also financing and other non-technical departments. In line with this perspective, MELiSSA promoted, as mentioned before, the ALiSSE methodology, intended to be used as a decision-making tool to assess life support systems. This methodology is based on three pillars: the metrics (mass, energy, safety, efficiency, crew time, reliability and sustainability), the reference model defining the interactions between physical elements and environments and the workflow which defines the information flow (Brunet et al., 2010).

2. OBJECTIVES

2.1. Scope of this Project

The goal of this study is to design and implement, in a virtual environment, a control architecture that would allow to operate the MELiSSA loop in a stable and optimal way. The following specific objective were pursued:

1. Provide a control architecture approach to manage the MELiSSA loop including:
    - Capacity to track setpoints
    - Rejection of deviations.
    - Control on the performance of the overall process.
    - Resource optimization.
2. Provide the mathematical development of the control architecture considering the requirements mentioned in the previous point as well as the use of model-based control algorithms to achieve the desired performance.
3. Implement and test the performance of the control architecture in a virtual environment based on the latest integration phase of the MELiSSA Pilot Plant. Two scenarios are used as case studies:
    - Case 1: Integration of the gas phases of C4a (photobioreactor), C5 (crew compartment) and C3 (nitrification reactor) and integration of the liquid phases of C4a and C3
    - Case 2: Integration of the gas phases of C3, C4a, C4b (Higher Plants Compartment) and C5 and the liquid phases of C3, C4a and C4b.
4. The development of a mathematical model for higher plants compartment (HPC) is a derived objective from point 3) since there are no available models of this compartment adapted to the MPP Higher Plants Chamber. This model has to be based on a mechanistic approach as well as contain metabolic information of the diel plant cycle.

2.2. Outline and contribution to the MELiSSA Project

The work presented in this study is a systems engineering work primarily focused on the adaptation of existing models of the MELiSSA compartments in a complex hierarchical control architecture which works using a predictive control approach aimed at optimizing and controlling the operation of the system under study. The different chapters are devoted to the following aspects:

- Chapter 1 and chapter 2 comprehend the introduction, context, contribution and objectives of the presented study.

- Chapter 3 is dedicated to the construction of a theoretical hierarchical control structure (HCS) based on an analogy of LSSs with Microgrids, which are complex engineering system that share conceptual similarities with LSSs, specially in their isolated mode of operation.
- Chapter 4 is devoted to the mathematical development of the HCS proposed in Chapter 3 and its implementation in a virtual environment. The MPP at its latest integration stage is used as a case study to test the proposed HCS because of the high degree of understanding of its different subsystems in standalone and in integrated mode of operation. Such case study is, more specifically, based on the integration of the nitrification compartment (C3) and the photobioreactor (C4a) in the liquid phase and C3, C4a, and the crew compartment (C5) in the gas phase (Garcia-Gragera et al., 2021). The objective of this integration campaign carried in 2021 was to achieve a 100% of O_2 regeneration in the system while satisfying the demands of a mock-up crew based on 3 rats. To achieve that, the C3 and C5 needs of O_2 were supplied on demand by the photobioreactor through a PFC-based cascade controller. In the simulation presented, the HCS defined in chapter 3 is designed to satisfy the demands of O_2 in C3 and C5 compartments, on top of coordinating the operation of the producer compartment, the photobioreactor C4a, and an added concentrated O_2 storing tank.
- In Chapter 5 a Higher Plants Chamber (HPC) model is presented based on an adaptation of previously published models to the subsystem of interest, which is the C4b compartment of the MPP. The model is conceived in a structural way, with different phenomena modelled in separate sub-models with information exchange between them. The effect of canopy on crop growth, the mass and energy balances, the enzyme kinetics, and the metabolic information for a *L. sativa* (lettuce) culture are contemplated. The proposed model strategy is validated with experimental data under different static and dynamic simulations.
- In Chapter 6 the integration of the HPC model presented in Chapter 5 with the HCS presented in Chapter 3 is addressed. In this study, the future integration step in the MPP is considered as a case study including the integration of the liquid phases of C3, C4a and C4b and of the gas phases of C3, C4a, C4b and C5. Different control configurations are tested as well as different process designs. On top of the control of O_2 in C5, the control of the use of the O_2 producers (C4a and the O_2 concentrated tank), the control of CO_2 has been included to explore both the capabilities of the HCS from a control perspective as well as to gain knowledge on the dynamics of the

internal resources of the MELiSSA loop, in this case the CO_2. A discussion of hardware and software co-design and their impact on the overall performance of the system operation is also presented.

3. DESIGN OF A HIERARCHICAL CONTROL STRUCTURE

Based on a paper published in the journal *IEEE Industrial Electronics Magazine*

Nomenclature

Acronyms

LSS	Life Support System
CES	Close Ecological System
MELiSSA	Micro-Ecological Life Support Systems Alternative
MPP	MELiSSA Pilot Plant
MG	Microgrid
HCS	Hierarchical Control Structure
DER	Distributed Energy Resource
ESS	Energy Storage System
MSS	Matter-Storing System
PV	Photovoltaic
RES	Renewable Energy Resource
ESA	European Space Agency
ALiSSE	Advanced Life Support Systems Evaluator
MPC	Model Predictive Control
PFC	Predictive Functional Control
HIL	Hardware-in-the-Loop
FPGA	Field Programmable Gate Array
SoH	State of Health
DT	Digital Twin (In other chapters, DT refers to Diluted Tank)

3.1. Introduction

A significant concern in integrating the complete compartments and developing a closed operational loop is related to designing an efficient, reliable, and dynamic control system that can fulfill system's requirements and guarantee its long-term performance.

From a systemic point of view, BLSSs are autonomous systems integrating various generation, recycling, and consumption subsystems with the storing capability to solve potential unbalance of key elements in the loop. Accordingly, a BLSSs share many similarities with other autonomous systems like islanded microgrids (MGs), which opens up new opportunities to benefit from the recent advances in modelling and control of such complex structures. In this regard, this study aims at exploring the similarities of the islanded MGs with CESs and benefit from MGs highly developed control structures to cope with the complex control tasks of closed ecosystems.

3.2. Controllability of BLSSs

As explained in the Chapter 1, the Russian project BIOS-3 represents one of the first closed ecosystem experiments relying both on microalgae and higher plant crops to convert the CO_2 released by the crew into O_2 with a negligible leak and a degree of closure of 100%, 85%, 40%, and 20 % for O_2, water, nitrogen, and minerals, respectively (Gitelson & Lisovsky, 2002). Most of the successful results of BIOS-3 inspired Biosphere-2, the biggest closed ecosystem facility focused on studying human-environment relationships to be used for future outer space habitat designs. It contained aquatic and terrestrial ecosystems colonized with model organisms mimicking the Earth, a totally sealed environment with energy from the sun. Biosphere-2 experiments in 1991 proved the importance and challenge of the controllability of closed ecosystems as microorganisms in the soil grew and released CO_2 into the atmosphere in an uncontrolled way exceeding the capacity of plants to revitalize the air while making the atmosphere unbreathable for the crew. Thus, the expected degree of closure of 100 % could not be guaranteed by controllability and leakage issues (Severinghaus et al., 1994). One of the longest runs of a closed BLSS was promoted by NASA in 1998 named Lunar-Mars Life Support Test, which involved the air revitalisation coupled to food supply from crop culture and waste processing in a 90-day test. One of the outcomes of this project was to boost an integrated control system design to consider the overall operation to reduce crew and ground personnel intervention time.

The recent promising integration results in the MPP connecting the gas phase of the crew chamber and the cyanobacteria bioreactor through a cascade controller serve as a platform to build an advanced control structure for the entire loop (Alemany et al., 2019).

From a control point of view, previous attempts to close an ecological system reported the importance of controllability in such complex systems. Even though there are different BLSSs strategies with advanced control structures, to the best of our knowledge there are not any hierarchical control structures (HCS) designed for the integrated operation management of BLSSs. Only in Farges et al. (2008), a HCS concerning the control of the biomass production in one of the compartments of the MPP through adjusting the light intensity is developed, but not extended to more compartments of the loop. Hence, this study will be focused on proposing a hierarchical control framework for BLSSs including several generation, consumption, and storage subsystems aiming at serving a BLSSs based on the advanced HCS of MGs.

3.3. From MGs to BLSSs

MGs are known as local aggregation of distributed energy resources (DERs), energy storage systems (ESSs), and loads with the capability of operating in either grid-connected or islanded modes (IEEE, 2018). Islanded MGs, MGs without power exchange with the main grid or adjacent MGs, have been implemented in many applications including geographical islands, rural areas, automotive, avionic, and marine industries (Guerrero et al., 2013). The main characteristics of an islanded MG include: The capability of locally solving energy balance problem; Performing several multi-time scale control tasks allied with different operational and technical requirements in system-level as well as component-level; Scheduling several micro-generation units characterizing different dynamical behavior; Supplying MG consumers with the reliable, clean, and sustainable energy taking into account the uncertainty involved in the generated and demanded power; and managing storage possibilities to cope with energy balance and enhance system reliability and performance. MGs are beneficial for both the main grid and MGs users. From the viewpoint of the main grid, a MG is regarded as a controllable entity, which can support the upstream network through providing ancillary services while from the MGs participants' point of view it can be seen as a highly reliable source of power, which can enhance the quality of life of its participants.

On the other hand, BLSSs represent a small-scale islanded system that aim to distribute matter through the loop in the form of mass flow. Hence, system's operation requires coordination between the energy resources, namely photosynthetic compartments that receive solar energy and convert it into chemical energy, matter-storing systems (MSSs), and matter sinks represented by different compartments including the crew compartment in the system.

Distributed Energy Resources: DERs in MGs include small on-site generation units called micro-sources such as diesel generators, micro turbines, wind turbines, photovoltaic (PV) systems, and

so on, which in comparison with conventional power generation systems enhance the reliability of the energy systems while reducing investments costs (Lopes et al., 2006). DERs in CESs are more limited due to the poor environment in terms of resources found in space. However, sunlight is the most abundant energy source on the Earth and outer Space and plays a crucial role in both renewable-based MGs and CESs. PV systems and photosynthetic complex harness the sunlight energy to produce electrical and chemical potential energy respectively. Although differences in the way of operation, the final product (electrical energy in PVs and energy carrier molecules in photosynthetic cells), and energy conversion efficiency, it is already known that they share many similarities (Blankenship et al., 2011; Kirk & Ferry, 2018). In a PV cell, the sunlight photon is absorbed by the semiconductor material (e.g. silicon) and results in generating an electron-hole pair. The energized electrons flow through the conductor as electrical current and the resulting electrical output power can be used immediately or stored for later usage. In natural photosynthesis, energy of the absorbed photon results in an excited state of chlorophyll. These high-energy electrons are used to produce the energy storing molecules NADPH and ATP in a series of light-driven reactions. The H_2O molecule as a donor of electron is broken and O_2 is produced as an important byproduct (Kirk & Ferry, 2018). Fig 3. 1 represents an illustration of both processes. It is worth mentioning that in BLSSs, it is not only important to be able to capture solar energy and distribute electrical energy, but to achieve high efficiencies in the conversion of electrical energy to chemical potential.

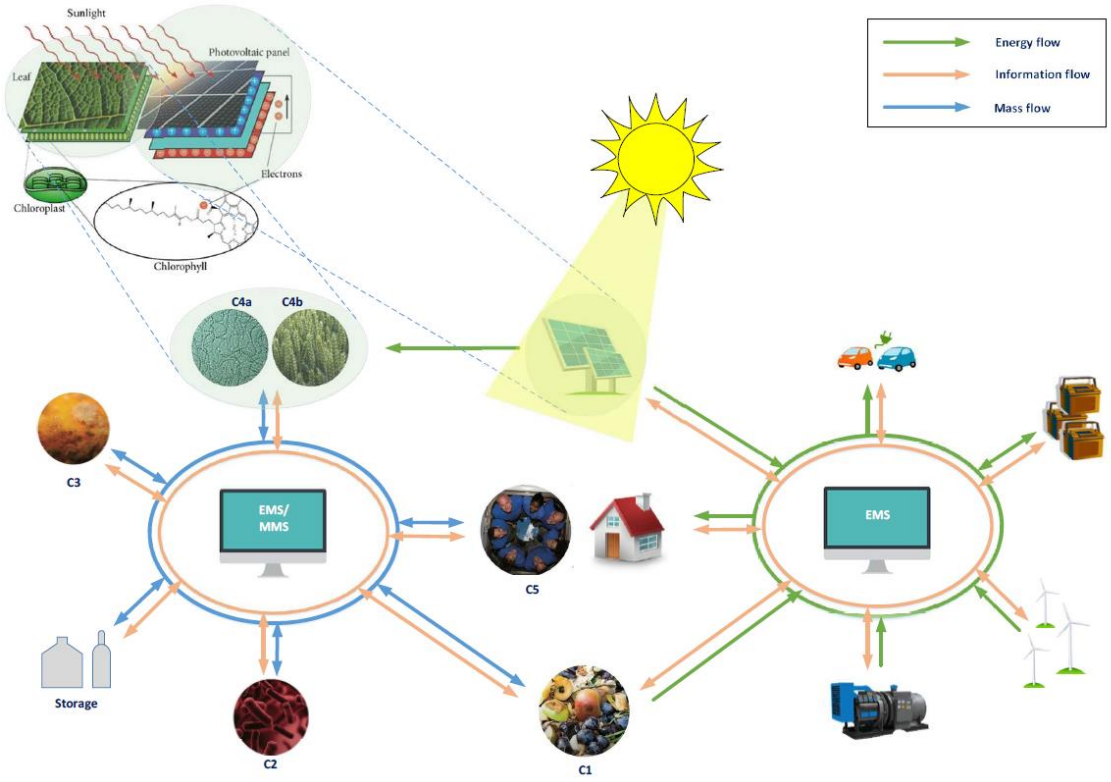

Fig 3. 1. Illustration of the comparison of MGs and BLSSs.

Like biogas generation technology in MGs, which can provide heat and energy cogeneration, CESs might also include an anaerobic digester to process the generated waste and produce CO_2 (Kojima et al., 2007). Analogous to micro-generation units in MGs, operational constraints such as minimum uptime/downtime limitations, ramp-rate constraints, and mass flow generation capacity are required to be respected in the control of BLSSs. As an example, the optimal higher plants growth rate in the MELiSSA loop is strongly conditioned by its activation time, which is related to the plants circadian rhythm (Kim et al., 2017), being the 16-hour day-light time when the maximum plants growth rate takes place in the current operational conditions used in the MPP. The minimum deactivation time of this compartment is also required to be longer than 8 hours for a proper functioning of the plants' metabolism (assuming certain variability between crops).

Energy and Mass Storing Systems: Storing systems are essential elements in both MGs and BLSSs. They can increase system's reliability and flexibility through providing the system with a backup source of energy and the capability of shifting energy production and consumption intervals. In MGs, uncertain nature of the power produced by renewable energy sources (RESs), asynchrony between the peak interval of power generation and consumption, as well as the different dynamical responses of various elements are among the main motivations of incorporating ESSs. In this sense, ESS management is a significant control task in the renewable-based MGs (Cagnano et al., 2018). In CESs, due to the day-night cycles of the plants and different dynamics of the loop elements, storage systems are used for buffering purposes. Increasing the cellular concentration or plant population, results in producing more O_2, water, and food, which can be stored for later consumption.

However, it is important to optimize the size of storing tanks to keep the system weight at its minimum, a requirement stated by ESA's ALISSE criteria (Brunet et al., 2010), which is also a main concern in isolated mobile MGs such as ships and space MGs. Besides, considering technical issues such as accumulation limitations and technical constraints of storage tanks (e.g. flow rate limitations, minimum and maximum storing capacity, etc.), including the MSSs will complicate the CES control process.

Hybridization is another efficient way to cope with different dynamics of the system components and benefit from advances in different technologies. As an example, in a hybrid MG including fuel cell, battery, and ultra-capacitors, the dynamic response of the system to power demand variations can be improved by utilizing the stored energy. This concept can be also applied to CESs where the two photosynthetic compartments based on cyanobacteria and higher plants feature different dynamic response characteristics. Besides, stored materials can

be used to respond to sudden changes in the system.

Energy/Mass Consumers: In a BLSSs, the crew consumption rate drives the entire operating loop. Survival of the crew is required to be ensured through satisfying specific conditions for the availability of water, food, and gas concentration. Like MGs, the consumers are considered one of the main sources of uncertainty besides the sunlight as their activities can considerably affect the supply of matter. Although we can have an estimate of the average O_2 consumption rate of the whole loop, many factors can affect this rate like the crew activity, the elemental composition of feces and urine and the consumption and generation rates of microbial communities.

MGs should be able to operate autonomously and interact with other MGs and the main grid while the state of the art of BLSSs are still not in a developed-enough stage to consider inter-connections between different CESs. In both MGs and CESs, DERs and ESSs/MSSs spread over the system and are connected to each other and loads.

Like in MGs, the design and planning of a BLSS is an important field of study, which needs to take into account different considerations such as the system scale, the degree of closure (variable accounting for the degree of internal regeneration), the efficiency of individual compartments and the whole system, the safety and the weight of the system. All the considerations affecting the design and operation of a BLSS are well described in the ALISSE criteria (Brunet et al., 2010), which is out of the scope of this study. This research is mainly focused on the control and operation management of BLSSs.

Although there are striking similarities between both systems, some of the specific characteristics of BLSSs make their design and operation more challenging than renewable-based MGs. As an example, despite light, which comes from an external source of energy, other energy sources are generated inside the loop. Hence, the generation capacity of different matter resources cannot be predetermined and are specified based on the current state of the dynamic system. However, the existing similarities offer the possibility to use the advanced control methodologies developed for MGs to BLSSs, a space application of increasing interest.

3.4. Control and Operation Managements of BLSSs

The integrated system of a BLSSs contains both the dynamics of the individual compartments as well as the interacting parts. The integrated system is very complex with many states and manipulated variables, non-linear interacting dynamics, and several varying operational and technical limitations. Besides, the dynamic response time of the processes in the various compartments are noticeably different. The impact of the dynamics of the different phenomena

that takes place in each compartment in the whole loop is strongly affected by both the volume, the residence time, and the nominal concentration of the compounds in each compartment.
The multi-objective control process requires meeting mainly two control objectives, namely balancing the consumption and production of oxygen, water, and food to guarantee life support, and to process the loop wastes to achieve high levels of recycling.
Due to the multiple time scales of the BLSSs and different time resolutions of the objectives, an integrated control structure may not be successful. The combination of the need of a long prediction horizon, in the order of several weeks, with short control time steps, in the order of a few minutes or seconds, results in a high-dimension control problem, which cannot be handled in real-time. Hence, a multi-time frame organization of the controller is required.
Furthermore, developing appropriate models to be used in different layers and sub-layers of the control hierarchy with different levels of abstraction is of vital importance. While non-linear mechanistic models provide a good representation of the real process behavior, they should be adapted for control purposes with small time resolution. Hence, developed models should provide a satisfactory compromise between the accuracy in their operating range and complexity.

Hierarchical Control of MGs: To accommodate different time scales, MGs control is organized in a HCS (Bidram & Davoudi, 2012). The significant objectives of MG mission including voltage and frequency regulation, power sharing, synchronization, resilient and economic operation, feature different time scales in the range of milliseconds to several days (Vu et al., 2020). There exist several standards related to MGs operation and control including IEC 62898-1, IEC/TS 62898-2, IEC 62898-3-1, and IEEE standard 2030.7-2017 (IEEE, 2018). ANSI/ISA-95 or ISA-95 is an international standard for automation system design and implementation for enterprise-control system integration in all industries, which is general-enough to be applied in chemical processes. In a HCS based on ISA-95, the control tasks are distributed in several levels following a functional and temporal decomposition. The standard multi-level HCS based on ISA-95 and its adaptation to the control strategy of MGs is represented in Fig 3. 2 (Guerrero et al., 2011).
In this scheme, the control levels are different from each other concerning the functionality, the speed of response, and the operation period as well as communication requirements (Olivares et al., 2014). Besides, the complexity of the required models differs in different layers. In an HCS, different control levels are interacting with each other by adjusting reference trajectories and constraints boundaries. To preserve stability and robust performance of the system, time-frame management of the reference signals and control commands of one level to the lower levels is of vital importance. Hence, the bandwidth is decreased with the increase of the control levels.

Adaptation of HCS of MGs for controlling BLSSs: The parallelisms between BLSSs and isolated MGs show the great potential of benefiting from the highly developed HCS of the islanded MGs to cope with the complex control tasks of BLSSs. Accordingly, hierarchical control for operation management of MGs is planned to be adapted for controlling the BLSSs in this study. Organizing the control strategy in several layers is also consistent with the variety of the control tasks and the different time scales of CESs. The significance of adopting a generic system model approach containing several layers is represented in Farges et al., (2008) for different purposes of control, management, test and optimization.

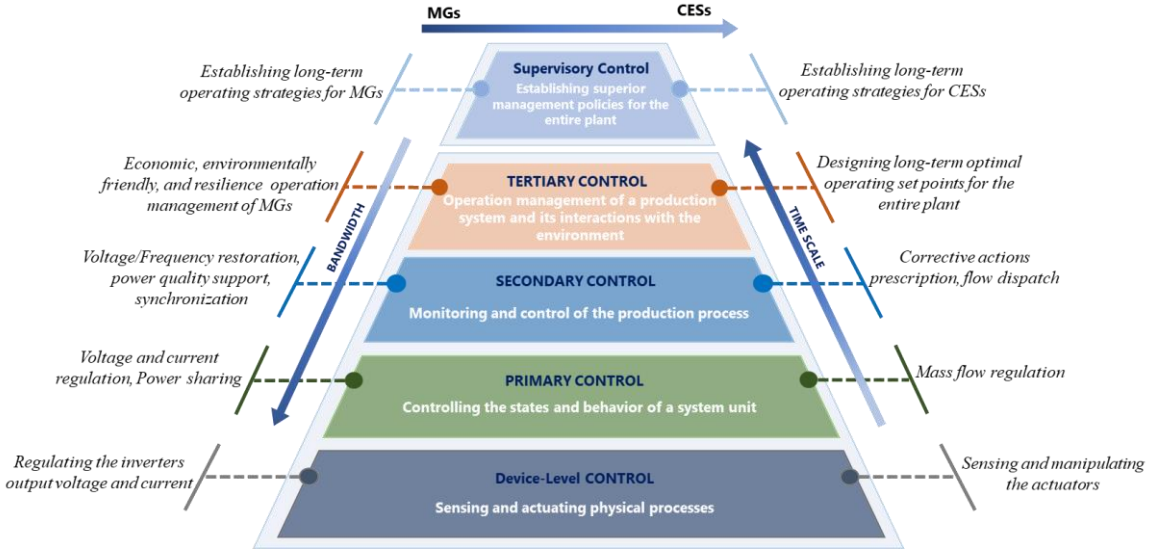

Fig 3. 2. Multi-level hierarchical control structure of MGs and CESs

Adopting the HCS of MGs, to deal with the complexity of the optimization and control of the entire loop of a BLSSs, the control process of the integrated system can be distributed in several levels as follows. The adaptation of the HCS of MGs to BLSSs is also outlined in Fig 3. 3, according to the following levels:

Level 0 (Device-level control): The controllers at this level are responsible for sensing and manipulating the actuators of the biochemical process to regulate the behavior of the associated compartment following control command signals.

Level 1 (Primary control): At this level, a local controller is responsible for devising appropriate control actions to follow the mass flow references received from the higher-level controllers. Besides, control agents at this level are responsible of sharing information about the dynamic compartment constraints so the higher-level controllers can have a global view of the whole process to optimally distribute resources (Vasquez et al., 2010). The strong coupling of variables and the interdependency of compartments may require the dynamically adjustment of the constraints.

Level 2 (Secondary control): To compensate for the set points deviations and to improve the tracking performance of the primary controllers, a secondary controller is required to provide local controllers with corrective actions. The corrective actions are obtained based on the feedback signals and the desired operating references and sent to the local controllers. To preserve stability of the system, the secondary controller is required to be faster than the tertiary control but slower than the primary controllers.

Level 3 (Tertiary control): The responsibility of this level is to guarantee long-term performance of the process and provide optimal operating set points based on the predicted evolution of the demand and supply of matter by different compartments while considering their dynamic operating constraints and technical limitations. In case matter exchange between different ecosystems is desired, the flow management can be also scheduled at this level.

Level 4 (Supervisory control): Supervisory controller is devoted to establish the operating strategies of the system following a set of main criteria such as ESA's ALISSE criteria (Brunet et al., 2010). Monitoring the state of health (SoH) of the system and projecting its states in the future using high-fidelity models and simulating the system in a faster than reality environment, the supervisory controller will be able to support reliable operation of the system through adjusting its operating strategies and predictive maintenance.

For accommodating the multiple time scale of the system, a temporal decomposition is also required at some levels (Bryds et al., 2008). As a result, the control levels might consist of several sublayers, which act on different time scales while handling the corresponding objective function and relevant constraints. The number of sublayers and associated prediction and control horizons, as well as the required sampling rate are determined based on the time scale properties of the system and the desired control tasks. Besides, the interactions between different layers and sublayers are required to be clearly defined to consider the functionality of a sublayer in determining reference trajectories or adjusting the constraints of other sublayer (Bryds et al., 2008). By applying the proposed HCS, different subsystems are integrated and the system operation can be controlled in a coordinated manner. Fig 3. 3 illustrates the proposed HCS for an exemplary pilot plant (MPP).

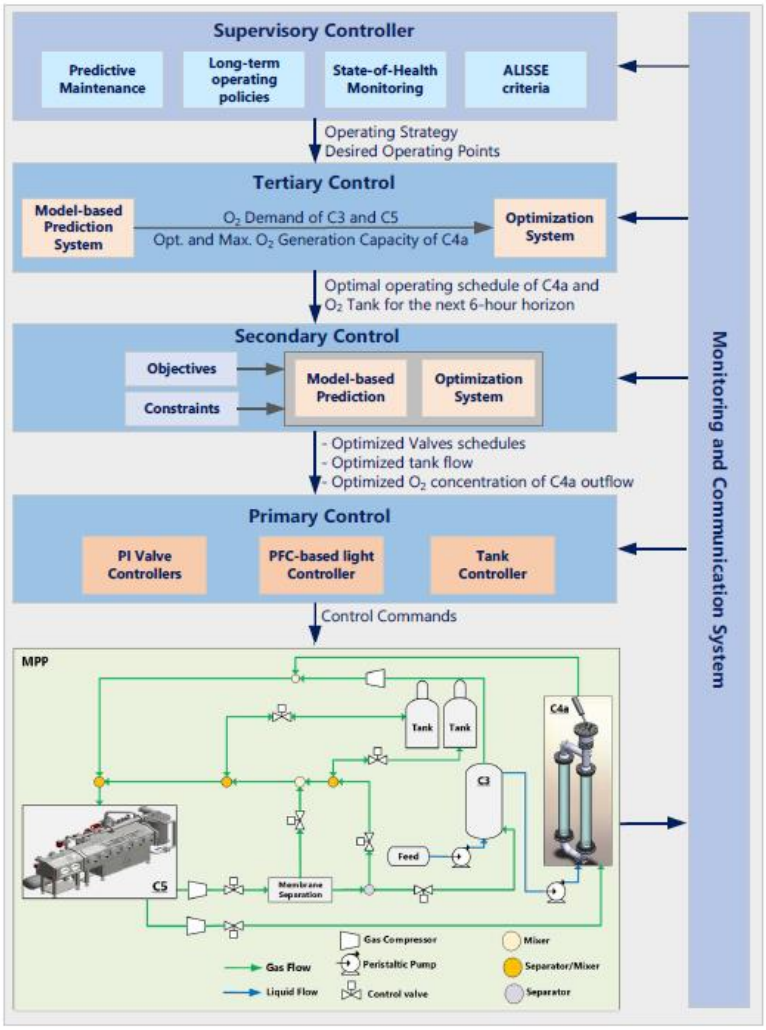

Fig 3. 3 Illustration of the proposed hierarchical control strategy for oxygen management applied to the MPP

Control Methodology: In the HCS for BLSSs, appropriate control methods are developed at each level considering the control requirements (such as control functionality or speed of controller response) and system characteristics among others. The capability of model predictive control (MPC) in considering system constraints and taking into account future predictions of the system behavior as well as its closed-loop control approximation makes it a good candidate for deriving the control strategy in the higher control levels, specifically tertiary and secondary levels. While at the lower levels, faster controllers such as PI, PID or predictive functional control (PFC) are highly preferred. PFC is a variant of MPC, which is characterized by its simple calculation algorithm and easy implementation. Using the two main characteristics of coincidence point (*h* steps later than the current step where the reference trajectory and the predicted process output will coincide) and basic control command functions distinguishes the PFC method from other predictive controllers. In the proposed control structure, MPC is used at tertiary and secondary levels while PFC is deployed for controlling the light intensity in compartment C4a

and the input gas flow in C3.

Prediction system and data exchange: To implement the HCS, the required information (state of the system, system parameters, prediction of disturbances, updated trajectories, constraints boundaries, etc.) at each control level and sub-level should be provided. Data gathering is conducted through reliable monitoring systems and relevant information is exchanged with the controllers through designated communication systems. Advanced estimation and prediction methods are required to find the latest values of the unmeasurable state variables and system dynamics evolution during the prediction horizon. The estimation and prediction methodologies should be fast-enough for online implementation. In this study, a model-based prediction system is deployed at the tertiary level using the high-fidelity models of the pilot plant and the data obtained through the monitoring system.

3.5. Simulation Analysis

In this Section, the performance of the proposed HCS will be evaluated using the MPP as a test case. The MPP was built in 2009 to integrate the individual compartments to have a complete operational loop in a testing facility with high quality standards. The demonstration scenario of the MPP is to achieve a closed liquid and gas loop fulfilling 100% of O_2 requirements and at least 20% of food requirements for 1 person. Fig 3. 5 illustrates four compartments of the MPP.

Fig 3. 4. MELiSSA Pilot Plant compartments following a left-right and top-down direction: Compartment CIII, Compartment C4a, Compartment C4b and Compartment C5.

Simulation analyses are based on a 25-day simulation period implemented in the MATLAB environment using the proposed HCS for the aggregation of three compartments and a gas storing system as shown in Fig 3. 3 and the nominal operating conditions used in the MPP (Alemany et al., 2019). The goal is to assess the long-term operation of the MPP using the proposed HCS with an O_2 reference of 21% in the crew compartment.

The prediction horizon of the MPC at the tertiary and secondary levels are set to 6 and 1 hours respectively, while the sampling time of the controller are equal to 1h, 6 min, and 36 sec for the controllers at tertiary, secondary, and primary levels, respectively. According to the simulation results represented in Fig 3. , the dynamics of the crew compartment correspond to a circadian rhythm of high O_2 consumption during the day and low O_2 consumption during the night (Fig 3. a). The secondary control is responsible for maintaining the O_2 concentration in the crew compartment within a specified boundary (19% - 24%) while following the references received from the tertiary controller regarding the storage tank charge/discharge rate and the O_2 supply rate of C4a. The scope of the tertiary control is to determine the optimal operating conditions for the plant taking into account the overall predicted O_2 consumption and production rates and certain operating criteria determined by the supervisory control. In the simulation presented, the supervisory control aims to keep the pressure of the storage gas tank around a reference level of 50% of the rated capacity and to use two nominal levels of light intensity in C4a operation, namely 225 W/m^2 and 84 W/m^2 for day and night shifts, respectively. In Fig 3. b-c it can be observed how the secondary control generates a conciliatory response between the references received from the tertiary level and the boundaries imposed on the O_2 concentration in the crew compartment. At primary control level, the light intensity in C4a fluctuates around the two nominal points for day and night shifts (Fig 3. d) and the O_2 tank pressure level remains close to the reference level (Fig 3. e).

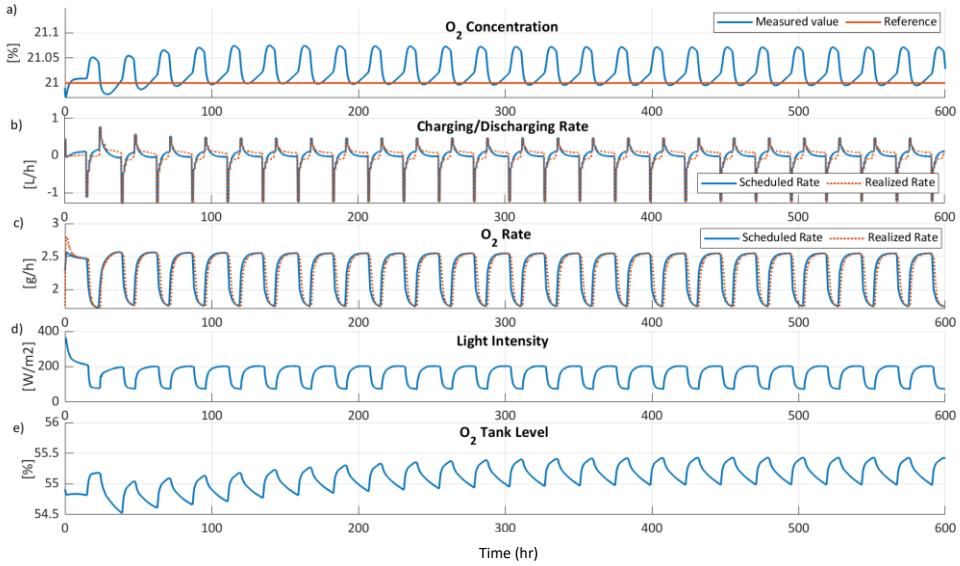

Fig 3. 5. (a) Concentration of O_2 in the crew compartment; (b) Scheduled storage charging(-)/discharging(+) rate of the storage tank by tertiary control and realized rate; (c) Scheduled O_2 supply assigned to C4a and realized rate; d) Light Intensity in C4a; (e) O_2 Tank pressure level.

3.6. Conclusions

Adapting the well-developed hierarchical control strategy of MGs to the control of BLSSs is a promising approach to deal with their complex control task. In this study, a hierarchical control strategy for BLSSs was introduced based on the multi-level control structure of MGs pointing out the similarities between both systems. The control structure can be extended for controlling other BLSSs, not only terrestrial LSSs, but also Mars or Lunar-based LSSs in the future. Besides, the hierarchical structure can be effectively scaled-up to include interconnection of several ecosystems. To design the HCS of BLSSs, digital twinning provides unique opportunities. Digital twinning is the virtual representation of a system to mirror the operating conditions of its corresponding twin in the real world. The digital twin (DT) allows the system designers and decision makers to assess the dynamic behavior of the system during the development stages, implementation, operation, and service phases for making well-informed decisions. DT is based on high-fidelity models of the physical system and is connected to the physical counterpart through bi-directional communication links. In this way, the real-time data obtained from the physical system will help improve the accuracy of the DT, while DT can support the optimal control and operation of the physical system through providing an advanced decision-support system and facilitating efficient in-house and remote monitoring. Considering the complexity involved in designing the control system of CESs, DT can provide an unprecedented, advanced platform to enhance the controller system performance during the CESs' life time.

Considering the recent advances in space exploration knowledge and technologies, and the increasing tendency towards long-term missions on Mars and Moon, developing efficient and reliable BLSSs is of vital importance. The design of efficient LSSs necessitates advanced control strategies with the capability of managing a highly complex process.

From a systemic point of view, BLSSs are autonomous systems integrating various generation, recycling, and consumption subsystems with the storage capability to locally solve potential matter and energy unbalance problems. From this perspective, BLSSs share striking similarities with isolated MGs developed for solving energy balance problems in an autonomous and independent manner. In this regard, a hierarchical control strategy for BLSSs was proposed based on the multi-level control structure of the MGs. Supervisory controller at the top of hierarchy decides about the operating policy of the plant through a human-machine interface. Strategical decisions related to operating priorities, predictive maintenance, SoH monitoring, and standard BLSSs criteria are performed at this level. Tertiary, secondary, and primary controllers at lower levels determine the optimal operating points of the system considering

specific requirements and operating goals at different time scales. Simulation results of applying the proposed method to MPP approved the effectiveness of the proposed control structure in achieving a desired performance while meeting the system's technical and operational requirements. Future works are related to enhance the controllers' performance in front of difference scenarios including the aggregation of other MELiSSA compartments in the loop. In the following chapters, the mathematical development of the HCS presented is described and different scenarios evaluated.

4. IMPLEMENTING A HIERARCHICAL CONTROL STRUCTURE TO INTEGRATE A NITRIFICATION REACTOR, A PHOTOSYNTHETIC BIOREACTOR AND A CREW COMPARTMENT

Based on a paper published in the journal *Computers and Chemical Engineering*

Nomenclature

Indexes

d	Phase: gas (g) or liquid (l)
x	Strain (i.e. *L. indica*, *N. winogradskyi, N. europaea*)
y	Compound index (i.e. O_2, CO_2)
z	Compartment index (C3, C4a, C5, membrane separation, concentrated gas tank, diluted gas tank)
n	C3 volume section nϵ{1..5}
i, j, m	Current sampling point at different control levels (3,2,1)
nom	Nominal point
ref	Reference
p	Sensor measurement. Ex. $C_y^z\|_d^p$ represents the measured value of $C_y^z\|_d$

Concentrated Gas Tank Parameters

$SOC^{CT,ref}$	Normalized reference level of the concentrated gas tank (0.5)
$SOC^{CT,max}$/ $SOC^{CT,min}$	Normalized max/min level of the concentrated gas tank (0.1/1)
SOC^{CT}	Normalized level of the concentrated gas tank
$P^{CT,max}$	Total maximum pressure of concentrated gas tank (50) [bar]
P^{CT}	Total pressure of concentrated gas tank [Pa]
$G^{CT/DT}$	Concentrated/Diluted gas tank discharging(+)/charging(-) rate [L h^{-1}]
$G^{CT,max}$/ $G^{CT,min}$	Maximum concentrated gas tank discharging/charging rate (15/-15) [L h^{-1}]
V^{CT}	Volume of the concentrated gas tank (10) [L]
N	Rate of moles [mole h^{-1}]
T	Temperature (298) [K]
R	Gas constant (8.314) [J K^{-1} $mole^{-1}$]

Internal Model Parameters

f_y	Dilution factor in the membrane separation for O_2, CO_2, and N_2 compounds

All Compartments

$\phi_y^z\|^l$	Rate of reaction of compound *y* in compartment *z* (subsection Iϵ{B_n} for C3) [g L^{-1} h^{-1}]
ϕ_x^z	Growth rate of strain *x* in compartment *z* [g L^{-1} h^{-1}]
$F_{in/out,I}^z$	Input/output liquid volumetric flow in compartment z. Subindex Iϵ{A, Bn, C, in, out, r} provides information about the flow localization within C3 reactor [L h^{-1}]
$G_{in/out,I}^z$	Input/output gas volumetric flow in compartment z. Subindex Iϵ{A, Bn, C, in, out, r} provides information about the flow localization within C3 reactor [L h^{-1}]

$M_y^z\|_d^{in/out}$	Input/Output mass flow of compound *y* in phase *d* in compartment *z* [g L^{-1} h^{-1}]. Extra superindex *in/out* can be included if referring to input/output mass flow.
Q_y^z	Production rate of compound *y* in compartment *z* [g h^{-1}]
$Q_y^{z,max/min}$	Max/min production rate of compound *y* in compartment *z* [g h^{-1}]
$C_y^z\|_d$	Concentration of compound *y* in phase *d* in compartment *z* [g L^{-1}]
$C_y^z\|_d^I$	Concentration of compound *y* in phase *d* in inflow/outflow of compartment *z*. *x* is used instead of *y* to refer to biomass. Superindex Iє{A, Bn, C, in, out, r} provides information about the localization within C3 reactor [g L^{-1}]
μ_x^z	Specific growth rate of strain x [h^{-1}] in compartment *z*
$\mu_x^{z,max}$	Maximum value of μ_x^z (0.059 for *N. europaea*, 0.024 for *N. winogradskyi*) [h^{-1}]
$K_{x,g/m}^y$	Saturation constant of compound *y* for strain *x*. Subindex *g/m* refers to growth/maintenance (0.0022 for *N. europaea* and NH_3, 0.000162 for *N. europaea* and O_2; 10^{-5} for *N. winogradksyi* and NH_3, 10^{-3} for *N. winogradskyi* and HNO_2 and $5.44 \cdot 10^{-4}$ for *N. winogradskyi* and O_2) [g L^{-1}]
d_x	Death rate of strain *x* (0.007 for *N. europaea* and 0.002 for *N. winogradksyi*) [h^{-1}]
m_x	Maintenance rate of strain *x* (0.3 for *N. europaea* and 3.51 for *N. winogradskyi*) [h^{-1}]
φ_y^z	Gas-Liquid transfer rate of compound *y* in compartment *z* [g L^{-1} h^{-1}]
$K_L a^z$	Gas-liquid transfer coefficient (reactor design parameter) in compartment z [h^{-1}]
q_y	Partition coefficient of compound *y*
$C_y^z\|_l^*$	Saturation concentration of compound y in z (*l* indicates liquid phase) [g L^{-1}]
$Y_{\frac{y}{x},g/m}$	Yield of compound y over *x*. A subindex *g/m* can be included referring to growth/maintenance
Ψ_y^z	Limiting factor associated to substrate y at compartment z
V_l^z	Volume of compartment z. Sub-index *l* ∈A, B_n, C, D_n provides information about the localization within C3 or C4a reactor (7.6 for C3 and 84 L for C4a) [L].

Compartment C3 Parameters

ε	Bead void volume (0.355)
ε_L	Liquid fraction of bed (0.92)
ε_G	Gas fraction of bed (0.08)
$V_{A/Bn/C}$	Volume of fraction (2.14, 1.6 and 3.03 for A, Bn, C) [L]
f	Liquid fraction of flow back-mixed (0.3)
f'	Gas fraction of flow back-mixed (0.3)
F_r^{C3}	Recirculation liquid flow (75) [mL/min]
G_r^{C3}	Recirculation gas flow (3) [L/min]

Compartment C4a Parameters

R_d	Radius of the bioreactor (0.076) [m]
I_{C4a}	Light intensity [W m^{-2}]
$I_{C4a}\|_{day}^{nom}$	Day nominal light intensity (225/84) [W m^{-2}]
$I_{C4a}^{min/max}$	Minimum and maximum light intensity (10/364) [W m^{-2}]
K_j	Saturation constant for light (20) [W m^{-2}]
α, δ	Radiative properties accounting for the absorption and scattering cross section of the cells and the fraction of radiant backscattered energy (0.90 for α and 0.9·$C_x^{C4a}\|_l$, being x the concentration of *L. indica*).
$V_{l/g}^{C4a}$	Gas (0.84 L) and liquid (83.1 L) volumes of C4a [L]

Compartment C5 parameters

$resp_y^{C5}$	Respiration rate of compound y in C5 (0.66 and 0.42 for oxygen in active/inactive photoperiods; 0.94 and 0.53 for carbon dioxide active/inactive photoperiods) [mole h^{-1}]

Controller parameters

ΔQ_{O2}^{C4a}	Span of the C4a production rate [g h^{-1}]
$\Delta C_{O_2}\|_g^z$	Span of O_2 concentration in gas phase in compartment z [%]
ΔG_{CT}	Span of the gas flow from CT [L min^{-1}]
ρ	Dispatch factor $G_{in}^{C4a}/G_{out}^{C5}$
ρ^{max}/ρ^{min}	Max/min dispatch factor
λ_i	The i^{th} weighting factor
$D_{O_2}^z$	O_2 consumption rate of compartment z [g h^{-1}]
N_{Pi}/N_{Ci}	Prediction/Control horizon at the i^{th} control level
$T_{m,PFCi}$	First order process time constant, i^{th} control level PFC [h^{-1}]
$K_{m,PFCi}$	First order process gain, i^{th} control level PFC
$T_{s,i}$	Sampling time at the i^{th} control level [h]
$CLRT_{PFCi}$	Closed loop response time at the i^{th} control level PFC
MV	Manipulating Variable

Acronyms

CELSSs	Controlled ecological LSSs
HCS	Hierarchical control structure
HPC	Higher Plants Chamber
ISS	International Space Station
LSS	Life support systems
MELiSSA	Micro-Ecological Life Support System Alternative
MG	Microgrid
MPC	Model Predictive Control

MS	Membrane separation
PFC	Predictive functional controller
VR-MPC	Varying-resolution MPC
PQ	Photosynthetic quotient

4.1. Introduction

In this chapter, the mathematical development of the different control layers introduced in the previous chapter (Chapter 3) are presented. The proposed hierarchical control structure (HCS) is implemented and tested on an exemplary case study based on the latest integration phase of the MELiSSA Pilot Plant, comprising C3, C4a, and C5 along with two gas buffer tanks, added in this study but not present in the MELiSSA Pilot Plant. C3 and C4a are connected through the liquid phase while C3, C4a, C5, and the gas storing tanks are connected through the gas phase. Mathematical models for the individual compartments and for the gas and liquid interfaces are briefly reproduced and used in simulations.

4.2. Modelling the Compartments

As can be seen in Fig 4. 1, starting from C5, the gas outflow of this compartment (G_{out}^{C5}), containing gas compounds with specific concentrations is split into two flows going to C4a (G_{in}^{C4a}) and the membrane separation unit (G_{in}^{MS}) whose output is a concentrated (G^{C}) and a diluted (G^{D}) O_2 flow. A specific fraction of the concentrated gas flow is the input of C3 (G_{in}^{C3}) that is determined based on the amount of ammonia to be oxidized in the liquid inflow being fed to C3 (F_{in}^{C3}). The other fraction ($\mathrm{G}^{C} - G_{in}^{C3}$) is sent back to C5 and can be used to fill the concentrated gas tank if needed. The gas outflow of C3 (G_{out}^{C3}) and C4a (G_{out}^{C4a}) are sent back to C5 together with the gas flows coming from the membrane separation closing the gas loop as shown in the following equations.

$$G_{in}^{C5} = G_{out}^{C4a} + G_{out}^{C3} + \mathrm{G}^{rich} + \mathrm{G}^{D} + \mathrm{G}^{DT} \quad (1)$$

$$\mathrm{G}^{rich} = \left(\mathrm{G}^{C} - G_{in}^{C3}\right) + \mathrm{G}^{CT} \quad (2)$$

The gas buffer tanks are appropriately sized to satisfy the O_2 demand of one human for 24 hours with a maximum pressure of 50 bar and 10L of volume. Considering that the MELiSSA Pilot Plant has not yet integrated the higher plant chamber (C4b), which represents the main producer of O_2, only 3 rats (out of the maximum capacity of C5 of 40 rats, approximately equivalent to one human in terms of physiological needs) are inhabiting C5, which have an O_2 consumption rate that can be supplied solely by C4a. Currently, the liquid phase loop is still not closed, but its closure is expected in the upcoming MELiSSA Pilot Plant activities.

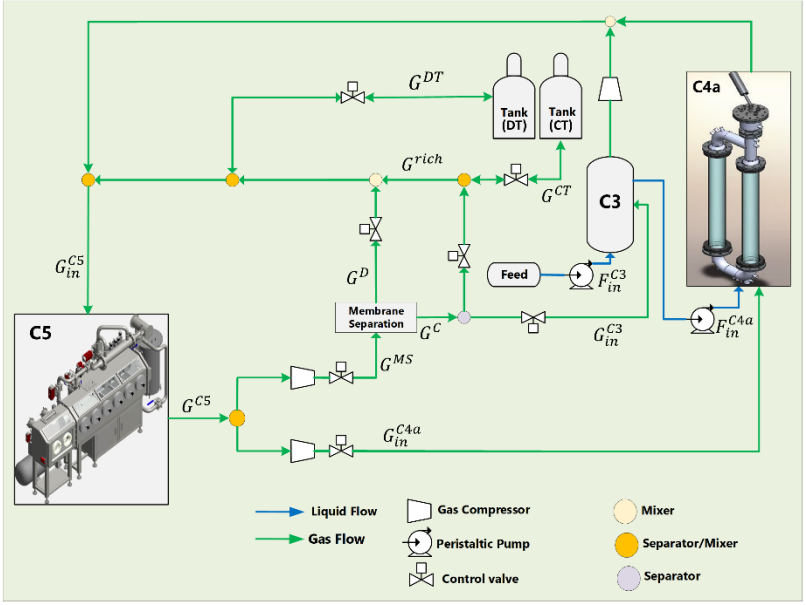

Fig 4. 1. The layout of the system under study

Non-linear mechanistic models are available for each of these compartments validated with massive experimental data obtained in the MELiSSA Pilot Plant testing campaigns. C3 model was validated and calibrated in a 120-day standalone experiment using step changes of ammonium loads (0.3-0.6 g N-NH4/L) and residence times (5 – 80 h) (Pérez et al., 2005a), while C4a and C5 models were evaluated in two 50 and 30-day integration tests by applying step changes to O_2 setpoints (19-22%) of the crew compartment (Alemany et al., 2019). Interested readers are referred to Cornet et al., (1995), Cruvellier et al., (2017), Dauchet et al., (2016a) and Poughon et al., (1999) for more information.

The process described in Fig 4. 1 operates in a continuous mode for both the liquid and gas phases. Thus, the law of conservation of mass needs to be satisfied in each of the biological compartments C3, C4a, and C5. A bioreactor working in continuous mode with a biochemical transformation of compound *y* can be defined with the following general form:

$$\dot{C}_y^z|_d = M_y^z|_d^{in} - M_y^z|_d^{out} + \phi_y^z + \varphi_y^z \tag{3}$$

$$\phi_x^z = \mu_x^z \cdot C_x^z|_l \tag{4}$$

$$\mu_x^z = \mu_x^{z,max} \cdot \Psi_y^z - d_x \tag{5}$$

$$\Psi_y^z = \frac{C_y^z|_l}{C_y^z|_l + K_{x,g}^y} \tag{6}$$

$$\phi_y^z = \phi_x^z \cdot Y_{\frac{y}{x}} \tag{7}$$

Notice in (4)-(7), rate of reaction (ϕ_y^z) only affects the liquid phase, being the rate of reaction

zero in the gas phase. According to (3), the changes in the concentration of the y^{th} compound ($\dot{C}_y^z|_d$) in compartment z in phase d (gas/liquid) is specified by the mass inflow ($M_y^z|_d^{in}$) and outflow ($M_y^z|_d^{out}$), the rate of reaction (ϕ_y^z) and the phase exchange rate (φ_y^z) in the associated compartment. In case of multiple substrates, (6) is modified to include the product of all participating substrates and Ψ_Π^z is defined for N_y compounds as follows:

$$\Psi_\Pi^z = \prod_{y=1}^{N_y} \frac{C_y^z|_l}{C_y^z|_l + K_{x,g}^y} \tag{8}$$

To obtain the production and consumption rates including maintenance costs, expression (7) becomes:

$$\phi_y^z = \left(\frac{\mu_x^{z,max} \cdot C_y^z|_l}{C_y^z|_l + K_{x,g}^y} \cdot Y_{\frac{y}{x},g} + \frac{m_x \cdot C_y^z|_l}{C_y^z|_l + K_{x,m}^y} \cdot Y_{\frac{y}{x},m} \right) \cdot C_x^z|_l \tag{9}$$

The gas-liquid transfer rate defined by φ_y^z takes the following form:

$$\varphi_y^z = K_L a^z \cdot \left(C_y^z|_l{}^* - C_y^z|_l \right) \tag{10}$$

$$C_y^z|_l{}^* = \frac{C_y^z|_l}{q_y} \tag{11}$$

Notice that considering the continuous mode of operation of the compartments and assuming that the biochemical transformation that takes place does not imply density changes in either of the liquid or gas phases, the volumetric input and output flow is maintained, i.e. $G_{in}^z = G_{out}^z$ and $F_{in}^z = F_{out}^z$.

4.2.1. C3 Compartment Model

The design of C3 is based on a packed-bed reactor with immobilized cells that carry the oxidation of ammonia to nitrate by ammonia-oxidizing *Nitrosomonas europaea* and nitrite-oxidizing *Nitrobacter winogradskyi*. To capture properly the C3 dynamics, the total module is discretized in seven volumes as shown in Fig 4. 2. In this figure, V_A and V_C are the volumes at the top and bottom of the reactor, which are used for probe location, gas, and liquid inlet, recirculation and outlet flows, but where no reaction takes place. V_B includes the packed-bed part of the bioreactor where cells are immobilized, and the reaction takes place. V_B is discretized in five parts to cope with the hydrodynamics and to account for non-ideal liquid mixing for implementing the reaction kinetics.

a)

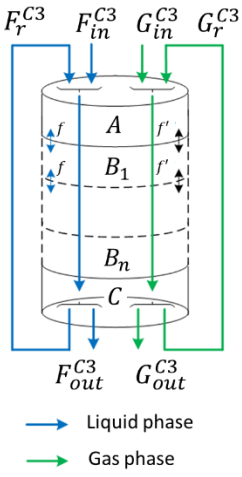

b)

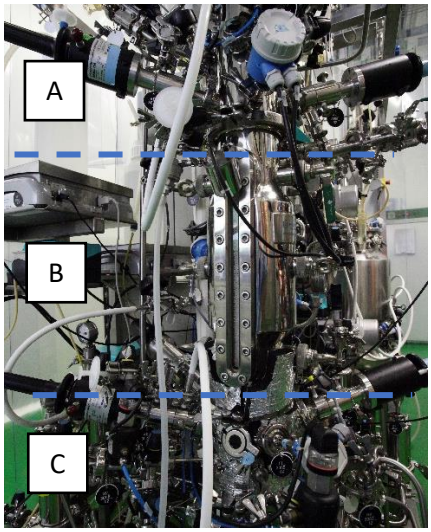

Fig 4. 2. Continuous mode of operation of C3. a) Scheme of the model. b) C3 in the MPP.

The dynamical evolutions of parts A, B, and C of the compartment in both liquid and gas phases are derived by the following general equations where $F_{int}^{C3}/G_{int}^{C3}$ is the sum of liquid/gas inflow to C3 (F_{in}^{C3}/G_{in}^{C3}) and recirculation liquid/gas flux (F_r^{C3}/G_r^{C3}) (Pérez et al., 2005b; Poughon et al., 1999):

Part A

$$V_A \cdot (1-\varepsilon_G) \cdot \dot{C}_y^{C3}|_l^A = F_{in}^{C3} \cdot C_y^{C3}|_l^{in} + F_r^{C3} \cdot C_y^{C3}|_l^r \quad (12)$$

$$-F_{int}^{C3} \cdot \left((f+1) \cdot C_y^{C3}|_l^A - f \cdot C_y^{C3}|_l^{B1}\right)$$

$$+V_A \cdot (1-\varepsilon_G) \cdot \varphi_y^{C3}$$

$$V_A \cdot (1-\varepsilon_L) \cdot \dot{C}_y^{C3}|_g^A = G_{in}^{C3} \cdot C_y^{C3}|_g^{in} + G_r^{C3} \cdot C_y^{C3}|_g^r \quad (13)$$

$$-G_{int}^{C3} \cdot \left((f'+1) \cdot C_y^{C3}|_g^A - f' \cdot C_y^{C3}|_g^{B1}\right)$$

$$-V_A \cdot (1-\varepsilon_L) \cdot \varphi_y^{C3}$$

Part B

$$V_{Bn} \cdot \varepsilon \cdot (1-\varepsilon_G) \cdot \dot{C}_y^{C3}|_l^{Bn} \quad (14)$$
$$= F_{int}^{C3} \cdot \left((f+1) \cdot C_y^{C3}|_l^{Bn-1} + f \cdot C_y^{C3}|_l^{Bn+1} - ((f+1) \cdot C_y^{C3}|_l^{Bn} + f \cdot C_y^{C3}|_l^{Bn})\right)$$

$$+V_{Bn} \cdot \varepsilon \cdot (1-\varepsilon_G) \cdot (\phi_y^{C3}|^{Bn} + \varphi_y^{C3})$$

$$V_{Bn} \cdot \varepsilon \cdot (1-\varepsilon_L) \cdot \dot{C}_y^{C3}|_g^{Bn} \quad (15)$$
$$= G_{int}^{C3} \cdot \left((f'+1) \cdot C_y^{C3}|_g^{Bn-1} + f' \cdot C_y^{C3}|_g^{Bn+1} - ((f'+1) \cdot C_y^{C3}|_g^{Bn} + f' \cdot C_y^{C3}|_g^{Bn})\right)$$

$$-V_{Bn} \cdot \varepsilon \cdot (1 - \varepsilon_L) \cdot \varphi_y^{C3}$$

Part C

$$V_C \cdot (1 - \varepsilon_G) \cdot \dot{C}_y^{C3}|_l^C = F_{int}^{C3} \cdot \left((f + 1) \cdot C_y^{C3}|_l^{B_5} - f \cdot C_y^{C3}|_l^C\right) - F_r^{C3} \cdot C_y^{C3}|_l^C - F_{out}^{C3} \cdot C_y^{C3}|_l^C \quad (16)$$

$$+V_C \cdot (1 - \varepsilon_G) \cdot \varphi_y^{C3}$$

$$V_C \cdot (1 - \varepsilon_L) \cdot \dot{C}_y^{C3}|_g^C = G_{int}^{C3} \cdot \left((f' + 1) \cdot C_y^{C3}|_g^{B_5} - f' \cdot C_y^{C3}|_g^C\right) - F_r^{C3} \cdot C_y^{C3}|_g^C - G_{out}^{C3} \cdot C_y^{C3}|_g^C \quad (17)$$

$$-V_C \cdot (1 - \varepsilon_L) \cdot \varphi_y^{C3}$$

4.2.2. C4a Compartment Model

The hydrodynamic pattern of C4a is approximated to a perfectly mixed photobioreactor, which is responsible for the conversion of CO_2 from C5 and nitrate from C3 into O_2 and biomass for human consumption while the reaction is controlled by light when no substrate is limiting. The reaction is carried by the cyanobacteria *Limnospira indica*. The general mass balance equation for this bioreactor is given in (3). The growth rate term in C4a is slightly different from (4) as light energy transfer is considered a rate-limiting process (Cornet, J F; Dussap, C G; Dubertret, 1992). The following equation is used to calculate the growth rate of *L. indica* and consumption or production rates of compound *y*:

$$\phi_x^{C4a} = \mu_x^{C4a,max} \cdot \Psi_\Pi^{C4a} \cdot \frac{1}{\pi \cdot R^2} \int_{r=Ril}^{r=R_d} 2\pi r \frac{4\pi J_r}{K_j + 4\pi J_r} dr \quad (18)$$

$$\phi_y^{C4a} = \phi_x^{C4a} \cdot Y_{\frac{y}{x},g} \quad (19)$$

J_r represents the profile of the light radiant energy, and it is expressed as a quotient of the modified Bessel functions of the first kind as follows:

$$4\pi J_r = \frac{2 \cdot I_{C4a} \cdot I_0(\delta \cdot R)}{I_0(\delta \cdot R) + \alpha \cdot I_1(\delta \cdot R)} \quad (20)$$

In (18), *Ril* is the illuminated radius defined as the photobioreactor radius where light reaches the compensation point (20 W m^{-2}). The illuminated radius can be found from (20), when the mean light radiant energy (J_r) becomes zero, which is the radius in the bioreactor where light cannot penetrate. Light is stopped due to biomass accumulation, which is integrated in the definition of δ (see nomenclature):

$$\frac{2 \cdot I_o(\delta \cdot R_{ill})}{I_o(\delta \cdot E) + \alpha \cdot I_1(\delta \cdot E)} - \frac{ComPoint}{I_{C4a}} = 0 \quad (21)$$

In (20), α and δ characterize the radiative properties of *L. indica*. The term Ψ_Π^{C4a} introduced in (8) considers the use of H_2NO_3, H_3PO_4, and CO_2 as substrates (Alemany et al., 2019).

The dynamic equations for the photobioreactor C4a are the following:

$$\frac{dC_{tic}|_l^{C4a}}{dt} = \frac{F_{in}^{C4a}}{V_l^{C4a}} \cdot \left(C_{tic}^{in}|_l^{C4a} - C_{tic}^{out}|_l^{C4a}\right) + \varphi_{CO2}^{C4a} + \phi_{tic}^{C4a} \quad (22)$$

$$\frac{dC_{co2}|_l^{C4a}}{dt} = \frac{F_{in}^{C4a}}{V_l^{C4a}} \cdot \left(C_{tic}^{in}|_l^{C4a} - C_{CO_2}^{out}|_l^{C4a}\right) + \varphi_{CO_2}^{C4a} + \phi_{CO_2}^{C4a} - R_{K1} \quad (23)$$

$$\frac{dC_{HCO_3}|_l^{C4a}}{dt} = \frac{F_{in}^{C4a}}{V_l^{C4a}} \cdot \left(C_{HCO_3}^{in}|_l^{C4a} - C_{HCO_3}^{out}|_l^{C4a}\right) + R_{K1} - R_{K2} + \phi_{HCO_3}^{C4a} \quad (24)$$

$$\frac{dC_{CO_3^{2-}}|_l^{C4a}}{dt} = \frac{F_{in}^{C4a}}{V_l^{C4a}} \cdot \left(C_{CO_3^{2-}}^{in}|_l^{C4a} - C_{CO_3^{2-}}^{out}|_l^{C4a}\right) + R_{K2} \quad (25)$$

$$\frac{dC_{O_2}|_l^{C4a}}{dt} = \frac{F_{in}^{C4a}}{V_l^{C4a}} \cdot \left(C_{O_2}^{in}|_l^{C4a} - C_{O_2}^{out}|_l^{C4a}\right) + \varphi_{O2}^{C4a} + \phi_{O2}^{C4a} \quad (26)$$

$$\frac{dX|_l^{C4a}}{dt} = \frac{F_{in}^{C4a}}{V_l^{C4a}} \cdot \left(-C_X^{out}|_l^{C4a}\right) + \phi_X^{C4a} \quad (27)$$

$$\frac{dHNO_3|_l^{C4a}}{dt} = \frac{F_{in}^{C4a}}{V_l^{C4a}} \cdot \left(C_{HNO_3}^{in}|_l^{C4a} - C_{HNO_3}^{out}|_l^{C4a}\right) + \phi_{HNO_3}^{C4a} \quad (28)$$

$$\frac{dNH_3|_l^{C4a}}{dt} = \frac{F_{in}^{C4a}}{V_l^{C4a}} \cdot \left(C_{NH_3}^{in}|_l^{C4a} - C_{NH_3}^{out}|_l^{C4a}\right) + \phi_{NH_3}^{C4a} \quad (29)$$

$$\frac{dO_2|_g^{C4a}}{dt} = \left(\frac{G_{in}^{C4a}}{V_l^{C4a}} \cdot \left(\frac{C_{O_2}^{in}|_g^{C4a}}{100 - C_{O_2}^{in}|_g^{C4a} - C_{CO_2}^{in}|_g^{C4a}} - \frac{C_{O_2}^{out}|_g^{C4a}}{100 - C_{O_2}^{out}|_g^{C4a} - C_{CO_2}^{out}|_g^{C4a}}\right) - \varphi_{O2}^{C4a} \cdot V_l^{C4a}/MW(O_2)\right)\frac{24}{V_G^{C4a}} \quad (30)$$

$$\frac{dCO_2|_g^{C4a}}{dt} = \left(\frac{G_{in}^{C4a}}{V_{C4a}} \cdot \left(\frac{C_{CO_2}^{in}|_g^{C4a}}{100 - C_{O_2}^{in}|_g^{C4a} - C_{CO_2}^{in}|_g^{C4a}} - \frac{C_{CO_2}^{out}|_g^{C4a}}{100 - C_{O_2}^{out}|_g^{C4a} - C_{CO_2}^{out}|_g^{C4a}}\right) - \varphi_{CO2}^{C4a} \cdot V_l^{C4a}/MW(OC_2)\right)\frac{24}{V_G^{C4a}} \quad (31)$$

4.2.3. C5 Compartment Model

The dynamic model of compartment C5 takes into account the respiration dynamics of the crew ($resp_y^{C5}$), which, as mentioned above, is simulated by a group of three rats. It should be mentioned that no liquid phase in C5 is considered in the simulation presented in this study. The general equation for the respiration dynamics in C5 is represented below.

$$\dot{C}_y^{C5}|_g = G_{in}^{C5} \cdot C_y^{C5}|_g^{in} - G_{out}^{C5} \cdot C_y^{C5}|_g + resp_y^{C5} \quad (32)$$

In (32), $resp_y^{C5}$ is assumed to take two values for day and night shifts for O_2 and CO_2. In addition, G_{in}^{C5} is the inflow of C5 coming from other compartments as represented in (1), while G_{out}^{C5} is the compartment outflow that is split between C4a and the membrane separator as shown in Fig 4. 1 (Alemany et al., 2019).

4.2.4. Membrane Separation

In the membrane module, compounds are distributed in a concentrated (G^C) and a diluted (G^D) flow, being the latter higher than the first, with a concentration of $C_y^C|_g$ and $C_y^D|_g$ respectively:

$$C_y^D|_g = \frac{f_y \cdot G^{MS} \cdot C_y^{MS}|_g}{G^D} \tag{33}$$

$$G^D = \sum_{y \in \{O_2, CO_2, N_2\}} f_y \cdot G^{MS} \cdot C_y^{MS}|_g \tag{34}$$

$$C_y^C|_g = \frac{G^{MS} \cdot (C_y^{MS}|_g - f_y \cdot G^{MS} \cdot C_y^{MS}|_g)}{G^C} \tag{35}$$

$$G^C = \sum_{y \in \{O_2, CO_2, N_2\}} G^{MS} \cdot C_y^{MS}|_g - (f_y \cdot G^{MS} \cdot C_y^{MS}|_g) \tag{36}$$

4.2.5. Storage Gas Tanks

The concentrated gas tank can be charged or discharged according to the O_2 needs of the overall system. The mission of the concentrated gas tank is to store concentrated O_2 to support C4a for supplying O_2 to the system. The ideal gas law is supposed to apply for the gas in the tank to calculate the rate of moles *(N)* introduced or removed during charging and discharging periods as shown below:

$$N = \frac{\mathrm{P}^{CT} \cdot \mathrm{G}^{CT}}{R \cdot T} \tag{37}$$

The normalized state of storage of the gas tank is calculated as follows:

$$SOC^{CT} = \frac{P^{CT}}{P^{CT,max}} \tag{38}$$

To maintain the mass flow in the loop, a diluted gas tank is included in the model as can be seen in Fig 4. 1, whose function is to release gas when the concentrated gas tank is filled and to be filled when the concentrated gas tank is emptied.

4.3. Method: HCS of the MELiSSA Pilot Plant

In this Section, the hierarchical control structure (HCS) presented in Chapter 3 is extended to CELSS. As explained in the previous chapter, the HCS includes three control levels, namely primary, secondary, and tertiary. In a CELSS, to accommodate different time scales of the various processes in the loop and considering the complexity of the integrated control problem, different control tasks including mass flow regulation, flow dispatch, and optimal resource utilization can be distributed in different control levels. Accordingly, the proposed control structure is organized into three levels. Since each level of control follows different operating goals and responds to different dynamics, different frequencies (clock signals in Fig 4. 3) are used for updating the control commands. While Level 3 aims at deriving long-term control commands for O_2 supply from C4a and the concentrated gas tank, the lower-level controllers are responsible for determining short-term detailed control signals ensuring gas balance, and

satisfying the system safety requirements. In Fig 4. 3, a general overview of the proposed control architecture is presented. A detailed description of each control level will be given in the following parts.

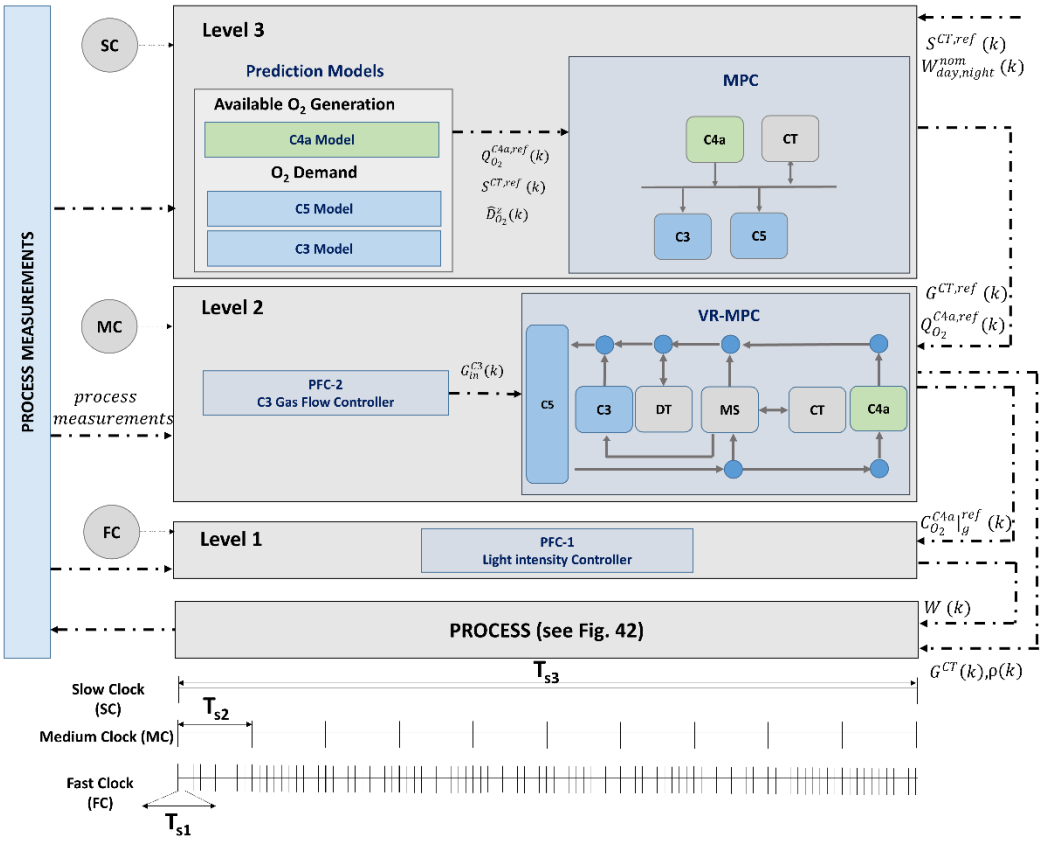

Fig 4. 3. The proposed hierarchical control structure

The main challenge is to design a control architecture that can manage the integrated operation of multiple producers and consumers of O_2. The most important priority of the process under study is to maintain the O_2 level in the crew compartment at a target level of around 21% at one bar of total pressure without violating the critical boundaries for CO_2. The definition of the upper boundary for carbon dioxide concentration in the crew compartment has been based on the maximum CO_2 concentration of 3% achieved in the MELiSSA Pilot Plant. This is acceptable for a test-bed hosting rats, as mock-up crew, whose environment control is ruled by the directive 2010/63/EU which suggests minimizing toxic pollutants (European Comission, 2010). For future human-based habitats, the environment control will be subject to the concentration range of 0.3-0.7% CO_2 defined by the NASA standard [V2-6004], which has become more restricted through the years according to the evidence from operational and research data. This can be more easily achieved through the inclusion of a higher plants compartment, which have a notably lower photosynthetic quotient (PQ) for most of the crops under consideration for Life

Support Systems compared to the PQ of *L. indica* used in C4a, driving the reduction of the overall carbon concentration in the system. This is included in the next MELiSSA Pilot Plant integration steps and discussed in Chapter 6. Regarding oxygen control, NASA standard [V2-6003] requires a mild hypoxia limit of 16% (NASA, 2019) with the reference established at 21%.

To achieve these requirements, besides tuning and properly scaling the process design, appropriate control methods are necessary at each control level considering the control performance such as control functionality or controller response time, among others. In this regard, model predictive control (MPC) is adopted at Levels 2 and 3 of the proposed structure taking into account its capability to consider for the future predicted behavior of the system, system constraints, its capacity to deal with non-linear multiple-input multiple-output processes (Michael A. Henson, 1998) and to express the desired performance specifications through adjusting control objectives (Ocampo-Martinez et al., 2012). Predictive functional control (PFC) is also used at Levels 1 and 2 because of its simplicity, low computational time requirement, and ease of implementation (Richalet, 1993).

PFC is a simplified variant of MPC that is characterized by replacing the control and prediction horizon of MPC with a coincidence point. When only one coincidence point is used, instead of minimizing the difference between the predicted output of the system and the desired trajectory over the desired horizon, the goal is to match the model output and the target trajectory at the coincidence point by solving a simple algebraic equation. In this study, PFC is applied to a simplified first-order approximation of subsystems assuming one coincidence point. Considering a first-order difference equation for a given compound $C_y^z|_d$ and a manipulated variable (MV):

$$C_y^z|_d(k+1) = \alpha_{m,PFC} \cdot C_y^z|_d(k) + K_{m,PFC} \cdot \beta_{m,PFC} \cdot MV(k) \tag{39}$$

$$\alpha_{m,PFC} = e^{-Ts/T_{m,PFC}} \tag{40}$$

$$\beta_{m,PFC} = 1 - \alpha_{m,PFC} \tag{41}$$

The reference trajectory ($C_y^z|_d^{ref}$) is considered to be of the first-order type whose starting point is equal to the value of the measured process output ($C_y^z|_d^p$) at the current time step. Assuming the coincidence point equal to one, the predicted value of the process output one step later than the present can be calculated as follows:

$$\Delta\hat{C}_y^z|_d(k+1) = \left[C_y^z|_d^{ref}(k) - C_y^z|_d^p(k)\right] \cdot \left[1 - e^{\left(\frac{-3 \cdot Ts}{CLRT_{PFC}}\right)}\right] \tag{42}$$

The parameter CLRT can be used to adjust the speed of response. After some algebraic operations using (39)-(42), it is straightforward to obtain the following control law:

$$MV(k) = \frac{\left[C_y^z|_d^{ref}(k) - C_y^z|_d^p(k)\right] \cdot lh_{PFC} + \beta_{m,PFC} \cdot \hat{C}_y^z|_d(k)}{K_{m,PFC} \cdot \beta_{m,PFC}} \quad (43)$$

$$lh = 1 - \left(e^{-3 \cdot Ts/CLRT_{PFC}}\right) \quad (44)$$

In the proposed control structure, PFC is used at Level 2 to adjust the input gas flow of C3 (G_{in}^{C3}) according to the amount of ammonium introduced in C3 that needs to be oxidized to nitrate. PFC is also used at Level 1 to adjust the light energy input in C4a. In the following, the control strategies at different control levels along with the associated control objectives and constraints are presented.

4.3.1. Level 3: Tertiary Controller

This is the system-level controller responsible for designing optimal long-term operating setpoints for the local controllers while optimizing the use of resources and satisfying different technical and operational constraints. To do so, a prediction is made based on the optimal operating criteria prescribed by the supervisory controller. These operating criteria include keeping the level of the concentrated gas tank around a reference level ($SOC^{CT,ref}$) of 50% over the total volume of 10 L and a maximum pressure of 50 bar and to operate C4a around two nominal light levels for day and night shifts (I_{C4a}). To draw the prediction, measurements are obtained from the monitoring system and used to initialize the internal model described. On the one hand, the upper bound of the O_2 production rate of C4a ($Q_{O2}^{C4a,max}$) is set by running the internal model using the maximum light intensity technically allowed while its reference production rate ($Q_{O2}^{C4a,ref}$) is determined using the nominal light intensity. On the other hand, O_2 consumption rates by C3 and C5 ($\hat{D}_{O_2}^{C3}$ and $\hat{D}_{O_2}^{C5}$ respectively) are predicted over the Level 3 prediction horizon. Hence, references regarding the predicted O_2 consumption and production rates are generated and used to solve the following optimization problem:

$$J_T = \min_U \lambda_1 J_1 + \lambda_2 J_2 \quad (45)$$

$$J_1 = \sum_{k=1}^{Np_1} \left(\widehat{SOC}^{CT}(i+k|i) - SOC^{CT,ref}\right)^2 \quad (46)$$

$$J_2 = \sum_{k=0}^{Nc_1-1} \left(\frac{Q_{O2}^{C4a}(i+k|i) - \hat{Q}_{O2}^{C4a,ref}(i+k|i)}{\Delta \hat{Q}_{O2}^{C4a}(k)}\right)^2 \quad (47)$$

$$U = \begin{bmatrix} Q_{O2}^{C4a}(i) \\ G^{CT}(i) \\ \vdots \\ Q_{O2}^{C4a}(i+Np_1-1) \\ G^{CT}(i+Np_1-1) \end{bmatrix} \quad (48)$$

$$U_3 = [Q_{O2}^{C4a}(i) \quad G^{CT}(i)] \tag{49}$$

Subject to:

(37)-(38)

$$\sum_{z\in\{C3,C5\}} \widehat{D}_{O_2}^{z}(i+k|i) = Q_{O_2}^{4a}(i+k|i) + \hat{Q}_{O_2}^{CT}(i+k|i) \tag{50}$$

$$G^{CT,min} \leq G^{CT}(i+k|i) \leq G^{CT,max} \tag{51}$$

$$Q_{O2}^{C4a,min}(i+k|i) \leq Q_{O_2}^{4a}(i+k|i) \leq \hat{Q}_{O2}^{C4a,max}(i+k|i) \tag{52}$$

$$SOC^{CT,min} \leq \widehat{SOC}^{CT}(i+k|i) \leq SOC^{CT,max} \tag{53}$$

In (50)-(53), k ∈ {0,...,Np_1-1}. $\hat{S}^{CT}(i+k|i)$, $\widehat{D}_{O_2}(i+k|i)$, $\hat{Q}_{O2}^{C4a,max}(i+k|i)$ and $\hat{Q}_{O_2}^{CT}(i+k|i)$ denote the predicted concentrated gas tank storage level, the total O_2 demand ($\widehat{D}_{O_2}^{C3} + \widehat{D}_{O_2}^{C5}$), the C4a maximum production rate and the concentrated gas tank production or consumption rate respectively at time step *i+k* using the internal model with the information available at time step *i*. The constraint represented in (50) indicates that the consumption rate expected for the compartments C3 and C5 must be satisfied with the production from C4a and the concentrated gas tank. The outputs of the tertiary controller stored in U_3 are considered as the reference for the secondary controller (see Fig 4. 3). In (46), $SOC^{CT,ref}$ represents the reference value for the state of the storage in the tank, which in this study is assumed to be fixed and time-invariant. In our future work, the operating criteria are expected to be dynamically adapted by the supervisory controller using a techno-economical and reliability analysis following the LSSs requirements such as the ALISSE criteria. Range parameters are included in the objective functions for normalization purposes due to the different magnitude of process variables.

4.3.2. Level 2: Secondary Controller

The main functionality of the secondary controller is to keep the gas concentration of the crew compartment within a safe boundary by manipulating the gas flows and the O_2 concentration in C4a. The output of this level of control is provided to local controllers as the reference trajectory for the following time intervals. The secondary controller needs to follow the outcome of the tertiary controller as it accounts for the optimal resource distribution and is based on the long-term prediction of the process. The sample time of this level is shorter than that of Level 3, in line with its scope to correct O_2 concentration deviations in C5. Two interrelated controllers work at the secondary level: (1) a PFC-based controller (PFC 2) that determines the flow of gas (G_{in}^{C3}) required to oxidize the nitrogen demands according to the ammonia concentration fed to C3 in the liquid phase (F_{in}^{C3}, see Fig 4.2), and (2) a non-linear varying-resolution MPC (VR-MPC) controller that generates the reference values for gas flows and the O_2 concentration in C4a to

be followed by the local controllers (see Fig 4. 3). To do so, the VR-MPC requires the information from PFC-2.

4.3.2.1. Predictive Functional Control

At the secondary level, a PFC-based control strategy is used to adjust the flow of enriched O_2 gas to convert ammonium into nitrate. The internal model used is based on a first-order approximation of O_2 concentration of C3 in the liquid phase ($C_y^{C3}|_l$) with the input gas flow (G_{in}^{C3}) as the manipulated variable. The first order process gain and time constant have been identified in Alemany et al., (2019) based on several experimental tests conducted in the pilot plant. Further details regarding the identification and validation of the first-order models for C3 and C4a controllers can be found in Alemany et al., (2019). It is worth mentioning that these parameters are assumed to be fixed in this study. However, as the system operating condition and the plant environment are exposed to changes over time, these parameters need to be re-tuned. Two different strategies can be followed for the re-tuning of the model parameters, a regular time-based re-tuning strategy or an event-based technique continuously monitoring a performance index to trigger the re-tuning process. In the former strategy, a fixed frequency is determined based on the historical data and experts' knowledge to re-tune the model parameters while in the latter, a performance index is defined for the model. Monitoring the performance index and comparing it with the desired threshold reflecting the permissible level of performance degradation, the time for triggering the re-tuning process is determined. Using the first-order model parameters given in Alemany et al., (2019) and (39)-(44), the following control law can be obtained:

$$G_{in}^{C3}(j) = \frac{\left[C_{O_2}^{C3}|_l^{ref}(j) - C_{O_2}^{C3}|_l^{p}(j)\right] \cdot lh_{PFC2} + \beta_{m,PFC2} \cdot \hat{C}_{O_2}^{C3}|_l(j)}{K_{m,PFC2} \cdot \beta_{m,PFC2}} \tag{54}$$

$$G_{in}^{C3}(j) \geq 0 \tag{55}$$

In (54), $C_{O_2}^{C3}|_l^{ref}$ is the reference of the O_2 concentration of C3 in the liquid phase, which is obtained from the O_2 demand predicted by the prediction system at the tertiary level. Hence, at the current time step of the tertiary and the secondary controllers:

$$C_{O_2}^{C3}|_l^{ref}(j) = \frac{\widehat{D}_{O_2}^{C3}}{V_{C3} \cdot K_L a^{C3}} \tag{56}$$

4.3.2.2. Varying-Resolution MPC

The output of this controller includes the gas flows to C4a (G_{in}^{C4a}) and to the membrane separation unit (G_{in}^{MS}), the gas flow to add or retrieve from the concentrated gas tank (G^{CT}) and the diluted gas tank (G^{DT}) and the O_2 concentration in the outflow of C4a ($C_{O_2}^{C4a}|_g$). The prediction and control horizons are set to one hour and the sample time is set to 6 minutes.

However, using a 6-min time resolution over the entire horizon of 1-hour results in a 10-step problem, which cannot be efficiently solved in a reasonable time. Hence, a homogeneous time resolution is not appropriate over the 1-hour time span. While in the first next steps, a higher resolution is preferred due to more accurate information, in the later steps, with fewer certain scenarios, the resolution can be decreased (Olivares et al., 2014). Accordingly, five-time steps with different time resolutions are considered: 2×6-min, 2×12-min, and 1×24-min time-steps. The multi-objective control problem at the secondary level is summarized below where λ_i represent weighting coefficients:

$$J_S = \min_{Y}(\lambda_3 J_3 + \lambda_4 J_4 + \lambda_5 J_5 + \lambda_6 J_6 + \lambda_7 J_7) \tag{57}$$

$$J_3 = \sum_{k=1}^{Np_2}\left(\frac{\hat{C}_{O_2}^{C5}|_g(j+k|j) - C_{O_2}^{C5}|_g^{ref}}{\Delta C_{O_2}^{C5}|_g}\right)^2 \tag{58}$$

$$J_4 = \sum_{k=0}^{Nc_2-1}\left(\frac{G^{CT}(j+k|j) - G^{CT,ref}(j+k|j)}{\Delta G^{CT}}\right)^2 \tag{59}$$

$$J_5 = \sum_{k=0}^{Nc_2-1}\left(\frac{\hat{Q}_{O2}^{C4a}(j+k|j) - Q_{O2}^{C4a,ref}(j+k|j)}{\Delta \hat{Q}_{O2}^{C4a}(j+k|j)}\right)^2 \tag{60}$$

$$J_6 = \sum_{k=0}^{Nc_2-1}(\rho(j+k|j) - \rho(j+k-1|j))^2 \tag{61}$$

$$J_7 = \sum_{k=0}^{Nc_2-1}\left(\frac{\hat{C}_{O_2}^{C4a}|_g(j+k|j) - \hat{C}_{O_2}^{C4a}|_g(j+k-1|j)}{\Delta C_{O_2}^{C4a}|_g}\right)^2 \tag{62}$$

$$Y = \begin{bmatrix} y_1 \\ \vdots \\ y_{Np_2-1} \end{bmatrix} \tag{63}$$

$$y_1 = \begin{bmatrix} \rho(j) \\ G^{CT}(j) \\ C_{O_2}^{C4a}|_g(j) \end{bmatrix}; y_{Np_2-1} = \begin{bmatrix} \rho(j+Np_2-1) \\ G^{CT}(j+Np_2-1) \\ C_{O_2}^{C4a}|_g(j+Np_2-1) \end{bmatrix} \tag{64}$$

$$U_2 = [\rho(j) \quad G^{CT}(j) \quad C_{O_2}^{C4a}|_g(j)] \tag{65}$$

Subject to:

$$System\ dynamics\ (32) - (38) \tag{66}$$

$$G_{out}^{C5}(j+k-1|j) = G_{in}^{C4a}(j+k|j) + G_{in}^{MS}(j+k|j) \tag{67}$$

$$\rho(j+k|j) = \frac{G_{in}^{C4a}(j+k|j)}{G_{out}^{C5}(j+k|j)} \tag{68}$$

$$G^{CT,min} \le G^{CT}(j+k|j) \le G^{CT,max} \tag{69}$$

$$SOC^{CT,min} \le \widehat{SOC}_{CT}(j+k|j) \le SOC^{CT,max} \tag{70}$$

$$C_{O_2}^{C5}|_g^{min} \leq \hat{C}_{O_2}^{C5}|_g(j+k|j) \leq C_{O_2}^{C5}|_g^{max} \quad (71)$$

$$C_{CO_2}^{C5}|_g^{min} \leq \hat{C}_{CO_2}^{C5}|_g(j+k|j) \leq C_{CO_2}^{C5}|_g^{max} \quad (72)$$

$$C_{O_2}^{C4a}|_g^{min} \leq C_{O_2}^{C4a}|_g(j+k|j) \leq C_{O_2}^{C4a}|_g^{max} \quad (73)$$

$$\rho^{min} \leq \rho(j+k|j) \leq \rho^{max} \quad (74)$$

The cost function (57) is the weighted sum of the normalized cost functions associated with the deviation of O_2 concentration in C5 from the reference as represented in (58), the deviation of the O_2 provided by the concentrated gas tank and C4a from the references scheduled at the tertiary level represented in (59) and (60) and the rate of change of manipulated variables represented in (61)-(62).

It is worth mentioning that due to the restricted computation time of the secondary controller, the dynamic equations corresponding to the evolution of O_2 and CO_2 in C3 and C5 have been reduced to fixed consumption rates. In addition, an empirical approximation has been used to estimate CO_2 concentration in C4a given the decision variable $C_{O_2}^{C4a}|_g$. Hence, all the models are discretized to be used in the above-mentioned MPC framework. The outputs of the secondary controller stored in U_2, together with the output of PFC2, become the references for the controllers at Level 1.

4.3.3. Level 1: Local Controllers

At this level, primary controllers, which receive the setpoints from the secondary controllers and send control actions to the process actuators are defined. Considering the need for a high-speed actuation and low computation time, a PFC-based (PFC1) control strategy has been chosen to control the O_2 concentration in C4a by adjusting the light intensity. The control law is derived based on the first-order model parameters identified in Alemany et al., (2019) and using (39)-(44) as follows:

$$I_{C4a}(m) = \frac{\left[C_{O_2}^{C4a}|_g^{ref}(m) - C_{O_2}^{C4a}|_g^{p}(m)\right] \cdot lh_{PFC1} + \beta_{m,PFC1} \cdot \hat{C}_{O_2}^{C4a}|_g(m)}{K_{m,PFC1} \cdot \beta_{m,PFC1}} \quad (75)$$

Level 1 is triggered every 36 seconds (fast clock in Fig 4. 3) to respond to O_2 fluctuations in the gas outflow of the C4a compartment ($C_{O_2}^{C4a}|_g$). A summary of the proposed HCS is represented in Fig 4. 3.

4.4. Simulation Results

4.4.1. Simulation Plan

In this section, the performance of the proposed control method is evaluated using the MELiSSA Pilot Plant as a test case under different operating scenarios. The time interval used for

simulation is 120 days. Simulations are conducted in MATLAB environment and Parallel computing Toolbox and Aalborg University cloud service (CLAAUDIA) are employed for parallel computations. Different controller specifications that are considered for the simulations are given in Table 4. 1.

Table 4. 1. Controller's specifications

Par	Value	Par	Value
$\mathrm{SOC}^{\mathrm{CT,ref}}$	0.5	$I_{C4a}\|_{day/night}^{nom}$	225/84 Wm^{-2}
$\mathrm{SOC}^{\mathrm{CT,min/max}}$	0/1	Np_3=$Nc3$	6
$I_{C4a}^{min/max}$	10/364 Wm^{-2}	Np_2=Nc_2	5
$\mathrm{G}^{\mathrm{CT,min/max}}$	-10/10 Lh^{-1}	λ_1	5
$\mathrm{P}^{\mathrm{CT,max}}$	50×10^5Pa	$\lambda_2 = \lambda_3$	1
V^{CT}	10L	$\lambda_4, \dots, \lambda_7$	0.1
$\mathrm{C}_{\mathrm{O}_2}^{\mathrm{C5}}\|_{\mathrm{g}}^{\mathrm{ref}}$	21%	$\mathrm{T}_{\mathrm{S},3}$	1h
$\mathrm{C}_{\mathrm{O}_2}^{\mathrm{C4a}}\|_{\mathrm{g}}^{\mathrm{min/max}}$	18/24%	$\mathrm{T}_{\mathrm{S},2}$	$0.1\mathrm{T}_{\mathrm{S},3}$
$\mathrm{C}_{\mathrm{O}_2}^{\mathrm{C5}}\|_{\mathrm{g}}^{\mathrm{min/max}}$	0/3%	$\mathrm{T}_{\mathrm{S},1}$	$0.1\mathrm{T}_{\mathrm{S},2}$
$\rho^{\mathrm{min/max}}$	0.1/0.9		

As mentioned in Section 4.3, the parameter identification of the PFC first-order models has been inferred based on the MELiSSA Pilot Plant experimental data, which has also represented a test-bed for the control implementation and large-scale validation. The controller parameters regarding PFC2 and PFC1 are listed in Table 4. 2.

Table 4. 2. Predictive functional controllers' parameter

Name	Control command	Time constant (h)	Gain	Coincidence point (h)	Closed loop response time (h)	Reference	HCS level
PFC2	G_{in}^{C3}	0.01	0.0459	0.1	0.03	$C_{O_2}^{C3}\|_l^{ref}$	2
PFC1	Light intensity (W/m^2)	0.15	0.007 % O_2 /W/m^2	0.01	0.45	$C_{O_2}^{C4a}\|_g^{ref}$	1

The data required for modelling the MELiSSA Pilot Plant can be accessed in Pérez et al., (2005a) for C3 and Alemany et al., (2019) for C4a and C5. A simulation with changing nitrogen load (ammonium load is also used indistinctively) in the input of C3 has been performed. By changing the nitrogen load, the overall demand of O_2 changes, and the response performance of the proposed HCS can be assessed. The details of the simulation schedule are given in Table 4. 3. As the nitrogen inflow increases/decreases, the required O_2 by C3 ($\widehat{D}_{O_2}^{C3}$) to oxidize it, also increases/decreases. The control system is responsible to coordinate all O_2 producer and consumer compartments as well as the concentrated gas tank to satisfy the main requirements of the loop.

Table 4. 3. Simulation Schedule

Step	Inlet Flow (mL/min)	[NH_4] (mg/L)	N Load (mg N L^{-1} day^{-1})	Time Interval (day)
Load1*	20.8	128.6	435	0-10
Load2	16.4	128.6	343	10-30
Load3	27.8	128.6	580	30-50
Load4	33.5	128.6	700	50-70
Load1	20.8	128.6	435	70-120

* Nominal operating condition

4.5. Results

4.5.1. Main Outcome

As the main outcome of the study, Fig 4. 4a demonstrates that O_2 in the crew compartment is appropriately maintained within the required limits while following the desired reference of 21%.

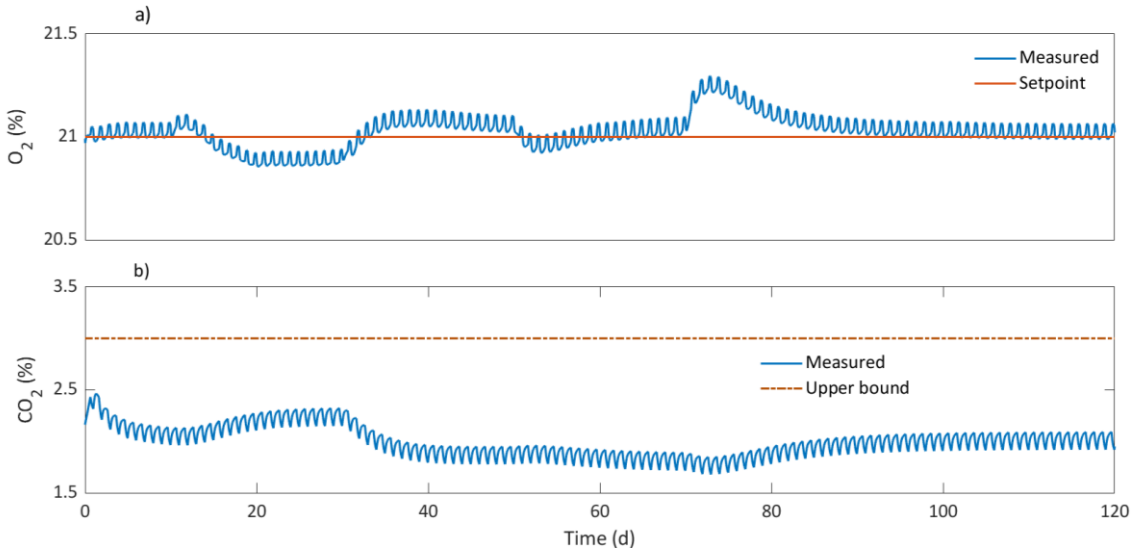

Fig 4. 4. Evolution of (a) O_2 and (b) CO_2 in the gas phase of C5

The reason for this fluctuation, which evolves according to the nitrogen load, lies in the fact that in the secondary controller, the O_2 reference-tracking requirement in C5 defined in (58) is introduced in the optimization problem as a soft constraint. Therefore, deviations from the reference are allowed under a penalization defined by the weight factor λ_3, without violating the limits as defined in (71). From a process point of view, when O_2 demand is high (for example when nitrogen load is at its highest point after 50 days), the concentration of O_2 in C5 decreases. The reason for this behaviour is that the optimization problem in Level 3 and Level 2 controllers provide a compromise between the precision of the reference tracking in C5 and the deviation of the operating conditions from the desired nominal operating points defined by parameters $SOC^{CT,ref}$, $I_{C4a}|_{day}^{nom}$ and $I_{C4a}|_{night}^{nom}$ in Table 4. 1. In opposite, when the process operates at its nominal condition, the concentration of O_2 in C5 can track the reference with high precision. In this study, CO_2 is not controlled, but with the operating conditions used, it can be kept below a critical level of 3% as can be seen in Fig 4. 4b. The already mentioned high degree of coupling between variables may makes it necessary to design a CO_2 trap or buffer tank, which introduces a degree of freedom in the system to be able to control CO_2.

4.5.2. Level 3 of the HCS

In Fig 4. 5, the optimal resource allocation scheduled by solving (45)-(53) is represented. Essentially, Level 3 is constrained by the mass balance in (50) considering a list of technical restrictions and operating criteria. If the process is operating in nominal conditions (Load 1 in Table 4. 3), O_2 is supplied mainly by C4a through adjusting light intensities close to the nominal values. It is important to notice that the oscillations of the system are due to the day-night dynamics of the mock-up crew respiration. During the night time, rats consume O_2 and produce CO_2 at a reduced rate in relation to the day shift causing the repeated oscillation observed in most of the variables represented in this section. This is also the reason why two nominal points of light intensity are used in C4a, so that the resource utilization can be optimized. In Fig 4. 5, it can be observed how the concentrated gas tank is coordinated with C4a to handle the excess and deficit of O_2 in the system. Thus, when the consumption rate of C3 and C5 exceeds C4a production capacity (from 25 to 30 days in Fig 4. 5b), the concentrated gas tank is mainly discharged (red area in Fig 4. 5b). On the contrary, if C4a has enough production capacity (from 30 to 38 hr in Fig 4. 5b), the concentrated gas tank is mainly charged (purple area in Fig 4. 5b).

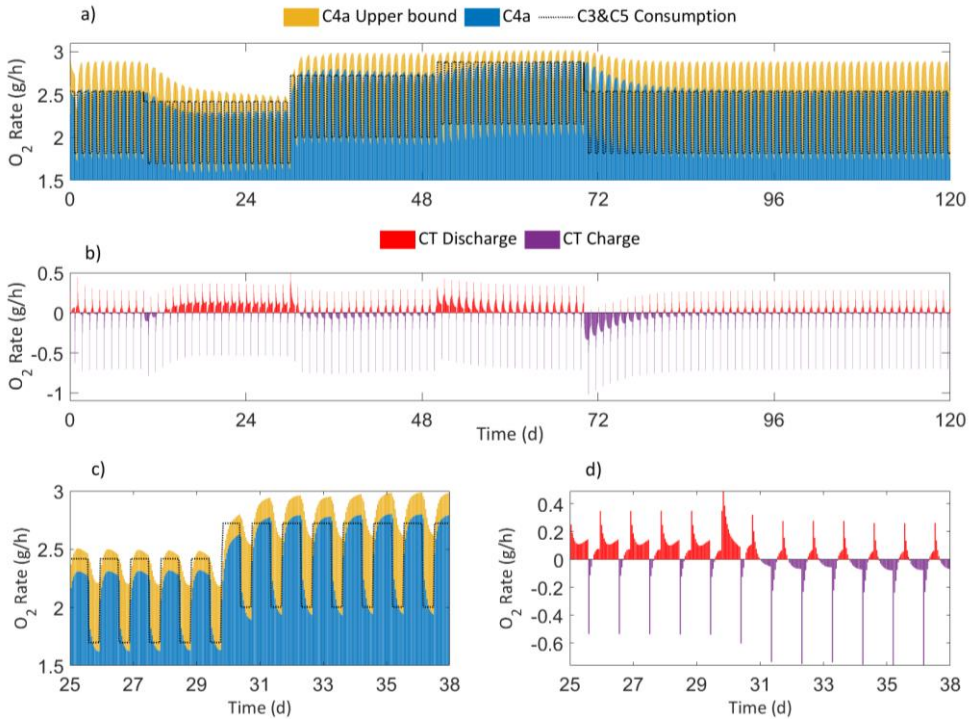

Fig 4. 5. Level 3: O_2 resource allocation. a) Overall demand of O_2 from C3 and C5 and the optimal resource allocation of C4a; b) Concentrated gas tank charging(-)/discharging(+) rates according to tertiary level decisions; c) and d) are zoomed plots of a) and b) respectively from day 25 to 38.

4.5.3. Level 2 of the HCS

Once Level 3 has determined the resource allocation in terms of O_2 production rates from C4a and the concentrated gas tank, references are sent to the secondary controller, which generates reference signals to be tracked by local controllers through solving the control problem presented in (57)-(74). In Fig 4. 6, where the output of the secondary controller is represented, a high performance can be observed in terms of precision in the tracking of the references received from Level 3. PFC2 performance will be assessed in the next section.

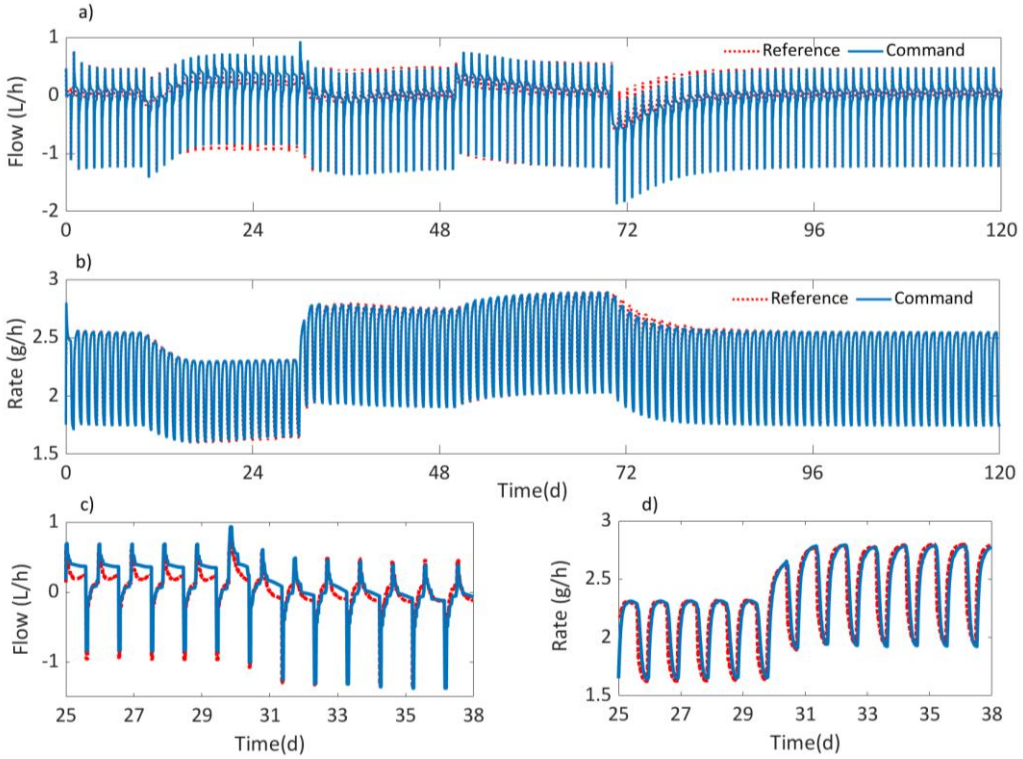

Fig 4. 6. Level 2 Controller: Reference Correction. a) Concentrated gas tank charging (-)/discharging(+) rate; b) Oxygen production rate of C4a; c) and d) Zoomed plots of a) and b) respectively from day 25 to 38.

4.5.4. Local Controllers and Process Performance

According to Table 4. 3, Load 2 corresponds to the lowest Nitrogen load in C3 which carries the lowest O_2 demand. Nevertheless, it is also observed in Fig 4. 6b that with this low amount of nitrogen load, the concentrated gas tank needs to be discharged to satisfy the overall O_2 demand. The reason for this apparent contradictory phenomenon about low O_2 demand and discharging of the concentrated gas tank can be explained by the resource limitation in C4a. According to (4)-(8), when the substrate *y* concentration decreases, the associated limiting factor decreases $\Psi_y^z < 1$, hence, cell growth and productivity of O_2 also decrease. In Fig 4. 7a, Ψ_y^z is represented for CO_2 and HNO_3, demonstrating that when nitrogen load is decreased in Load 2 scenario, C4a

receives less nitrate and its O_2 productivity is threatened. It is also important to highlight that according to Table 4. 3 the concentration of NH_4 in the input of C3 is not changed, but the flow of input liquid (F_{in}^{C3}) is changed. Hence, the concentration of nitrate in the input of C4a is time-invariant, considering that C3 operates at full nitrification. The cause of the limitation is that reducing the flow involves increasing the residence time in the photobioreactor C4a, increasing its biomass concentration (increasing the population) until the consumption rate of nitrate crosses a boundary that implies nitrogen (resource) limitation (Fig 4. 7b). This is a paradigmatic example of the degree of interdependency between variables involved in biochemical reactions.

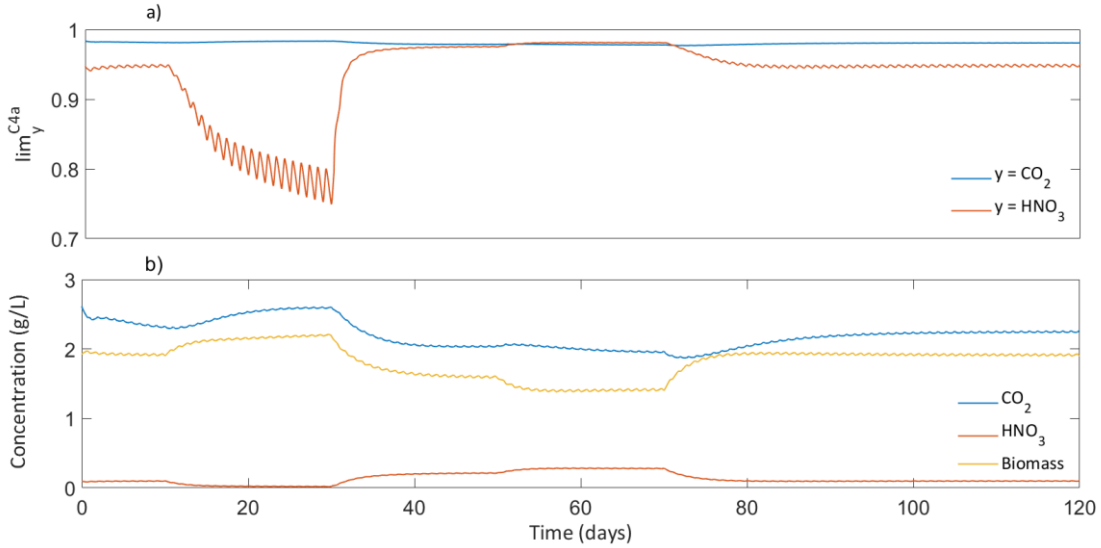

Fig 4. 7. a) Substrate limitation in C4a associated to Carbon and Nitrogen sources b) Concentration of compounds in the liquid phase in the output of C4a

The control system proposed in this study can overcome this type of limitation by deploying efficient predictions. The tertiary controller uses the measurements obtained from the plant, which in combination with the internal model presented in Section 4.2, can anticipate some of the negative phenomena that the process can face as long as they are properly considered in the internal model. When the nitrogen load is at its highest level (Load 4), it can be observed in Fig 4. 5b that the concentrated gas tank needs to be discharged, not because of a nitrogen limitation in C4a, but because of the high O_2 demand in the system. At this point, C4a approaches its maximum production capacity, which is penalized by the objective function. As can be observed, the HCS defines an optimal strategy for charging and discharging the concentrated gas tank for compensating, either the default of nitrogen availability or the excess in O_2 demand of the system.

According to the diagram in Fig 4. 3, the secondary controller requires information about the gas inflow in C3 to be able to generate the rest of the control references. By applying the PFC in (54),

the gas flow is determined based on the expected O_2 demand, which is predicted at the tertiary level. Fig 4. 8a demonstrates that whenever nitrogen load is increased, so does the reference dissolved O_2 in C3 following (56). To track these reference changes, the input gas flow (Fig 4. 8b) is modified to inject more concentrated O_2 from the membrane separation unit when more nitrogen is loaded in C3. As it can be seen in Fig 4. 8c, PFC is proven to be very efficient in guaranteeing that no NH_4 is sent to C4a.

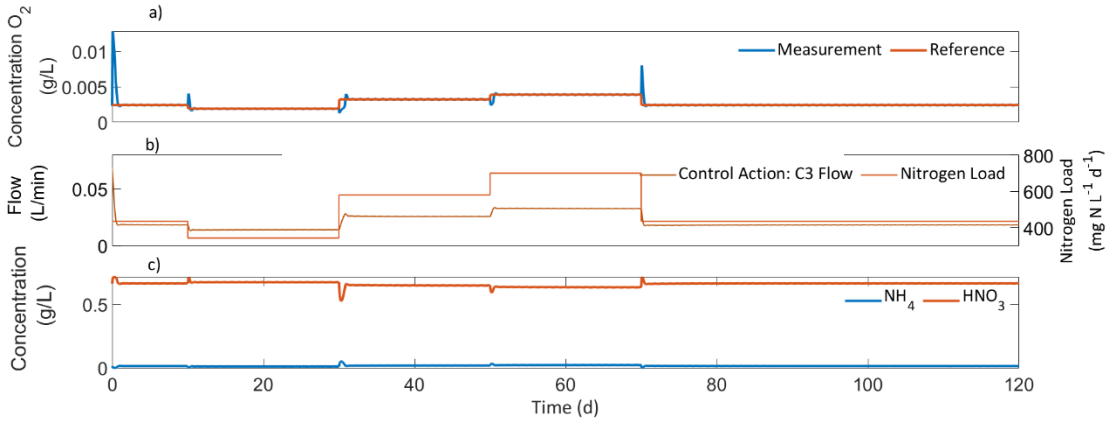

Fig 4. 8. Summary of oxygen controller in C3. a) Dissolved oxygen tracking to guarantee ammonia oxidization to nitrate b) C3 Gas inflow representation as a control command in response to varying nitrogen load c) Distribution of nitrogen compounds of C3 in the liquid phase.

Regarding the output of the secondary controller, the concentrated gas tank flow (Fig 4. 6a) can be directly sent to the local controller, but the O_2 production rate assigned to C4a (Fig 4. 6b) depends on the C4a gas flow and the O_2 concentration in the output of C4a. Thus, secondary controller determines optimal flows and concentration setpoints to be tracked by the local controllers given the flow rate generated by Level 2, the control of O_2 concentration in C4a is performed by adjusting the light intensity in the primary controller. As mentioned, the operating criteria for C4a is to work with two nominal levels of light intensity. In Fig 4. 9a, it can be observed that the O_2 concentration in C4a follows with good precision the reference received from Level 2. The performance of the PFC controller has been already validated in the MELiSSA Pilot Plant. In Fig 4. 9b it is shown that when the process operates at the nominal operating condition (Load 1) the light intensity is close to the day and night nominal points (225 and 84 W/m^2 respectively), while in scenarios when different nitrogen loads are applied, light intensity tends to deviate from the nominal levels following the priority given to different objective functions of the secondary controller. Fig 4. 9c shows the evolution of the concentrated gas tank storage level over the simulation time, tracking the desired reference imposed by the supervisory controller at a value of 50%. As the reference for concentrated gas tank is set to 50%, as soon as the production capacity of C4a can satisfy the overall O_2 demand, the tank is charged to restore its desired level.

This is observed in Fig 4. 9c when the nominal operating conditions are restored from day 70 until the end of the simulation. Hence, the light intensity profile in C4a is never saturated as it stays around the nominal point and similarly, the concentrated gas tank level fluctuates around 50%.

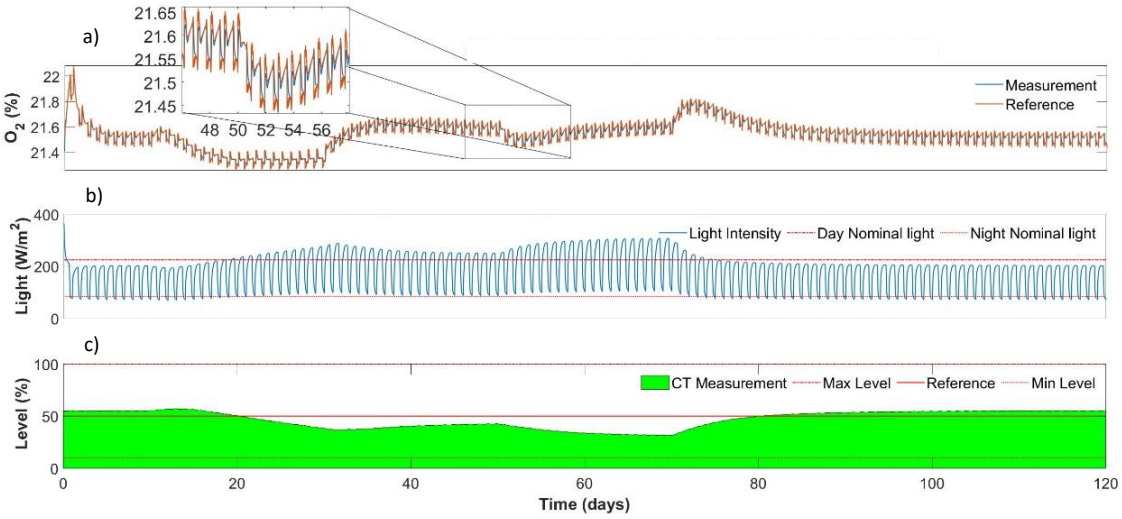

Fig 4. 9. Performance of the controllers in Level 1: a) Oxygen reference tracking in C4a, b) C4a light adjustment, c) Concentrated gas tank level.

Satisfactory results have been achieved regarding both the operation of the system following the desired references guaranteeing a safe environment for the crew and the achievement of a high degree of resilience to changes. The computational time required at different levels in the proposed HCS is also satisfactory, given the complexity of the MPC used for Levels 3 and 2. Details about the computational cost of different controllers can be found in Table 4. 4.

Table 4. 4. Controllers Computational Cost

Level in HCS	Maximum (sec)	Minimum (sec)	Mean (sec)
Prediction	122.15	65.74	70.06
Level 3	2.72	0.55	0.62
Level 2	9.38	1.07	2.065
Level 1	<0.1	<0.1	<0.1

4.6. Conclusions

In this study, the HCS presented in the previous chapter is implemented to control ecological LSSs, which have a very complex nature reflected in the mathematical modeling and present many challenges including non-linearities, interrelated system dynamics, hard constraints, scarce resources, and degrees of freedom, and especially a high degree of variable and functions coupling. All this requires a HCS with different levels to supervise (Supervisory Level), manage (Level 3), adjust (Level 2), and execute (Level 1) control commands. The platform presented will be used in the future to adapt the proposed HCS to further integration steps pursued in the MELiSSA Pilot Plant. Increasing the number of compartments will naturally increase the control complexity. Among others, it will force to include carbon dioxide, water or edible material production for the crew, to assess the use of buffer elements to ensure optimal control of the plant, as well as to appraise the control architecture resilience and robustness. Aligned with this expected growing complexity associated to the integration of more compartments, the following chapters will be focused on the modelling of the higher plants chamber and the inclusion of this compartment in the presented HCS. Among several challenges presented by the introduction of a higher plants chamber (HPC) compartment in the loop, it is of special relevance the way to cope with a higher redundancy (multiple oxygen producers), higher degrees of freedom (HPC provides one more degree of freedom) and how to benefit from that.

5. MULTILEVEL MECHANISTIC MODEL OF A HIGHER PLANTS CHAMBER

Based on a paper published in the journal *Frontiers in Plant Sciences*

Nomenclature

Morphological module

LA	Leaf area [m^2 leaves]	
L	Leaf length [m leaves]	
M_x	Dry biomass [g]	

Irradiance module

I	Irradiance [moles m^{-2} ground s^{-1}]	
I_u	Irradiance at LAI = 0 [moles m^{-2} ground s^{-1}]	
$I_{s,g}$	Direct irradiance over ground surface [moles m^{-2} ground]	
$I_{d,g}$	Diffuse irradiance over ground surface [moles m^{-2}]	
I_s	Direct irradiance over leaf surface [moles m^{-2} ground s^{-1}]	
I_d	Diffuse irradiance over leaf surface [moles m^{-2} ground s^{-1}]	
LAI	Leaf area index [m^2 leaves m^{-2}]	
LAI_s	LAI exposed to direct irradiation [m^2 leaves m^{-2}]	
LAI_d	LAI exposed to diffuse irradiation [m^2 leaves m^{-2}]	
k	Extinction coefficient (0.5)	MELiSSA Pilot Plant
f_s	Direct irradiance fraction (0.7)	Thornley (1980)
$BCmol$	C-mole molecular weight (27) [g mol-C^{-1}]	MELiSSA Pilot Plant

Energy Balance

T_l	Leaf temperature [K]	
k_t	Heat transfer coefficient [m s^{-1}]	
E_{hs}	Direct irradiance energy [J s^{-1}]	
E_{hd}	Diffuse irradiance energy [J s^{-1}]	
E_r	Radiation energy [J s^{-1}]	
E_{conv}	Convection energy [J s^{-1}]	
E_{tr}	Transpiration energy [J s^{-1}]	
Na	Avogadro number ($6.02 \cdot 10^{23}$) [Pa]	
c	Light velocity ($3 \cdot 10^{9}$) [Pa]	
h	Planck constant ($6.63 \cdot 10^{-34}$) [m^2 kg s^{-1}]	
ε	Leaf emissivity (0.97)	Poulet et al., (2020)
σ	Stefan-Boltzman constant ($5.67 \cdot 10^{-8}$) [J s^{-1} K^{-4}]	Poulet et al., (2020)

R	Ideal gas constant (8.314) [m^3 Pa K^{-1} mol^{-1}]	
C_p	Molar air specific heat capacity (29.3) [J mol^{-1} K^{-1}]	Poulet et al., (2020)
λ_{mol}	Water latent heat of vaporization ($4.0788 \cdot 10^4$) [J mol^{-1}]	Poulet et al., (2020)

Gas exchange module

Ex_{CO_2}	CO_2 exchange rate [moles m^{-2}]	
Ex_{O_2}	O_2 exchange rate [moles m^{-2}]	
Ex_{H_2O}	H_2O exchange (transpiration) rate [moles m^{-2}]	
G_z	Conductance compound z [moles m^{-2}]	
P_b^z	Bulk partial pressure compound z [Pa]	
P_l^z	Leaf partial pressure compound z [Pa]	

Biochemical module

F_{LETC}	Light electron transport chain rate [moles m^{-2}]	
F_{LETC}^{max}	Maximum light electron transport chain rate [moles m^{-2}]	
J	Ribulose 1,5-biphosphate regeneration [moles m^{-2}]	
Γ	Carbon dioxide compensation point [moles m^{-3}]	
V_c	Carboxylation rate [moles m^{-2}]	
V_{cmax}	Maximum carboxylation rate [moles m^{-2}]	
V_o	Oxygenation rate [moles m^{-2}]	
C_i	Carbon dioxide leaf concentration [moles m^{-3}]	
O_i	Oxygen leaf concentration [moles m^{-3}]	
P_g	Gross photosynthesis rate [moles m^{-2}]	
P_n	Net photosynthesis rate [moles m^{-2}]	
θ	Convexity coefficient (0.8)	Farquhar et al., (1980)
f	Energy loss for LETC (0.045)	Nikolov et al., (1995)
K_c	Carboxylation half-saturation constant (460) [µbar]	Farquhar et al., (1980)
K_o	Oxygenation half-saturation constant (330) [mbar]	Farquhar et al., (1980)
F_{LETC}^{max25}	F_{LETC}^{max} at 25ºC (100) [µmol m^{-2} s^{-1}]	Nikolov et al., (1995)
$V_{cmax_{25}}$	V_{cmax} at 25ºC (31.31) [µmol m^{-2} s^{-1}]	Nikolov et al., (1995)
E	Activation energy of reaction (81993) [J mol^{-1} K^{-1}]	Nikolov et al., (1995)
S	Entropy (711.36) [J mol^{-1} K^{-1}]	Nikolov et al., (1995)
H'	Energy of deactivation (219814) [J mol^{-1} K^{-1}]	Nikolov et al., (1995)
M_c	C-molar molecular weight (27) [g mol-C^{-1}]	MELiSSA Pilot Plant

DM	Dry Biomass fraction (0.045) [g/g]	MELiSSA Pilot Plant

Boundary layer module

g_{BL}^{z}	Boundary layer conductance of compound z [moles m^{-2}]	
g_{s}^{z}	Stomatal conductance of compound z [moles m^{-2}]	
δ	Boundary layer thickness [m]	
T_{bl}	Average leaf-bulk temperature [K]	
D^{z}	Diffusion coefficient of compound z [m^2 s^{-1}]	
v_{bulk}	Bulk velocity [m s^{-1}]	
v_{free}	Free velocity [m s^{-1}]	
ρ_{l}	Leaf air density [kg m^{-3}]	
η	Air kinematic viscosity ($1.8 \cdot 10^{-5}$) [m^2 s^{-1}]	Poulet et al., (2020)
α	Leaf angle in relation to the vertical axis (0.1) [º]	Poulet et al., (2020)
g	Gravity force (9.8) [m s^{-2}]	
ρ_{b}	Bulk air density (1.186) [kg m^{-3}]	

Acronyms

BLSS	Bioregenerative Life Support System
FBA	Flux Balance Analysis
MPC	Model Predictive Control
SSTO	Steady-State Target Optimization
MELiSSA	Micro-Ecological Life Support Systems Alternative

5.1. State of the art of modelling higher plants

Modelling crop growth has been a topic of research since the mid-twentieth century given the relevance that agronomic-related activities have in the global economy, but the focus on plant modelling research has evolved in the last decades moving towards new applications (Louarn & Song, 2020). A lot of attention has been placed on developing full canopy models to assess climate change from different perspectives, such as its effect on crop physiology, the higher plants adaptive strategies or the contribution of forestry and agricultural systems on carbon dioxide capture, to mention a few (Peng et al., 2020; Soussana et al., 2010). Besides responding to the current global climate and demographic challenges, the need for more efficient forms of horticulture to increase productivities, improve yield and optimize crop growth has also contributed to the generation of mathematical models to support agronomic activities. Still much progress is required in the field of biological systems modelling and this is especially relevant in the case of higher plants due to the complexity of their underlying growth mechanisms. Modelling complex systems like higher plants may be an objective by itself as before-mentioned but they may also lead to other interesting applications like the development of model-based control methodologies. Particularly, space research and the development of bio-regenerative life support systems have exploited the use of controllers based on first principles in opposition to surrogated and reduced order models, to improve both the management of missions under operation as well as to improve the design of future missions (Fulget et al., 1999). One remaining task, which is in turn one of the most relevant consensuses of the development of BLSSs shared by the major space agencies, is the importance of developing technologies and mathematical models to grow plants on space, which are expected to be the major source of edible biomass and oxygen in BLSSs (Dong et al., 2017a; Gitelson & Lisovsky, 2002; Poughon et al., 2009).

Even though current models can cope with the evolution of biomass, the compounds involved in photosynthesis and respiration (O_2 and CO_2) and the nutrients uptake by the roots, most of the phenomena involved in plants growth are not addressed given their complexity and lack of knowledge. This complexity is associated to several factors; higher plants are multicellular, compartmentalized organisms undergoing strong metabolic changes associated to the cyclic switch between light and dark phases of the day. They are also characterised by having a complex substrate partitioning strategy with different parts being coordinated to uptake and distribute specific compounds. This has contributed to the preference of empirical at the expense of mechanistic models due to the usually satisfactory information provided by the former, especially in nominal conditions (Amitrano et al., 2020; Boscheri et al., 2012). Empirical models

cover a limited range of operating conditions though, thus the scope of their use is narrow and cannot contemplate all scenarios that plant culture may undergo. As an alternative, mechanistic approaches have also been deployed to understand the first principles behind higher plants growth, standing out the Farquhar model (Farquhar et al., 1980) to calculate photosynthesis rates based on the enzyme kinetics of principal metabolic pathways. However, out of the photosynthesis process, many key mechanisms like respiration, substrate accumulation and management, tissue morphology or multi-tissue interactions have not completely been mathematically characterised yet. To treat such a complex system, the use of metabolome information has attracted the attention of plant modellers as an alternative to gather multiple biological reactions formalized as a constraint-based metabolic model (Gomes et al., 2015). It should be highlighted that constraint-based metabolic models have been demonstrated to successfully address the plant diel cycle with a light phase with resource accumulation and a dark phase with resource depletion (Cheung et al., 2014), a critical phenomenon in higher plants metabolism very difficult to deal through first-principle approaches thus far. Several efforts have been recently placed on integrating available mechanistic information and *omics* data in a common multi-scale modelling framework that could potentially be used by the plant computational biology research community to feed data in a single converging platform (Marshall-Colon et al., 2017; Xiao et al., 2017).

In this study, the modelling of higher plants is approached through the design of a multi-level organization of the mechanistic processes that takes place during crop growth. To present the results, *L. sativa* has been used as an exemplary higher plant. The higher level in the hierarchy copes the mechanistic phenomena corresponding to a higher characteristic length (i.e. crop chamber scale) whereas the lower the level the smaller the characteristic length of the modelled phenomena (i.e. enzyme rate). Information follows a top-bottom flow and it is eventually used to calculate the metabolic flux distribution by applying a flux balance analysis (FBA). This multi-level modelling approach is firstly validated with experimental data and secondly integrated in a model-based predictive control, representing, to the best of the authors, the first attempt to incorporate cell metabolism in an advanced control strategy.

Overall, the modelling and control methodology presented in this study may pave the way for a more efficient and sustainable agriculture either for intensive cultivation systems or as a part of BLSSs in space exploration.

5.2. Model Proposal

5.2.1. Multilevel Mechanistic Model

The model developed here is organized following a multilevel approach, considering the different levels of the plant, from canopy to metabolic level, and uses the output of the higher levels as the input to the lower levels. In this section, the models used in the different levels are explained. A graphical description of the model organization is presented in Fig 5. 1 and detailed in the following paragraphs. Model parameters are described in the nomenclature of this Chapter.

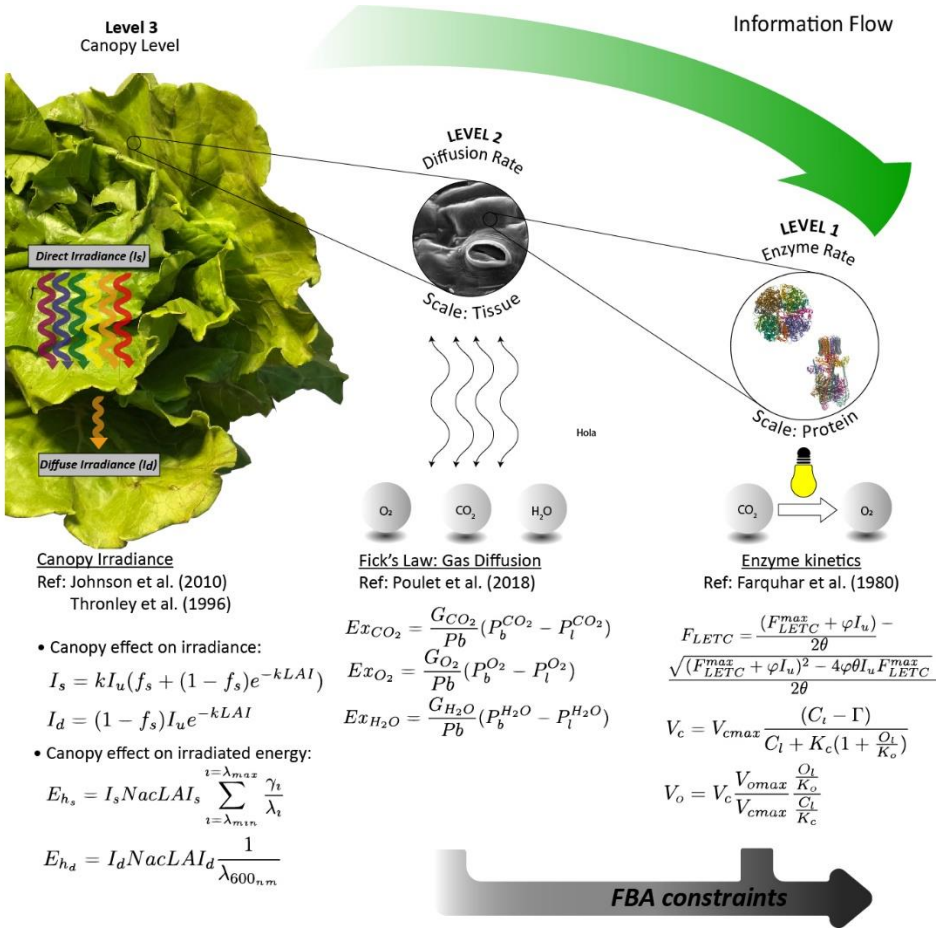

Fig 5. 1. Graphical scheme of the multilevel mechanistic model approach used for L. sativa prediction growth.

5.2.1.1. Level 3: Modelling Canopy Growth

When dealing with whole leaf or canopy modelling it is necessary to consider the effect of shading among leaves, which is not accounted in single-leaf models (Poulet et al., 2018). The common practice is to use the leaf area index (LAI) as an indicative parameter of the leaf area density over ground surface. The photon flux density inside the canopy I declines along the canopy exponentially and is a function of the leaf area index:

$$I = I_u e^{(-kLAI)} \tag{76}$$

Parameter I_u represents the photon flux density at the top of the canopy and k represents the extinction coefficient. Extending (76), leaves can receive direct photon flux density (I_s) or diffuse photon flux density (I_d) as stated by Thornley (2002), which are expressed in terms of µmol m^{-2} leaf s^{-1} by using the extinction coefficient *k:*

$$I_s = k \cdot f_s \cdot I_u + k \cdot (1 - f_s) \cdot I_u \cdot e^{(-k \cdot LAI)} \tag{77}$$

$$I_d = k \cdot (1 - f_s) \cdot I_u e^{(-k \cdot LAI)} \tag{78}$$

Notice in (77) that the parts of the canopy under direct irradiance also receive diffuse irradiance. The LAI term should be differentiated between the fractions exposed to direct and diffuse light sources (LAI_s and LAI_d respectively) as suggested by Thornley (2002):

$$LAI_s = (1 - e^{-kLAI})/k \tag{79}$$

$$LAI_d = LAI - LAI_s \tag{80}$$

The derivative of LAI_s and LAI_d should be obtained and used to integrate I_s and I_d to calculate the overall irradiance received by the canopy:

$$dLAI_s = e^{-kLAI}\, dLAI \tag{81}$$

$$dLAI_d = (1 - e^{-kLAI})\, dLAI \tag{82}$$

$$I_{s,l} = \int_0^{LAI} I_s dLAI_s \tag{83}$$

$$I_{d,l} = \int_0^{LAI} I_d\, dLAI_d \tag{84}$$

The way how light irradiates exposed and shadowed leaves strongly affects the energy balance in the leaves surface, being the shadowed leaves irradiated by diffused light mainly of a wavelength of 600 nm corresponding to the green colour spectrum of transmitted light. Energy received by irradiance contains the direct (E_{hs}) and diffuse (E_{hd}) terms, which are expressed as follows:

$$E_{h_s} = I_s \cdot Na \cdot c \cdot h \cdot LAI_s \sum_{i=\lambda_{min}}^{i=\lambda_{max}} \frac{\gamma_i}{\lambda_i} \tag{85}$$

$$E_{h_d} = I_d \cdot Na \cdot c \cdot h \cdot LAI_d \frac{1}{\lambda_{600nm}} \tag{86}$$

Na represents the Avogadro number, c represents the velocity of light and γ is the fraction of wavelength λ that compose the light directly irradiating the canopy. The total energy irradiated to the leaves is the summation of both equations (85)-(86). The radiation energy emitted by the

plants (E_r), the energy lost by convection (E_{conv}) and the energy lost by transpiration (E_{tr}) are determined by the following equations:

$$E_r = \varepsilon\sigma\left({T_{leaf}}^4 - {T_b}^4\right) \tag{87}$$

$$E_{conv} = C_p k_t \frac{P_b}{RT_b}\left(T_{leaf} - T_b\right) \tag{88}$$

$$E_{tr} = \lambda_{mol} Ex_{H_2O} \tag{89}$$

In (87), ε and σ represent the leaf emissivity and the Stefan-Boltzmann constant respectively. In (88), C_p and k_t represent the molar specific heat capacity at constant pressure and 298.15 K and the heat transfer coefficient respectively, the latter being a function of the diffusion coefficient and the boundary layer thickness as follows (see Appendix 1 for details on D^t calculation and for an extended description of the boundary layer model):

$$k_t = \frac{\mathrm{D}^t}{\delta} \tag{90}$$

In (89), λ_{mol} is the water latent heat of vaporization and Ex_{H_2O} the transpiration rate defined in the following section. Finally, T_{leaf} is the leaf surface temperature, T_b is the bulk temperature, R is the ideal gas constant.

5.2.1.2. Level 2: Modelling Gas Exchange Rates

This level is dedicated to calculate the uptake and release rates between the atmosphere and the leaves concerning the exchange gases (Ex_{CO_2}, Ex_{O_2} and Ex_{H_2O}). The approach to model gas exchanges between the leaves and the atmosphere follows Fick's law, being the concentration gradient the driver of the molecular transport:

$$Ex_{CO_2} = \frac{\mathrm{G}^{CO_2}}{P_b}\left(P_b^{CO_2} - P_l^{CO_2}\right) \tag{91}$$

$$Ex_{O_2} = \frac{\mathrm{G}^{O_2}}{P_b}\left(P_b^{O_2} - P_l^{O_2}\right) \tag{92}$$

$$Ex_{H_2O} = \frac{\mathrm{G}^{H_2O}}{P_b}\left(P_b^{H_2O} - P_l^{H_2O}\right) \tag{93}$$

In (91)-(93), the atmospheric partial pressure is calculated assuming gases behave following the general gas equation, whereas the conductance for the different gases (G^{CO_2}, G^{O_2} and G^{H_2O}) and the internal (i.e. leaf) partial pressure ($P_l^{CO_2}$, $P_l^{O_2}$, $P_l^{H_2O}$) as well as the leaf area (LA) are calculated according to Poulet et al., (2018) and explained in Appendix 1.

5.2.1.3. Level 1: Modelling Enzyme kinetics

The gross photosynthesis rate (P_g) is calculated using the Farquhar model (Farquhar et al., 1980), which has been widely used to model photosynthesis phenomena (Arnold & Nikoloski, 2011; Harley et al., 1992; Morgan & Rhodes, 2002). In this model, P_g is determined through finding the limiting rate of the photosynthesis, which is either caused by the regeneration of Ribulose 1, 5-biphosphate (J), substrate of the ribulose-1,5-biphosphate carboxylase (RuBisCo), or by the RuBisCO carboxylation rate itself (V_c).

On the one hand, the regeneration of Ribulose 1, 5-biphosphate depends on the potential rate of the light electron transport chain (F_{LETC}) and its capacity to generate reducing power. Thus, it is necessary to define an expression for F_{LETC}, which can be approximated by a quadratic equation (Nikolov et al., 1995):

$$F_{LETC} = \frac{(F_{LETC}^{max} + \varphi I_u) - \sqrt{(F_{LETC}^{max} + \varphi I_u)^2 - 4\varphi\theta I_u F_{LETC}^{max}}}{2\theta} \tag{94}$$

$$\varphi = \frac{(1 - \mathrm{f})}{2} \tag{95}$$

In (94), the maximum F_{LETC} is represented by F_{LETC}^{max} (see Appendix 1 for calculation details). The photosynthetic photon flux density used is represented by I_u and θ is a convexity coefficient. The efficiency of energy conversion is represented by φ, which is a function of the fraction of absorbed photon flux unavailable for photosynthesis (f). As previously demonstrated, it is necessary to consider the direct and diffuse irradiances when considering the whole canopy. Therefore, combining with (79)-(80):

$$F_{LETC(I_s,I_d)} = \int_0^{LAI} \frac{F_{LETC}(I_s)\, dLAI_s}{2} + \int_0^{LAI} \frac{F_{LETC}(I_d)\, dLAI_d}{2} \tag{96}$$

Considering that two electrons are necessary per molecule of NADPH generated, the light electron transport chain rate resulting from (96) is divided by 2. This is necessary to provide information to the FBA with consistent units considering the stoichiometry matrix used.

As mentioned before, in Farquhar et al., (1980) approach, it is necessary to convert F_{LETC} defined in (96) to a flow of Ribulose 1, 5-biphosphate (Ru5P) regeneration (J), through the following expression derived from the stoichiometry of the light electron transport chain and the Calvin Cycle (Farquhar et al., 1980):

$$J = \frac{F_{LETC}}{2(2 + 2\emptyset)} \tag{97}$$

Rubisco carboxylation (V_c) kinetics is of Michaelis-Menten type and is a function of the leaf internal oxygen (O_i) and carbon dioxide (C_i) concentrations:

$$V_c = V_{cmax} \frac{(C_i - \Gamma)}{C_i + K_c \left(1 + \frac{O_i}{K_o}\right)} \tag{98}$$

In (98), V_{cmax} represents the maximum carboxylation velocity of RuBisCo, K_c and K_o are the Michaelis Menten half saturation constants for the carboxylation and oxygenation activities of RuBisCo respectively whereas Γ represents the carbon dioxide compensation point. Details about the calculation of the internal carbon and oxygen concentrations can be found in the Appendix 1, based on the boundary layer approach defined by Poulet et al. (2018; 2020). V_c can be directly used to feed the FBA as an upper bound.

Finally, the gross photosynthesis rate (P_g) is determined by finding the minimum between the Ru5P regeneration rate (J), the RuBisCo carboxylation rate (V_c) and the gas exchange rate (Ex_{CO_2}) and the net photosynthesis rate (P_n) is determined by retrieving the RuBisCo oxygenation (V_o) to P_g as follows:

$$P_g = min\left(V_c, Ex_{CO_2}, J\right) \cdot LA \tag{99}$$

$$V_o = V_c \cdot \frac{V_{omax}}{V_{cmax}} \cdot \frac{\frac{O_l}{K_o}}{\frac{C_l}{K_c}} \tag{100}$$

$$P_n = P_g - V_o \cdot LA \tag{101}$$

Notice that equation (99) can be formalized due to the conversion applied in equation (97) considering J represents the regeneration rate of Ru5P and V_c represents its carboxylation rate. Parameter A indicates surface of crop growing area. In this study, the use of a metabolic matrix makes the conversion from light electron transport flux (F_{LETC}) to RuBP regeneration (J) unnecessary, because this information is already included in the stoichiometric matrix. Similarly, the discontinuity introduced by Farquhar et al. (1980) in (99) can be prevented with a FBA formulation as addressed in the following section.

5.2.1.4. Level 0: Stoichiometry matrix

In this level, a simplified network model of the photosynthetic leaves' metabolism of *L. sativa* is described. The stoichiometry matrix is based on the work of Sasidharan (2012), which contains the distinguishing characteristics of *L. sativa*, such as the reduced starch content to store carbon and the definition of the elemental composition that makes up the macromolecules of the biomass. This model though, has been extended to include relevant reactions like the pentose

phosphate pathway or the photorespiration cycle, originally missing. In the model used, the cellular organelles are described as different compartments The model also describes dark and light phases of the day by duplicating each one of the reactions. Hence, a diel model is achieved where both light and dark phases of the day account for separate pools of metabolites and organelle compartments. Here, only those metabolites that have been reported to be accumulated in one phase and consumed in the other are connected by exchange reactions that simulate the transference of nutrients between phases. For example, sugars that are synthesised in the light phase can be used in the dark phase due to the addition of exchange reactions among day phases. In Fig 5. 2, the metabolic model is presented in a simplified way including the cellular compartmentalization, the pathways involved and the connections between them as well as the exchange reactions with the atmosphere and between day periods.

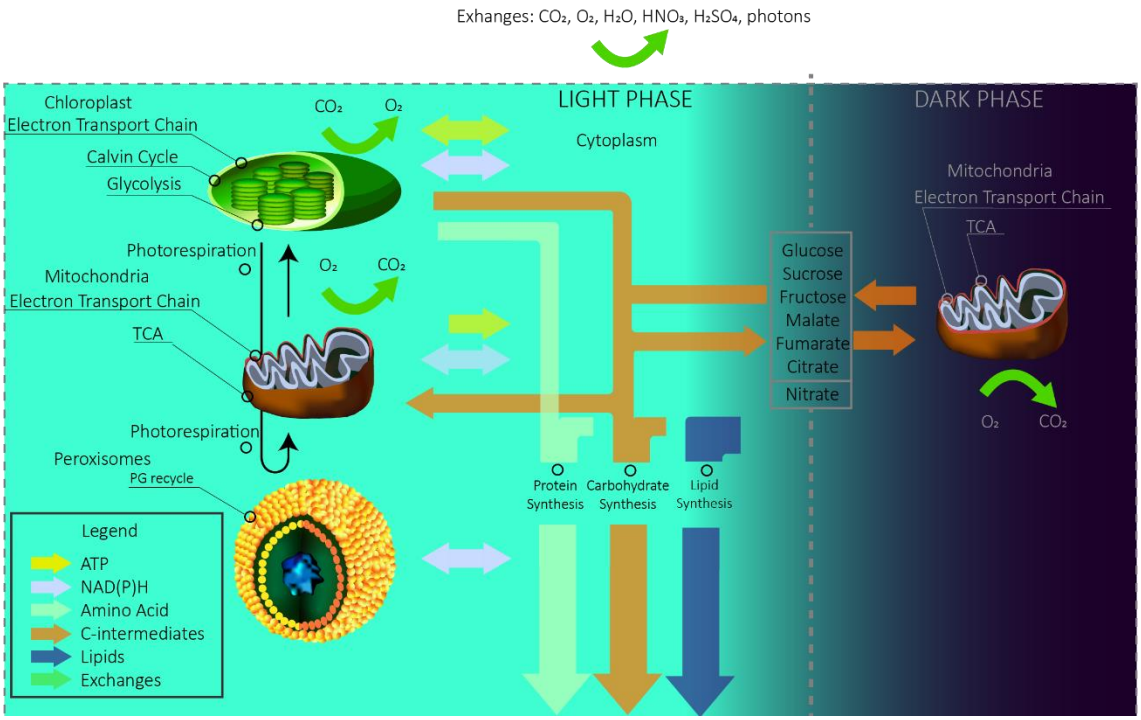

Fig 5. 2. Structure of the diel model presented. Four compartments (chloroplast, mitochondria, peroxisomes and cytoplasm) and the two phases of the day (light and dark) are considered with exchange reactions including metabolites diffused through leaves (CO_2, O_2, H_2O, light photons) and through the roots (HNO_3 and H_2SO_4). PG represents 2-Phospho-glycolate

The diel model is composed by different organelles including chloroplasts, mitochondria, peroxisomes, and cytoplasm. The proposed model also features plants simultaneity of metabolic pathways (i.e. glycolysis in chloroplast and cytoplasm or the folate metabolism in chloroplasts, cytoplasm and mitochondria) as well as the aforementioned coordination between day phases. A summary of the metabolic model can be found in Appendix 2 and the model in SBML format

can be accessed in the github link of the author (https://github.com/HigherPlantsModelling/Frontiers-in-Plant-Science).

The metabolic network model is mathematically formalized as a constraint-based model and the fluxes are calculated by applying a flux balance analysis (Cheung et al., 2014):

$$\begin{aligned} &\underset{v}{max} && (v_{biomass}[d]) \\ &subject: && lb \leq Sv \leq ub \\ & && Cv = F \end{aligned} \tag{102}$$

In the FBA formulation in (102), the objective function refers only to the daily biomass production. It is well known for other crop species like *Arabidopsis thaliana* that biomass growth also takes place during the dark phases of the day (Gomes et al., 2015). However, night metabolism of non-starchy crops like *lettuce* is still not clear so in the current approach maintenance-associated reactions are limited to night metabolism whereas metabolism associated to light periods of the day concentrates, on top of maintenance, also biosynthetic reactions. Letter v represents the array of fluxes for each of the reactions of the model. The lower and upper bounds (lb and ub) are fixed only for those fluxes indicated in Table 5. 1. Matrix C contains the information regarding the flux ratios specified in Table 5. 1 and matrix F represents the resulting flux. The inequality constraints represented in Table 5. 1 are generated in levels 3 and 2 of the model and are used to feed the FBA. $ATP_{maintenance}$ and $NAD(P)H_{maintenance}$ includes the reactions that contribute to the consumption of ATP and the reducing agent for respiration purposes. As suggested in Cheung et al., (2013), this can be achieved including generic ATPase and NAD(P)H oxidase reactions. Finally, the enzyme rates included are those related to constrain the reducing power supply in the cytoplasm. At night, plastidic NADP-malate dehydrogenase and glyceraldehyde 3-phosphate dehydrogenase are downregulated(Mekhalfi et al., 2014; Miginiac-Maslow & Lancelin, 2002). Finally, minimums and maximums for a set of reactions are defined given the presence of thermodynamically infeasible loops when no restrictions are applied. These reactions include: PYK, Pyruvate kinase; PGM: Phosphoglycerate mutase; ENO: Enolase; EB1: Inorganic pyrophosphatase; EB2: Inorganic pyrophosphatase; ACS: Acetyl-CoA synthetase; Ser_bio_cl: Phosphorylated Serine pathway; GOGAT: Glutamate synthase; Prot32: 3 Mercaptopyruvate Sulfurtransferase/cytoplasmic aspartate aminotransferase; OASTL: Cysteine synthase; GS: Glutamine synthetase. The FBA presented is implemented in both Matlab ® 2021 using the Cobra Toolbox (Becker et al., 2007a) and in python 3.0 using Cobrapy (Ebrahim et al., 2013) and can be found in the github link of the author (https://github.com/HigherPlantsModelling/Frontiers-in-Plant-Science).

Table 5. 1. Flux Balance Analysis equality, inequality and flow ratio restrictions. [d] and [n] indicate day and night phase period respectively. Subscripts c, m, cl and p indicate cytoplasmic, mitochondrial, plasmidic and peroxisomal location. lb and ub represent lower and upper bound respectively. List of enzyme abbreviations: GAPN: Cytosolic Non-phosphorylating NADP-Glyceraldehyde-3-phosphate dehydrogenase. GAPDH: Cytosolic Glyceraldehyde 3-phosphate dehydrogenase. MDH: Cytosolic Malate dehydrogenase. OPPP: Glucose-6-Phosphate dehydrogenase and 6-phosphogluconate dehydrogenase. ICDH: Isocitrate dehydrogenase. MDH: Malate Dehydrogenase. SGT: Serine-glyoxylate aminotransferase. GT: Glutamate-glyoxylate aminotransferase

Inequality Constraints	**Type**	**Description**
$v_{Ex_{CO_2}}$	lb	Gas Exchange
$v_{Ex_{O_2}}$	ub	Gas Exchange
$v_{Ex_{H_2O}}$	lb	Gas Exchange
$v_{F_{LETC}}$	ub	Light ETC
v_{V_c}	ub	Carboxylation
v_{V_o}	lb	Oxygenation
Flux Ratios	**Value**	
$v_{Ex_{O_2}}[d]: v_{Ex_{CO_2}}[d]$	1.22:-1	Photosynthesis Rate (MELiSSA Pilot Plant)
$v_{ATPmaintenance}[d/n]: v_{NADPHmaintenance}[d/n]^*$	3:1	Maintenance (Cheun et al., 2019)
$v_{Ex_{CO_2}}[d]: v_{Ex_{CO_2}}[n]$	-1:0.25	Respiration (MELiSSA Pilot Plant)
$v_{ATPmaintenance}[d]: v_{ATPmaintenance}[n]$	1:1	Respiration (MELiSSA Pilot Plant); (J. Liu & van Iersel, 2021)
$v_{NADPHmaintenance}[d]: v_{NADPHmaintenance}[d]$	1:1	Respiration (MELiSSA Pilot Plant); (J. Liu & van Iersel, 2021)
$v_{OPPP_{[c,m,cl]}}[d/n] + v_{ICDH_{[c,m]}}[d/n] + v_{ME_{[c,m]}}[d/n]: v_{NADPHmaintenance}[d/n]$	1:1	(Corpas & Barroso, 2014)
$v_{SGT_{[p]}}[d/n]: v_{GT_{[p]}}[d/n]$	1:1	(Yu et al., 1984)
Enzyme Rates	**Value**	
$v_{GAPN_{[c]}}$	ub: 0.33	(Shameer et al., 2019)
$v_{GAPDH_{[c]}}$	lb: -93	(Shameer et al., 2019)
$v_{MDH_{[c]}}$	lb: -0.75	(Shameer et al., 2019)

*NADPH oxidation and ATP hydrolysis associated to maintenance reactions include plasmidic, cytoplasmic and mitochondrial locations.

5.2.1.5. Dynamic Model

The evolution of the different states of interest through time either for dry biomass, leaf temperature or gas compositions, can be obtained integrating their rates of generation or consumption over time. For dry biomass, this can be done straightforward from Pn, considering all carbon molecules captured by the plant are fixed into structural biomass:

$$M_x = \int_{t=t0}^{t=t_f} Pn \cdot BCmol \cdot dt \tag{103}$$

For the evolution of leaf temperature, it is necessary to solve an energy balance between the leaf temperature and the environment and to convert energy units to temperature degrees:

$$T_l = \int_{t=t0}^{t=t_f} \frac{(E_{hs} + E_{hd})A - (E_r + E_{conv} + E_{tr})LA}{C_p \frac{M_x}{DM}} \cdot dt \tag{104}$$

Finally, the oxygen concentration can be obtained by solving a mass balance within the growing crop chamber:

$$O_2 = \int_{t=t0}^{t=t_f} \frac{u \cdot (O_2^{in} - O_2) + v_{Ex_{O_2}}}{\mathrm{V}} \cdot dt \tag{105}$$

In (105), gas flow is represented by u, oxygen concentration in the input flow by O_2^{in} and the chamber volume is V.

5.3. Integration of the Multilevel Mechanistic Model with Advanced Control Architectures

Once defined the modelling strategy for higher crops, the second scope of this study is to integrate the use of metabolic models into and advanced control strategy. In different complex systems ranging from microgrids (Vasquez et al., 2010), life support (Ciurans et al., 2021) or water distribution systems (Ocampo-Martinez et al., 2012) to chemical plants (Marchetti et al., 2014; Scattolini, 2009), the use of advanced control architectures have been proven to be efficient in terms of optimal management and control. Advanced control architectures are characterized by hierarchically distributing management and control functions in different levels. In this study, an adaptation of a common control architecture used in process plants is adapted to control oxygen in a crop-growing chamber. The top layer called Steady-State Target Optimization (SSTO) aims at finding reference values for the controlled and manipulated variables given a specific setpoint through solving a mass balance problem at steady state. The output of SSTO are the controlled and manipulated variables that give the closest estimation of the controlled variables to the setpoint at steady state. This output becomes the input of the following control step in the hierarchy, which is a model-based predictive control (MPC). MPC uses a discretized model of the process to be controlled and aims at finding the sequence of control commands along a prediction horizon that brings the predicted controlled variables the closest to the reference given a set of hard and soft constraints. MPC works based on a rolling-horizon approach, which essentially solves the minimization problem along the defined prediction horizon but sends solely the control command corresponding to the first step. This process is repeated every time

the controller is executed (Pannocchia & Bemporad, 2007). In Fig 5. 3, a schematic representation of the advanced control architecture with details on the communication among its levels is presented. In the presented study, the controlled variable is the oxygen concentration in the chamber whereas the manipulated variable is the gas flow.

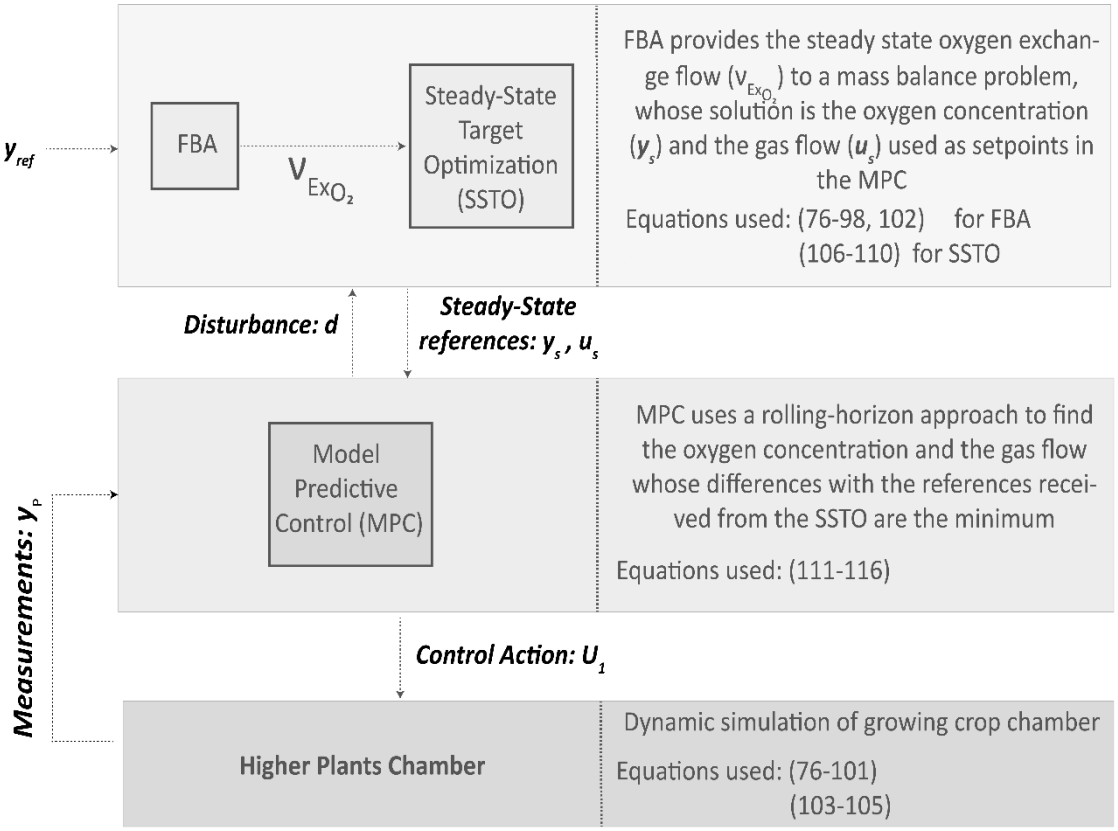

Fig 5. 3. Scheme of the advanced control architecture proposed to integrate metabolic models

The SSTO solves the following system of equations using the output of FBA, considering oxygen exchange rate ($v_{Ex_{O_2}}$) as the generation rate in a steady-state mass balance:

$$u_s\left(O_2^{in} - x_s\right) + v_{Ex_{O_2}} = 0 \tag{106}$$

$$x_s + d = y_s \tag{107}$$

$$y_s = y_{ref} \tag{108}$$

s.t.

$$y_L \leq y_s \leq y_U \tag{109}$$

$$u_L \leq u_s \leq u_U \tag{110}$$

The output of the SSTO is provided as a reference to the MPC, which in this case is the concentration of oxygen in the chamber (x_s) and the external gas flow (u_s) both at steady state. The internal model at steady state is defined in (78) being the generation term ($v_{Ex_{O_2}}$) the output of the FBA, O_2^{in} the input oxygen concentration and the internal model prediction defined by x_s. A disturbance (d) is incorporated in (107) to take into account any possible plant-model mismatch or a measured perturbation and must be taken into account for the new reference generation. Hence, the final prediction value (y_s) at steady state considering the presence of any given disturbance will match the process measurement guaranteeing offset-free control (Pannocchia & Bemporad, 2007). The expression to obtain the disturbance is defined in the MPC development hereafter. The technical upper and lower bounds of controlled and manipulated variables are summarised in (109)-(110) and thus do not need to be defined in the MPC. It is then possible to violate constraints on controlled and measured variables during transition states but not at steady state (Marchetti et al., 2014).

The MPC solves a rolling horizon nonlinear optimization problem taking the output of the SSTO as the reference to track:

$$J = \min_{U} \lambda_1 \sum_{i=k}^{i=N_p} \frac{|\hat{x}(i|k) - x_s|^2}{\Delta x} + \lambda_2 \sum_{i=k}^{i=N_c} \frac{|u(i|k) - u_s|^2}{\Delta u} + \lambda_3 \sum_{i=k}^{i=N_c} \frac{|u(i|k) - u(i-1|k)|^2}{\Delta u} \tag{111}$$

s.t.

$$\hat{x}(i+1|k) = \hat{x}(i|k) + U(i|k)\left(O_2^{in} - \hat{x}(i|k)\right)\frac{T_s}{V} + v_{Ex_{O_2}}\frac{T_s}{V} \tag{112}$$

$$\hat{y}(i|k) = \hat{x}(i|k) + \mathrm{d}(i|k) \tag{113}$$

$$\mathrm{d}(i|k) = y_p - \hat{x}(2|k-1) \tag{114}$$

$$\mathrm{d}(i+1|k) = \mathrm{d}(i|k) \tag{115}$$

$$U = \begin{bmatrix} U(i|k) \\ \vdots \\ \mathrm{U}(N_c|\mathrm{k}) \end{bmatrix} \tag{116}$$

The cost function in (111) includes penalization terms to the deviation of the internal prediction ($\hat{x}$) and the control command (u) from the concentration (x_s) and the gas flow (u_s) references generated in the SSTO. A third penalization term to the rate of change of the manipulated variable is also included in (111) aimed to adjust the speed of the controller response. All three penalization terms are normalized using the range of possible maximum and minimum values for both controlled and manipulated variables (defined by Δx and Δu) and are subject to a scaling

factor (λ). Prediction and control horizons are represented by N_p and N_c respectively. Constraint in (112) reflects the dynamics of the growing crop chamber with T_s as the sample time of the MPC. The internal model is initialized with the current process measurement (y_p). In (114) the disturbance is integrated to the internal model prediction as similarly done in the SSTO in (107). This disturbance is estimated at each sampling time and is defined as the difference between the process measurement (y_p) and the first step prediction of the previous MPC execution ($\hat{y}(2|k-1)$) as stated in Tatjewski et al., (2017). It is assumed in (40) the disturbance to be constant through the whole prediction horizon. The output matrix of gas flows (U) is expressed in (116) and only the control action for the first step of the control horizon is sent to the control actuators until next SSTO and MPC execution. This control strategy is implemented in Matlab ® 2021 using the Optimization Toolbox for solving nonlinear programming problems and Cobra Toolbox – 2022 for the FBA resolution(Becker et al., 2007).

5.4. Simulation Scenarios

Two simulation packages are presented. First, the results of the multilevel model presented in Section 5.2.1 and their validation with experimental data. Second, a dynamic simulation presenting the response of the control architecture presented in Section 5.2.2 under different perturbations.

5.4.1. Simulation conditions for Multilevel Model Validation

CO_2-response curves were generated using the fixed light intensity indicated in 4 and the following range of internal CO_2 values in µmol CO_2/mol: 100, 225, 300, 450, 600, 850, 1000, 1100. Light-response curves were generated using the fixed internal carbon dioxide concentration indicated in Table 5. 2 and the following range of light intensity values in µmol/m^2/s: 100, 200, 350, 500, 600, 800, 1000, 1200. Considering the conditions listed in Table 5. 2 and the model equations (76) -(101), it is possible to retrieve the inequality constraints described in Table 5. 1 and thus the FBA can be resolved. Results are represented in section 5.3.1. The distribution of fluxes is analysed for both light and dark metabolism using atmospheric conditions for CO_2 which are 400 ppm and a light intensity of 400 µmole/m^2/s. Results are graphically represented in Section 5.3.2.

Table 5. 2. List of operating parameters used in FBA simulation

Parameter	Value	Units
Leaf area (LA)	25	m^2 leaf
Leaf area index (LAI)	5	m^2 leaf/ m^2 ground
Growing Area (A)	5	m^2 ground

Chamber Height (H)	1	m
Bulk Temperature (T_b)	25	ºC
Bulk Pressure (P_b)	101300	Pa
Relative Humidity (RH)	70	%
Light Intensity (I_u)	800	µmol/m²/s
Internal CO_2 concentration (C_i)	400	µmol/mol
Forced Velocity (v_{forced})	0.3	m s^{-1}

5.4.2. Advanced Control Architecture Configuration

In Table 5. 3, the controller specifications and parameter values are indicated. On top of the control objective defined in Section 5.2.2, atmospheric CO_2 is controlled at 800 ppm with external addition of pure CO_2.

Table 5. 3. Controller specifications including SSTO and MPC algorithms.

Parameter	**Value**	**Units**
Input Oxygen Concentration (O_2^{in})	0	%
Oxygen setpoint (y_{ref})	21	%
Carbon dioxide setpoint	800	ppm
Lower and upper bounds oxygen Concentration ($y_L - y_U$)	18-24	%
Lower and upper bound flow (($u_L - u_U$))	0-1	m³/h
Scaling factor ($\lambda_1, \lambda_2, \lambda_3$)	10,1,1	
Prediction horizon (N_p)	4	
Control horizon (N_c)	3	
Sample time (T_s)	720	s

Noteworthy, the scaling factors are used to promote the control of the system close to the setpoint but at the expense of having a more aggressive control. Prediction and control horizons are important tuning parameters of the controller increasing its sensitivity but also the computational cost of the calculation. Finally, the sampling time also affects the control performance. For slow systems like a plant cultivar, sample times should not be too short because the prediction would not have enough perspective to take correct decisions. Tuning model based predictive controllers is critical to achieve a good process operation and represents a trade-off between the expected performance and the controller and system capabilities. The

metabolic-based control architecture represented in Fig 5. 3 is tested in a 24-hour dynamic simulation using the operating conditions listed in Table 5. 2.

5.5. Results

This section is divided in two parts, the first dedicated to present the output of the multi-level model and its validation with experimental data and the second related to the integration of that modelling approach containing metabolic information into an advanced control architecture.

5.5.1. Validating Photosynthesis Rates

The results of the model introduced in Section 5.2.1 are represented in Fig 5. 4, where modelled and experimental results for mature leaves (28 days after transplanting) are compared.

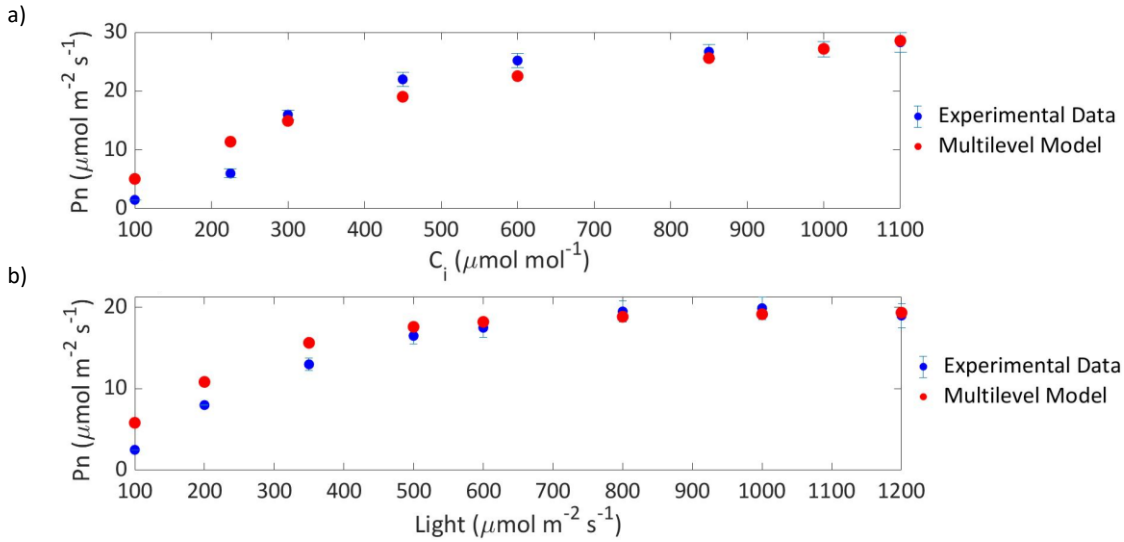

Fig 5. 4. Model validation through the comparison of the photosynthesis rate expressed as net carbon assimilation (Pn) as a function of internal carbon concentration and light irradiance. In a) a fixed light intensity of 800 µmole/m²/s is set; in b) a fixed internal carbon concentration of 400 µmol/m²/s is set. Experimental data is based on Zhou et al. (2020).

Fig 5. 4a represents the RuBisCo saturation curve showing a fast rate of change in the smaller range of internal carbon dioxide concentrations, a pattern which is reproduced in Fig 5. 4a which shows the light electron transport chain saturation curve. The maximum net photosynthesis rate achieved in the light-response curve is lower than the maximum achieved in the CO_2-response curve because in the former the internal CO_2 concentration used for the simulation is 400 µmole CO_2/mol reaching the expected photosynthesis rates if compared to Fig 5. 4a. Finally, the output of the model is comparable to the reported experimental results by J. Zhou et al., (2020) under the same operating conditions. Overall, the error observed in the modelled results in relation to

the experimental values is higher at low internal carbon concentrations and at low light intensities.

5.5.2. Distribution of Metabolic Fluxes using a Metabolic Diel Model

In this section, the flux distribution of day and night metabolites obtained after the resolution of the FBA introduced in (102) are presented. The parameters used for the simulation are those provided in Table 5. 1.

5.5.2.1. Day Flux Distribution

The day flux distribution is presented in Fig 5. 5. The central carbon metabolism of plants in light conditions is well represented in this model with the main fluxes located in the Calvin Cycle associated reactions. The results indicate that, as has been extensively studied and published (Michelet et al., 2013; Tan & Cheung, 2020), the flow through the Calvin Cycle generates triose phosphate (g3p) from ribulose 1,5-biphosphate (RuBP), consuming part of the reducing power and ATP molecules synthesized during the light electron transport chain. Triose phosphate is used to feed the rest of the Calvin Cycle machinery aimed at restoring the ribulose 1,5-biphosphate while it is also partially used to generate photosynthetic end products (McClain & Sharkey, 2019).

As previously stated, higher plants store carbon during the light phase of the day, to be used during night respiration and fuel maintenance processes. For non-starchy crops, even though they can still generate starch, most of the carbon fixed during the light phase is stored as soluble sugars or organic acids. In this study, the sugar molecules stored and mobilized between light and dark periods of the day have not been restricted and, as Fig 5. 5 suggests, sucrose, glucose, citrate and malate and with a lower flux fumarate are the metabolites used for carbon exchange. This modelled result fits well the reported experimental concentrations of sugars in lettuce at harvest, being glucose, sucrose and fructose, the main carbohydrates found for carbon exchange between phases of the day (Chen et al., 2019b) and also predicting with accuracy the role of malate accumulation during light phase of the day in vacuoles for its use in dark (Lee et al., 2021). Not all carbon compounds mobilized from light to night metabolism are consumed during the latter. Therefore, some carbon intermediates need to be exported from night to light metabolism too. Specifically, citrate imported from dark periods is used in light phase of the day to generate oxoglutarate which is important for the nitrogen assimilation mechanism and for the synthesis of nitrogen-rich amino acids. The citrate cycle and its interactions with amino acid biosynthesis is well covered by the presented model, both suffering a flux reduction when nitrate uptake is limited. (Morcuende et al., 1998; Weiwei Zhou et al., 2021).

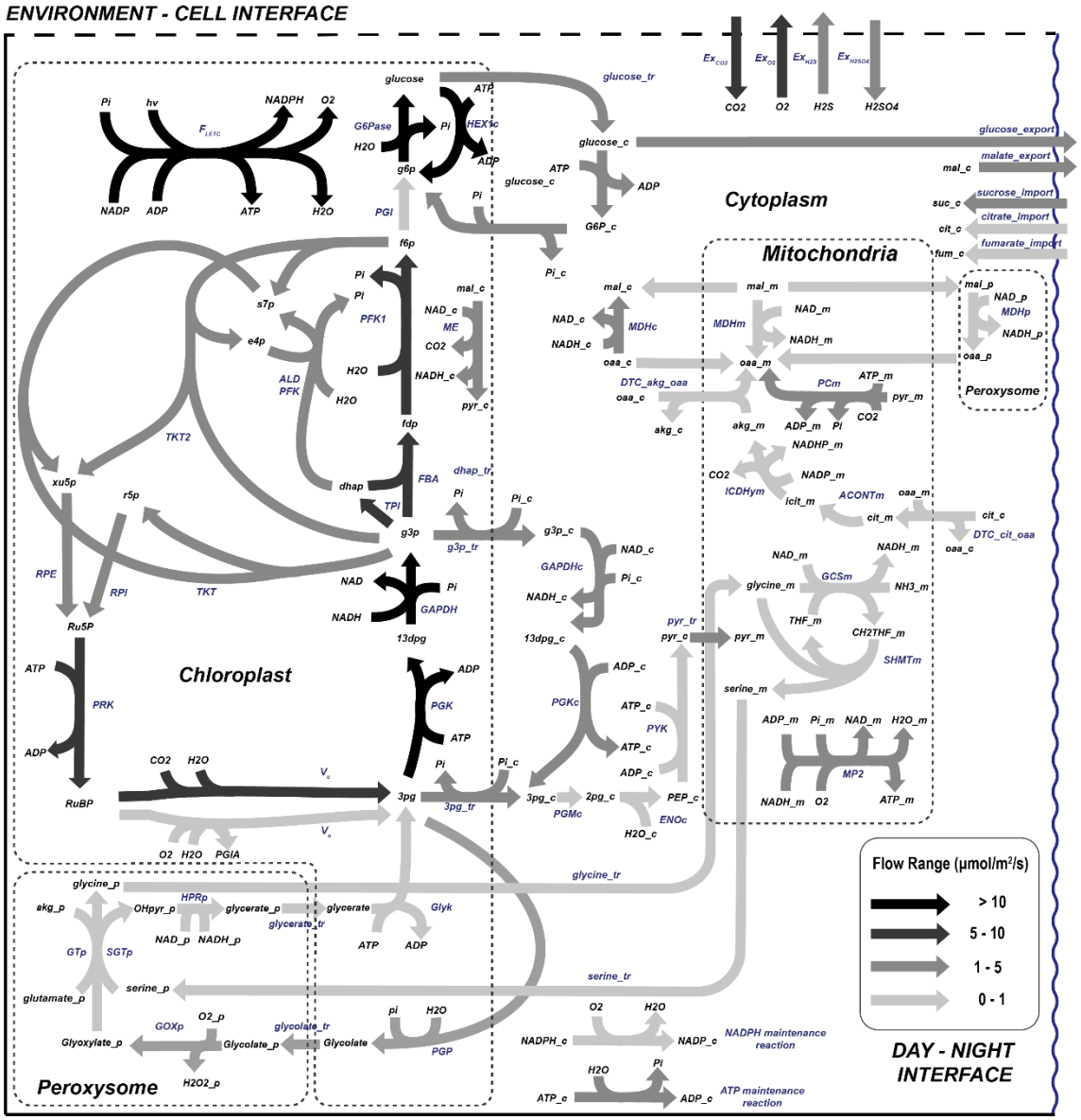

Fig 5. 5. Flow distribution of the central carbon metabolism during L. sativa grown during the light photoperiod. List of abbreviated enzymes or enzyme reactions. In chloroplast: F_{LETC}: Flow of light electron transport chain, G6Pase: Glucose-6-phosphatase, PGI: Glucose-6-phosphate isomerase, MDH: Malate dehydrogenase, FBPase: Fructose-1,6-biphosphatase, PFK: Phosphofruktokinase-1, ALD: aldolase TKT: Transketolase, TKT2: Transketolase 2, FBA: Fructose-1,6-biphosphate aldolase, TPI: Triose-phosphate isomerase, RPI: Ribose-5-phosphate isomerase, RPE: Ribulose-phosphate 3-epimerase, GAPDHy: NADP-Glyceraldehyde-3-phosphate dehydrogenase, PGK: Phosphoglycerate kinase, PRK: Phosphoribulokinase, V_c: Rubisco carboxylation, V_o: Rubisco oxgygenation, Glyk: D-Glycerate 3-kinase, PGP: Phosphoglycolate phosphatase. In peroxisome: GOXp: Glycolate oxidase, SGTp: Serine-glyoxylate transaminase, GTp: Glycine transaminase, HPRp: Hydroxypyruvate reductase, MDHp: Malate dehydrogenase . In cytoplasm: PGMc: Phosphoglycerate mutase, ENOc: Enolase, PYKc: Pyruvate kinase, PGKc: Phosphoglycerate kinase, GAPDHc: NAD-Glycerate-3-phosphate dehydrogenase, MDHc: NADH malate dehydrogenase. In mitochondria: ACONTm: Aconitase, ICDHm: Isocitrate dehydrogenase MDHm: Malate dehydrogenase, GCSm: Glycine cleavage system, SHMTm: Serine hydroxymethyltransferase, CSm: Citrate synthase, PCm: Pyruvate carboxylase, MP2: Mitochondrial phosphorylation 2.

One of the critical phenomena of plant photosynthetic cell metabolism is the coordination of photosynthesis and respiration, which essentially determines how and where are energy carrier molecules (ATP and NAD(P)H) produced. Most of the ATP and NAD(P)H used for catabolic reactions are produced in the light electron transport chain in chloroplasts for amino acid and

lipid production. Part of the ATP synthesized in chloroplasts is exported to the cytosol through the 3PG-G3P shuttle, satisfying the ATP demand together with ATP exported from mitochondria (Gakière et al., 2018; Shameer et al., 2019). The resulting metabolic network shows the mechanisms of redox power balancing in the different organelles of photosynthetic leaves enabled by the metabolite shuttles represented by the malate/oxalacetate and the triose phosphate/3-phosphoglycerate shuttle in Fig 5. 5 (and the glutamate/2-oxoglutarate and the malate/aspartate shuttle, not represented)(Taniguchi & Miyake, 2012). Around half the NAD(P)H generated in mitochondria comes from the glycine decarboxylation, which in turn generates the serine used in the serine-glyoxylate aminotransferase (SGT) in the peroxisome. It has been reported that malate dehydrogenase seems to regulate the reducing power in mitochondria based on the reduction state of the cells, removing, and restoring NAD(P)H at low and high-light conditions responding to changes in the photosynthesis rate (Bykova et al., 2014; Schertl & Braun, 2014a). This is validated in the presented fluxome, where mitochondrial malate dehydrogenase (MDHm) restores NAD(P)H together with the glycine cleavage system (GCS, also known as Glycine decarboxylase system) but behaves in the opposite direction, that means removing excess NAD(P)H in the mitochondria, at higher carbon dioxide concentration when photosynthesis rate is increased (see S7 and S8 for flux distribution at a CO_2 concentration of 1000 ppm and 400 µmole/m^2/s). The metabolic flux distribution represented in Fig 5. 5 also shows that TCA cycle is not complete during light photoperiods. This is mainly because most TCA intermediates are dedicated to anabolic reactions and pyruvate dehydrogenase (PDH) is photo-inhibited (Schertl et al., 2014b).

5.5.2.2. Night Flux Distribution

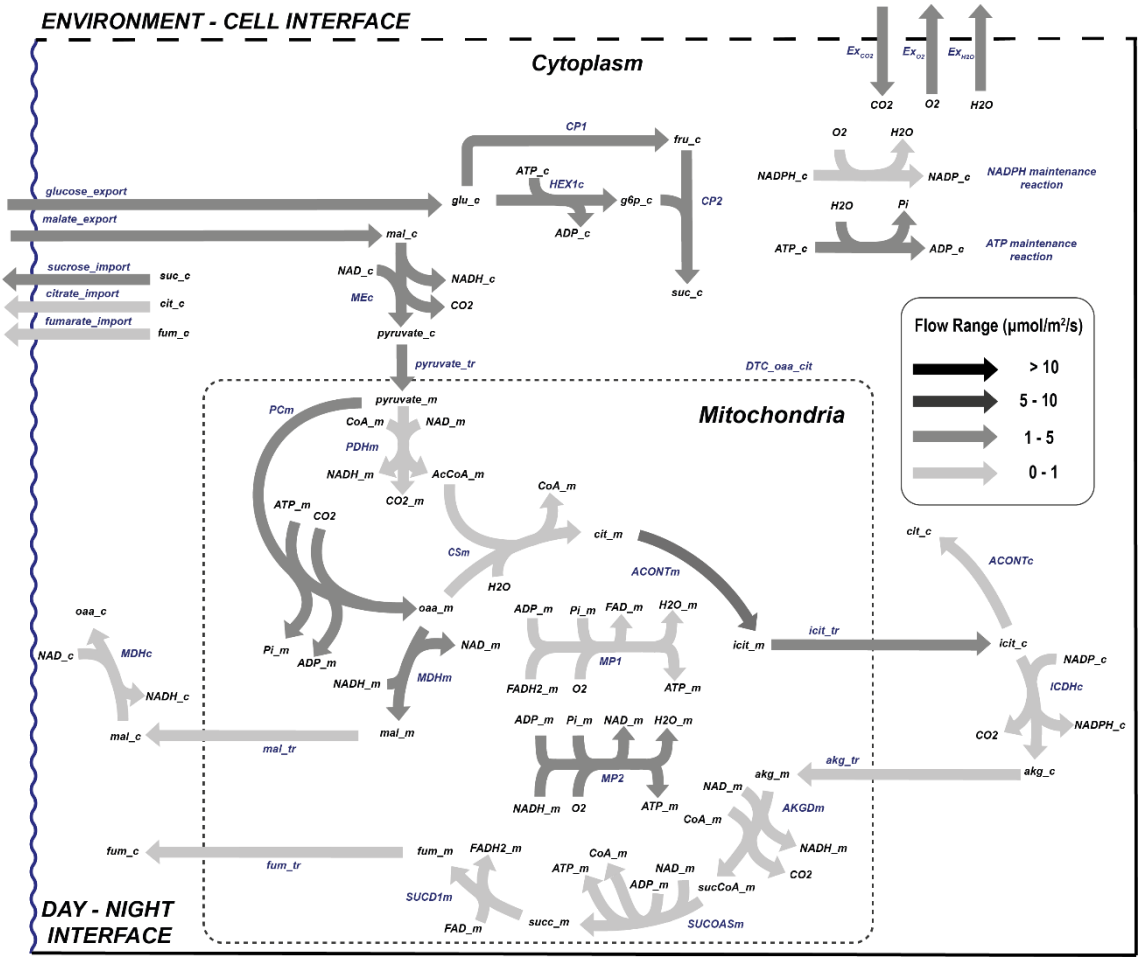

Fig 5. 6. Flow distribution of the central carbon metabolism during L. sativa dark phase. List of abbreviated enzymes or enzyme reactions. In cytoplasm: MDHc: Malate dehydrogenase, ICDHyc: NADPH isocitrate dehydrogenase, ACONT: Aconitase, MEc: Malic enzyme, CP1: Glucose isomerase, CP2: sucrose-6-phosphate synthase; In mitochondria: ACONTm: Aconitase, PDHm: Pyruvate dehydrogenase, PCm: Lyruvate carboxylase, CSm: Citrate synthase, AKGDm: α-oxoglutarate dehydrogenase, SUCOASm: Succinyl-CoA synthetase, SUCD1m: Succinate dehydrogenase complex, MDHm: Malate dehydrogenase, MP1/2: Mitochondrial phosphorylation 1/2

During the dark phase of the day in Fig 5. 6, ATP can only be produced in mitochondria being NAD(P)H the electron donor and thus completely modifying the flow distribution within the cell. Autotrophic organisms like plants, use the sugars generated and stored during the day to feed TCA, which is cyclic in dark conditions. In lettuce and other non-starchy vegetable, instead of mobilizing starch, glucose, sucrose or fructose are broken down to pyruvate at very similar proportions (Chen et al., 2019a) even though in this study the proportion of soluble sugar utilization has not been constrained. The pyruvate produced in the glycolysis is then transferred to the mitochondria to regenerate the reducing power needed to fuel the mitochondrial respiration. In dark conditions, the exchange rates are completely opposite to those observed in light conditions, being carbon dioxide and water released and oxygen consumed. In a way, respiration and photosynthesis are opposite processes, but complementary as demonstrated during crop growth. The governing rule of night metabolism is represented in Table 5. 1 in the

ratio of consumed CO_2 during day phase over produced CO_2 due to night respiration (Ex_{CO2}[d]:Ex_{CO2}[n]) which sets the night carbon conversion.

5.5.3. Sensitivity Analysis

FBA is a powerful tool but strongly affected by its mathematical formalization and particularly by the flux boundaries choice (Raposo et al., 2020; Nobile et al., 2021). A sensitivity analysis on the selected boundaries is very useful for detecting those constraints (either hard or soft constraints) that generate the highest impact on the flux distribution and thus requires a thorough parameter identification. But sensitivity analysis can also be used to detect those fluxes with the highest variability in relation to a given boundary, metabolic model shortcomings or fluxes that are invariable to the boundaries. A local sensitivity analysis is presented, with a focus on the flux ratios defined in Table 5. 1, which are either defined empirically or based on literature and may be prone to uncertainty. The sensitivity analysis has also been explored for the light irradiance. Details on the ranges of flux ratios explored for this analysis are presented in Table 5. 4.

Table 5. 4. Range of values explored in sensitivity analysis. The percentage is applied to the nominal ratio (i.e. for the photosynthesis rate ratio, the range explored is from 0.8:1 to 1.59:1). The whole range is splitted in 6 points.

Flux Ratios	Nominal Ratio	Range	Description
$Ex_{O2}[d]$: $Ex_{CO2}[d]$	1.22:1	[-30%, +30%]	Photosynthesis Rate
$ATP_{maintenance}[n]$:$NADPH_{maintenance}[n]$	3:1	[-30%, +30%]	Maintenance
$ATP_{maintenance}[d]$:$NADPH_{maintenance}[d]$	3:1	[-30%, +30%]	Maintenance
$Ex_{CO2}[n]$:$Ex_{CO2}[d]$	0.25:1	[-30%, +30%]	Respiration
I_u	400 µmol m^{-2} s^{-1}	[-30%, +30%]	Irradiance

The sensitivity analysis has been based on the variability of the fluxes along the range of flux ratios allowed. Such variability is expressed as the normalized summation of the slopes in each of the steps of the range of flux ratios explored:

$$FV_{j,z} = \sum_{i=1}^{i=6} \frac{\frac{v_{i+1,j,z} - v_{i,j,z}}{\Delta r_z}}{\Delta v_{j,z}} \tag{117}$$

$$\Delta v_{j,z} = \max(v_{j,z}) - \min(v_{j,z}) \tag{118}$$

In (117), *i* index refers to the discrete steps in which the range of flux ratios has been divided (a total of 6 steps for each flux ratio) whereas index *j* and *z* refers to the reaction and the flux ratio respectively. The parameter Δr_z is the increment in the flux ratio expressed as a fraction and

equivalent to 0.1 for all cases. The denominator $\Delta v_{j,z}$ is used to normalize the summation of slopes and it represents the range of values for a given reaction *j*. The sensitivity analysis has been carried for light and night metabolism and is represented in Fig 5. 7 considering an atmospheric concentration of CO2 of 1000 ppm in order not to limit by carbon substrate and a nominal light intensity of 400 µmole/m^2/s.

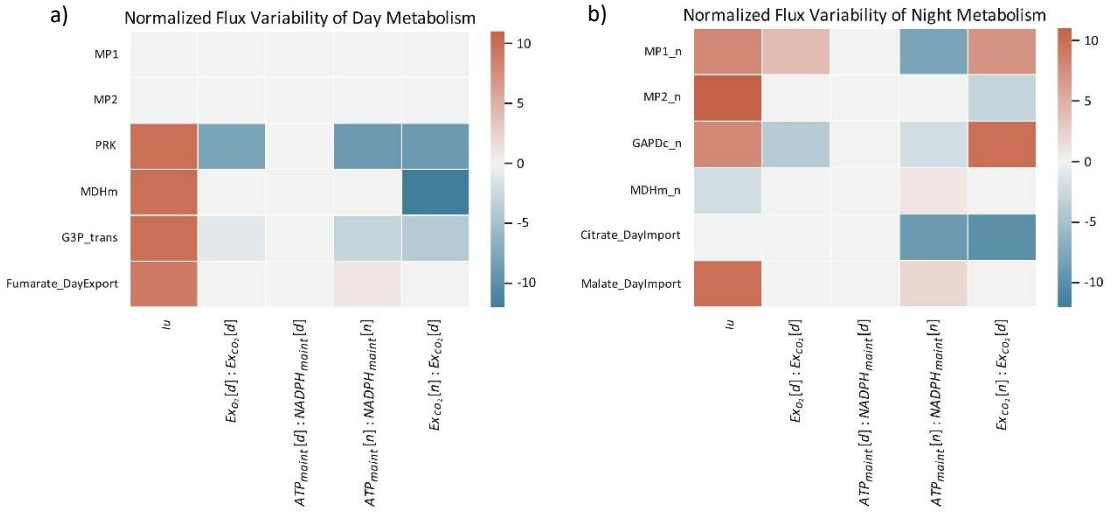

Fig 5. 7. Normalized sensitivity analysis result of a selection of day (A) and night (B) metabolic fluxes (B) according to a given range of ratios and constraints explored

Considering the light metabolism sensitivity analysis (Fig 5. 7), the light phase of day-time mitochondrial respiration is never active. In the predicted fluxome for all range of flux ratios applied, the ATP production comes mainly from chloroplast activity. The main mitochondrial NADH producer in light conditions is the GDC system, being consumed mainly by the malate dehydrogenase activity and not by the electron transport chain (Bykova et al., 2014). The lack of the electron transport chain in day metabolism is due to the lack of maintenance reactions during light period. When light is increased, the reactions associated to the regeneration of RuBP are activated. This is the case of the phosphoribulokinase (PRK), which restores the ribulose 1,5-biphosphate. An increase in the triose phosphate export activity (G3P_trans) is also detected responding to the increase in the carbon fixation. The mitochondrial malate dehydrogenase (MDHm) is also augmented in first place to respond to the increased anabolic demands and in second place given the increased flux through photorespiration that triggers the GCS and the consequent increased consumption of NADH through MDHm to keep the redox balance in mitochondria (Schertl & Braun, 2014b). The sensitivity analysis of the day metabolism also highlights that, when the night respiration flux in relation to the daily carbon fixation is increased relative to the nominal value of 0.25, the associated photosynthetic reactions (PRK and G3P_trans) are reduced.

Regarding night metabolism (Fig 5. 7B), the variability of the represented reactions is higher than in day metabolism. When light intensity (I_u) is increased, night mitochondrial activity (MP1_n and MP2_n) is also increased to respond to the maintenance reactions demands (Frantz et al., 2005). The activity of glyceraldehyde 3-phosphate dehydrogenase (GAPDc_n) responds to the increased flux towards glycolytic pathways to process the carbon compounds converted during night metabolic activities (Schneider et al., 2018; Gaude et al., 2018). In the dark phase, with the cyclic TCA cycle re-stored, the excess TCA intermediates and soluble sugars not used to fuel dark metabolism are stored and re-used in light metabolism for nitrogen assimilation and biosynthesis reactions(Igamberdiev & Eprintsev, 2016; Popova & Pinheiro De Carvalho, 1998). In this way, the pool of organic carbon compounds and reducing equivalents is managed by the plants as a response to variations in the day carbon fixation efficiency and night respiration activities. GAPDc_n is also positively affected when the ratio of respiratory produced over photosynthetically consumed CO_2 is increased (Ex_{CO2}[n]:Ex_{CO2}[d]) with the availability of citrate and the other TCA intermediates usage in light photoperiods reduced given the night metabolic increased activities as suggested by the citrate import flux. Therefore, an increased night CO_2 release is corresponded by an increased glycolytic activity represented by GAPDC_n, also impacting the TCA intermediates and soluble sugar accumulation at night.

5.5.4. Testing the integration of Multilevel Model Approach to Advanced Control Architectures in Dynamic Simulations

The control strategy presented based on a new approach combining the prediction capacity of MPC and the integration of constraint-based metabolic modelling has been tested in a 24-hour dynamic simulation. To do that, different perturbations have been included at different points of the simulation to test the resiliency of the proposed control approach, its capacity to overcome common control challenges and to analyse its versatility:

- At 5hr of simulation time, a plant-model mismatch has been introduced by adding a perturbation in the form of a multiplication factor to the gas flows in (106):

$$2u_s\left(O_2^{in} - x_s\right) + v_{Ex_{O_2}} = 0 \tag{119}$$

$$\hat{x}(i+1|k) = \hat{x}(i|k) + 2U(i|k)\left(O_2^{in} - \hat{x}(i|k)\right)\frac{T_s}{V} + v_{Ex_{O_2}}\frac{T_s}{V} \tag{120}$$

- At 10hr of simulation time, a perturbation in the process output has been introduced by adding a sudden decrease in the oxygen concentration from the measurement to 20.8%.
- At 16hr of simulation time, a change in the oxygen setpoint from 21% to 21.2% has been included.

The results of this simulation schedule are presented in Fig 5. 8. It is observed that when a plant-model mismatch is deliberately included, the controller can keep minimising the offset of the O_2 measurement in relation to the reference (Fig 5. 8a). Similarly, when an abrupt perturbation is added at 10hr of simulation, the gas flow is stopped to restore the oxygen concentration rapidly. Finally, when the reference is modified from 21% to 21.2%, the gas flow is also reduced in order to accumulate oxygen in the growing chamber and reduce the tracking error (Fig 5. 8b). The control of CO_2 is achieved by externally injection of pure CO_2 (Fig 5. 8C).

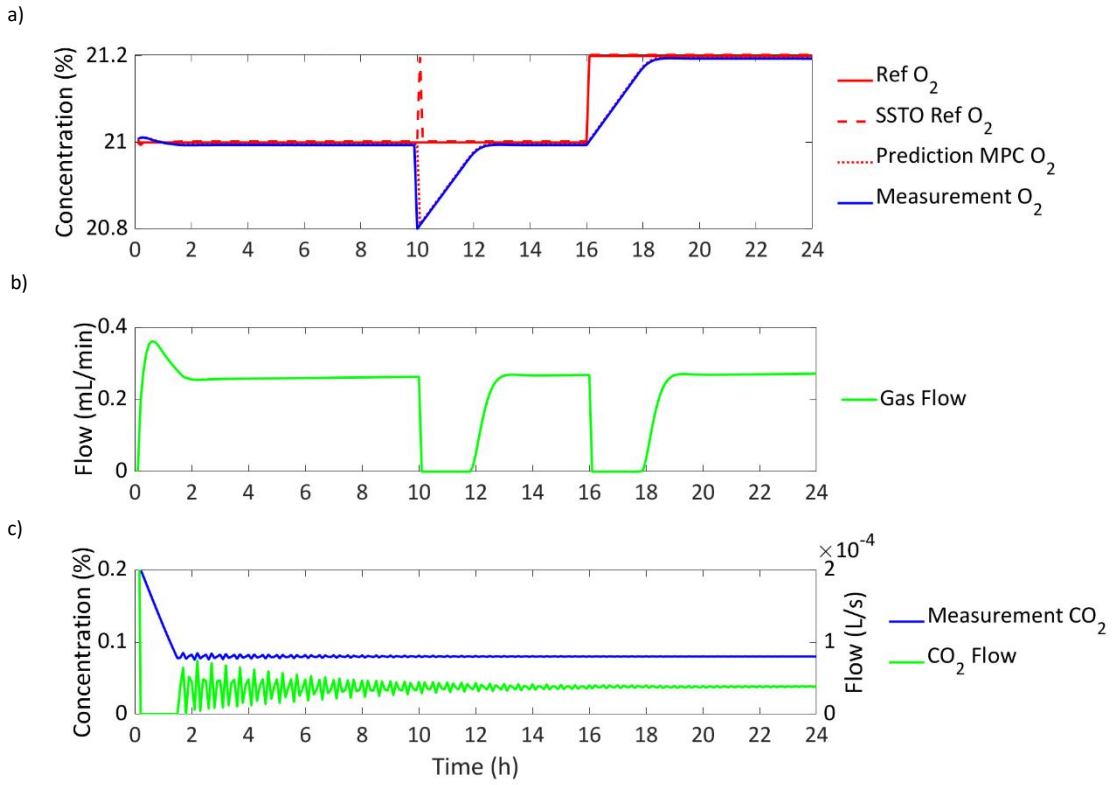

Fig 5. 8. Dynamic control performance under introducing different perturbations at 5, 10 and 16 hours as described in the text. a) Evolution of O_2, the controlled variable; b) and c) Evolution of the manipulated variables flow and CO_2 injection respectively

The controller is thus demonstrated to be resilient and smooth to overcome any of the perturbations applied as well as on the nominal operation. This performance is due to the reliable metabolic-based model introduced in the MPC and largely due to the integration of a disturbance specially to achieve offset-free control. In Fig 5. 9, the comparison of the controller performance with and without disturbance integration is represented. It can be observed that under different perturbations, when disturbance is integrated in the internal model of both the SSTO and the MPC, offset is reduced and thus the reference tracking is improved. Nevertheless, not all disturbances can be rejected using a constant state disturbance prediction as defined in

(107), especially in scenarios where plant-model mismatch are bigger, that is when models are less reliable than the one presented in this study. In the case of higher model disagreement, disturbance integration approaches should be considered like integrating the error in the multistep model prediction (Tian, X.; Wang, P.; Huang, D.; Chen, 2007) or integrating a moving horizon estimation (MHE) and MPC to estimate uncertainty parameters and to include them in the MPC algorithm (Huang et al., 2010). Disturbance rejection especially in the situation of plant-model mismatch has been highly analysed within MPC development and certainly, the future metabolic-based controllers will need to deal with a wide diversity of model typology from simplified and surrogated models to complex genome-scale metabolic models.

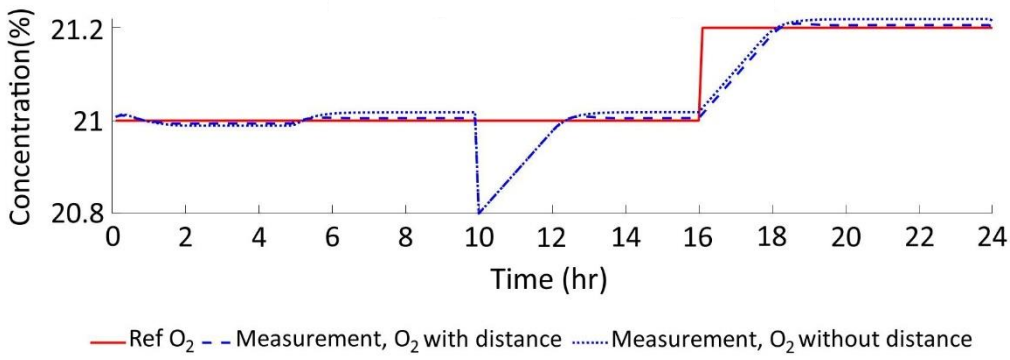

Fig 5. 9. Comparison of the controller performance in terms of reference tracking between controllers including or not disturbance rejection in the internal SSTO and MPC models

5.6. Conclusions

Modelling higher plants has major challenges to deal with. These challenges include huge metabolic changes associated to the light and night photoperiods, substrate partitioning given the heterogenic requirements of the different tissues present in higher plants, organelle coordination, complex morphologies that condition the interaction with the environment and many other phenomena still not fully understood. In this study, a multi-level model has been designed with the main mechanistic phenomena that drives crop grow distributed into different levels in decreasing order of scale length. The output of the mechanistic multilevel model has been connected to a constraint-based metabolic model providing information of high interest about cell metabolism. The presented multilevel model offers the advantage to merge all the available information related to plants growth in a structured way ensuring the solution found to be feasible for all the phenomena described in the different layers in the model hierarchy, from light reception and biochemical conversion down to specific metabolic pathways, a feasibility that cannot be granted in only mechanistic or metabolic-based models using stand-alone modelling strategies. This method has been validated with experimental data, integrated and tested in a novel advanced control strategy with promising results. Computational

capabilities are less constraining nowadays, making it more realistic to contemplate the design of control strategies that can integrate more information about the system under operation. In this study, the focus has been placed in the use of metabolic information embedded in a model predictive control providing promising results in a dynamic simulation of a growing crop chamber with a range of applications going from agriculture to life support systems. It is in the framework of the MELiSSA project and by extension to the field of fully regenerative life support systems where structural multi-level models, integrating from physical to metabolic information, emerges as an opportunity to design model-based predictive controller techniques. These advanced control strategies should be further explored with different levels of metabolic complexity, in different control formulations and applied to different bio-based processes as they may contribute improving the overall performance through exploiting the increasingly available metabolic information.

5.7. Appendixes

5.7.1. Appendix 1: Boundary Layer Model

In this appendix the boundary layer model is presented based on the work by Poulet et al., (2020)

Morphological module

Leaf area (LA) is expressed as a function of biomass accumulated following a logistic approximation:

$$LA = 3(1 + e^{(220 - \frac{0.016 M_x}{DM})}) \tag{121}$$

Being DM the dry mass ratio fraction and M_x the accumulated dry biomass. Leaf length (L) is approximated considering a circular shape:

$$L = 2\sqrt{\frac{LA}{\pi}} \tag{122}$$

Biochemical module

According to Harley et al. (1992), the temperature dependence of F_{LETC}^{max} and V_{cmax} is described by the following expressions:

$$F_{LETC}^{max} = F_{LETC}^{max25} \frac{exp\,[(3.3621 \cdot 10^{-3} T_l - 1)E/(RT_l)]}{1 + exp\,[(ST_l - H')/(RT_l)]} \tag{123}$$

$$V_{cmax} = V_{cmax25} \frac{exp\,[46.9411 - 116300/(RT_l)]}{1 + exp\,[(650T_l - 202900)/(RT_l)]} \tag{124}$$

In (49) k_c is the turnover number of carboxylase sites, which in this model a value of 2.5 s^{-1} has been used as suggested by Farquhar et al. (1980). At 25ºC the value of k_o, the equivalent of k_c for oxygenase sites is 0.21 times that of k_c.

Gas exchange module

In (3) the conductance of the different gases through the leaves is introduced. Two layers are considered to calculate the leaf conductance for a given gas *z* (G^z), the boundary layer (g_{BL}^z) and the stomatal conductance (g_S^z). Considering an electrical resistance analogy for each of these layers, the following expression for calculating the overall leaf conductance can be used:

$$G^z = \frac{g_{BL}^z \cdot g_S^z}{g_{BL}^z + g_S^z} \tag{125}$$

The conductance through the boundary layer depends on the diffusion coefficient (D^z), which is species-specific:

$$g_{BL}^{z} = \frac{D^{z} P_b}{\delta \cdot R \cdot T_{bl}} \quad (126)$$

In (126), P_b represents the bulk pressure, T_{bl} is the average temperature between the bulk air and the leaves, R is the ideal gas constant and δ the boundary layer thickness.

The diffusion coefficient for the different gases uses depend on the environmental conditions in the following way:

$$D^{H_2O} = 0.242 \frac{Tb/293^{3/2}}{0.1P_b} \quad (127)$$

$$D^{CO_2} = 0.177 \frac{Tb/317^{3/2}}{0.1P_b} \quad (128)$$

$$D^{O_2} = 0.176 \frac{Tb/298^{3/2}}{0.1P_b} \quad (129)$$

$$D^{t} = 0.2207 \frac{Tb/300^{1.81}}{0.1P_b} \quad (130)$$

In (125), the conductance through the stomata for each of the gas species is proportional to the conductance of water:

$$g_s^{CO_2} = g_s^{H_2O} \frac{D^{CO_2}}{D^{H_2O}} \quad (131)$$

$$g_s^{O_2} = g_s^{H_2O} \frac{D^{O_2}}{D^{H_2O}} \quad (132)$$

The boundary layer thickness δ also depends on the conditions of the bulk air, more specifically on the air density and the bulk velocity:

$$\delta = 2\sqrt{\frac{L \cdot \eta}{v_{bulk}}} \quad (133)$$

$$v_{bulk} = \sin(\alpha) \cdot v_{forced} + \cos(\alpha) \cdot v_{free} \quad (134)$$

$$v_{free} = \sqrt{2 \cdot g \cdot H \cdot \Delta_\rho} \quad (135)$$

$$\Delta_\rho = \left| \frac{\rho_b - \rho_l}{\rho_b} \right| \quad (136)$$

In (133)-(136), η is the air kinematic viscosity, v_{bulk}, v_{forced} and v_{free} are the resulting bulk velocity parallel to the leaf surface, the free convection velocity and the forced convection velocity respectively, g is the gravity force, H is the chamber height and α is the leaf inclination in relation to the vertical direction. The leaves air density (ρ_l) depends on gas species concentrations in the following way:

$$\rho_l = \frac{P_l^{CO_2} \cdot MW_{CO_2} + P_l^{O_2} \cdot MW_{O_2} + P_l^{H_2O} \cdot MW_{H_2O} + P_l^{N_2} \cdot MW_{N_2}}{R \cdot T_l} \quad (137)$$

Finally, the internal concentration of the different species can be derived from (3):

$$P_l^{CO_2} = P_b^{CO_2} - \frac{P_b}{LA \cdot G_{CO_2}} Pn \quad (138)$$

$$P_l^{O_2} = P_b^{O_2} + \frac{P_b}{LA \cdot G_{O_2}} Pn \quad (139)$$

$$P_l^{H_2O} = P_b^{H_2O} + \frac{P_b}{LA \cdot G_{H_2O}} Ex_{H_2O} \quad (140)$$

For the sake of clarity, the main difference between the classical way of solving plant photosynthesis model and the methodology presented in this study is on the way to obtain the net photosynthesis (P_n). The net photosynthesis is usually obtained by finding the phenomena that limits the photosynthesis and can either be due to a biochemical machinery limitation (J, V_c) or by a mass transfer limitation (Ex_{CO_2}):

$$P_g = min\left(V_c \cdot LA, Ex_{CO_2} \cdot LA, J \cdot A\right) \quad (141)$$

$$P_n = P_g(1 - R_d) \quad (142)$$

The multilevel modelling approach presented provides the net photosynthesis directly from the resolution of the FBA:

$$P_n = \upsilon_{Ex_{O_2}} \quad (143)$$

5.7.2. Appendix 2: Summary of metabolic reactions

Compartment	Pathway	Number of Reactions
Chloroplast	Amino Acid Synthesis	38
	Calvin Cycle	17
	Connecting Reactions	4
	Exchange	1
	Folate Cycle	1
	Glutathione Cycle	2
	Glycolysis	5
	Light ETC	1
	Lipid Synthesis	3
	Malic Enzyme	2
	Nitrogen Assimilation	5
	Pentose Phosphate Pathway	2
	Photorespiration	2
	Sulphate Cycle	3
	Transport	38
Mitochondria	Amino Acid Synthesis	3
	Connecting Reaction	6
	Folate Cycle	6
	Lipid Synthesis	2
	Malic Enzyme	1
	Nitrogen Assimilation	2
	Respiratory ETC	2
	Transport	43
Cytoplasm	Amino Acid Synthesis	8
	Calvin Cycle	5
	Carbohydrate Synthesis	7

	Connecting Reaction	10
	Exchange	9
	Folate Cycle	6
	Glycolysis	11
	Lipid Synthesis	17
	Malic Enzyme	2
	Nitrogen Assimilation	3
	Pentose Phosphate Pathway	2
	Photoperiod Exchange	7
Peroxisome	Photorespiration	5
	Transport	4

6. CONTROL-BASED OPTIMIZATION OF OXYGEN AND CARBON DIOXIDE DISTRIBUTION IN A BIOREGENERATIVE LIFE SUPPORT SYSTEM

Nomenclature

Indexes

d	Phase: gas (g) or liquid (l)
y	Compound index (i.e. O_2, CO_2)
z	Compartment index
nom	Nominal point
ref	Reference

All compartments

Q_y^z	Production rate of compound y in compartment z [g/h]
$G_{in/out}^z$	Input/output gas volumetric flow in compartment z.
$C_y^z\|_d$	Concentration of compound *y* in phase *d* in compartment *z* [g L^{-1}]. If compartment localization is included, nomenclature for concentration is $C_y^{in/out}\|_d^z$
ϕ_y^z	Reaction rate of compound *y* in compartment *z* [g h^{-1}]
Ts	Integration time for the system of differential equations
MW_y	Molecular weight of compound y [g/mol]

Concentrated Gas Tank Parameters

$SOC^{CT,ref}$	Normalized reference level (also referenced as State of Charge) of the concentrated gas tank (0.5)
$SOC^{CT,max}$/ $S^{CT,min}$	Normalized max/min level of the concentrated gas tank (0.1/1)
SOC^{CT}	Normalized level of the concentrated gas tank
$P^{CT,max}$	Total maximum pressure of concentrated gas tank (50) [bar]
P^{CT}	Total pressure of concentrated gas tank [Pa]
$G^{CT/DT}$	Concentrated/Diluted gas tank discharging(+)/charging(-) rate [L h^{-1}]
$G^{CT,max}$/ $G^{CT,min}$	Maximum concentrated gas tank discharging/charging rate (15/-15) [L h^{-1}]
$V^{CT,max}$	Maximum volume of the concentrated gas tank (10) [L]
V^{CT}	Volume of the concentrated gas tank [L]
N	Rate of moles [mole h^{-1}]
T	Temperature (298) [K]
R	Gas constant (8.314) [J K^{-1} $mole^{-1}$]

Compartment C4a Parameters

R_d	Radius of the bioreactor (0.076) [m]
I_{C4a}	Light intensity in C4a [W m^{-2}]
K_j	Saturation constant for light (20) [W m^{-2}]

α, δ	Radiative properties accounting for the absorption and scattering cross section of the cells and the fraction of radiant backscattered energy (0.90 for α and 0.9·$C_x^{C4a}|_l$, being x the concentration of *L. indica*).
R_{Ki}	Equilibria constant for the carbonate system (indexes 1, 2 and 3 refers to carbon dioxide, carbonate and carbonic acid equilibria respectively)
V_l^{C4a}	Volume of the liquid fraction of C4a [L] 84L
V_g^{C4a}	Volume of the gas fraction of C4a [L] 1L
φ_g^{C4a}	Gas-liquid mass transfer

Compartment C4b Parameters

A^{C4b}	C4b growth chamber area (5) [m^2]
I_{C4b}	Total light irradiance (550) [µmole m^{-2} s^{-1}]
$I_{C4b,RGB}$	Light irradiance. RGB indicate the irradiance color [µmole m^{-2} s^{-1}]
$I_{abs,RGB}$	Light absorbance [µmole m^{-2} s^{-1}]
$I_{tr,RGB}$	Light transmittance [µmole m^{-2} s^{-1}]
$I_{ref,RGB}$	Light reflectance [µmole m^{-2} s^{-1}]
k_{RGB}	Extinction coefficient as per color [m^2 ground m^{-2} leaf]
LAI	Leaf Area Index [m^2 leaf m^{-2} ground]
LA	Leaf Area [m^2 leaf]
QY_{RGB}	Quantum yield [mol C mol $photon^{-1}$]
V_c	Carboxylation rate associated to the activity of Rubisco [µmole m^{-2} s^{-1}]
F_g	Gross carbon fixation rate [µmole m^{-2} s^{-1}]
F_n	Net carbon fixation rate [µmole m^{-2} s^{-1}]
R_n	Respiration rate (0.3) [µmole m^{-2} s^{-1}]
V^{C4b}	C4b volume (9.7) [m^3]

Energy Cascade Model

HCG	Hourly Carbon Consumption [µmole h^{-1}]
HOP	Hourly Oxygen Production [µmole h^{-1}]
OPF	Oxygen Production Fraction
HCP	Hourly Carbon Production [µmole h^{-1}]
HOC	Hourly Oxygen Consumption [µmole h^{-1}]

Compartment C5 parameters

$resp_y^{C5}$	Respiration rate of compound y in C5 (0.66 and 0.42 for oxygen in active/inactive photoperiods; 0.94 and 0.53 for carbon dioxide active/inactive photoperiods) [mole h^{-1}]

Controller parameters

λ_i	The i^{th} weighting factor
$D_{O_2}^z$	O_2 demand rate of compartment z [g h^{-1}]
H_i	Prediction/Control horizon at the i^{th} control level

T_m	First order process time constant for PFC [h^{-1}]
K_m	First order process gain for PFC
T_i	Sampling time of the i^{th} control level
$CLRT$	Closed loop response time for PFC
MV	Manipulating Variable

Acronyms

CELSSs	Controlled ecological LSSs
HCS	Hierarchical control structure
ISS	International Space Station
LSS	Life support systems
MELiSSA	Micro-Ecological Life Support System Alternative
MPC	Model Predictive Control
MS	Membrane separation
PFC	Predictive functional controller

6.1. Introduction

The increase in space research activities driven by both economic and scientific interests during the last decades has been substantial. Unlike in mid 20-th century, during the outbreak of the space race, many private and public agencies and enterprises are currently devoted to cooperate, as stated by the International Space Exploration Coordination Group (ISECG) in the "Annual Report 2020" (ISECG, 2020), to deploy a wide range of spatial technologies including space exploration, micro and nano-satellite design or rocket development to mention a few (Pekkanen, 2019). According to the space exploration roadmap, current and mid-term scheduled exploration activities comprehend from the on-going robotic exploration of Mars to the eventual long-term presence of humans on Martian surface (Laurini et al., 2018). One of the main requirements of a successful crewed mission to Mars, among many other scientific and technical colossal challenges, is to design a BLSS with enough degree of closure and recycling to guarantee a safe trip, stay, and return for the crew (ISECG, 2018). During the engineering development process that will bring humankind to Mars, the ISS has been a platform for technology testing. Currently, BLSS in the ISS is limited to the recovery of water from urine and regeneration of O_2 from electrolysis of H_2O as has been presented in Chapter 1. Also, O_2 can be generated through a Sabatier reaction using H_2, product of water electrolysis, and the CO_2 generated by the crew respiration (Metcalf et al., 2012). Currently, the ISS is necessarily dependent on Earth provisions to guarantee regular food supply, apart from other kind of maintenance, hardware, and research-related cargo. This dependency from Earth scheduled re-supply is viable for low-Earth orbit habitat like the ISS but not for long-term missions such as a trip to Mars which would take approximately 3 years, which for a crew of 4-6 members would require a quantity of food difficult if not impossible to be supplied from Earth (Barta, 2017). The way to tackle this challenge is photosynthesis, which, as pointed in (Cogdell, 2013), is the essence of the natural Earth's BLSS and crucial for BLSS in Space. In Chapter 4 it was already discussed the use of a photosynthetic compartment based on the activity of cyanobacteria to satisfy the oxygen demands of a crewed mission. In the current chapter, higher plants are included together with a cyanobacteria culture as oxygen producers. Higher plants can develop a triple role: regenerating the atmosphere by consuming CO_2 and producing O_2 through photosynthesis, furnishing food, and producing filtered pure H_2O from transpiration (Galston, 1992). Most Space agencies worldwide are developing research on plants growth with potential CELSS applications like the Veggie project (already under operation in the ISS) the Higher Plants Chamber in the MPP, the PaCMAN Unit Laboratory in the University of Naples Federico II managed by ESA in the framework of the MELiSSA project and also the Lunar Palace of the China Manned Space Engineering Office.

6.1.1. Main Contribution

In this Chapter, two main goals are targeted. First, the assessment of the integration of the higher plants compartment into the current MPP integration phase; Secondly, designing a Higher Control Structure to manage the target BLSS (the MPP) with the integration of a higher plants chamber while assessing different control strategies. In summary, a HCS is designed to control an exemplary LSS, the MPP, and to assess from a process and control perspective the integration of the higher plants compartment C4b into the current MPP integration phase. The available models for each of the compartments (introduced and validated in previous studies) are used to simulate the non-linear behavior of the system under study and to design the model-based controllers that conform the proposed HCS. Due to the reliability of the modelling resources, an integrated process design and control analysis is carried out to find the optimal process configuration in terms of operation performance and controllability that can be used to assess further integration steps.

The rest of this Chapter is organized as follows: The MELiSSA Loop is introduced in Section 6.2 while Section 6.3 is dedicated to the MPC-based control strategy. The case study and simulation parameters are introduced in Section 6.4 and simulation analysis are presented in Section 6.5. Finally, the concluding remarks of this chapter are provided in Section 6.6

6.2. The MELiSSA Loop and the MELiSSA Pilot Plant integration phase

6.2.1. The MELiSSA Pilot Plant

As mentioned in the previous Chapters, the scope of the MPP is to provide a test-bed for the MELiSSA BLSS design, characterization, demonstration and integration activities on Earth conditions. The latest integration phase completed in the MPP comprises the liquid phase connection between C3 and C4a and the gas phase connection between C3, C4a, and C5 which was finalized in 2021, whereas next integration steps will involve the higher plants compartment. This is certainly a substantial landmark in the completion of the MELiSSA loop.

Within the knowledge developed in the MPP, special efforts have been devoted to the generation of mechanistic models for each of the compartments in standalone and integrated operation modes. These modelling tools are used to support the pilot plant activities but also to develop model-based predictive controls (Farges et al., 2008). Predictive controllers are of high interest due to their capability to explicitly account for process constraints, considering future behavior of the plant, and easiness of handling Multiple-input Multiple-output processes (Bemporad, 2017).

6.2.2. Integration Scenarios

As previously mentioned, the scope of this study is to make a model-based assessment of potential integration scenarios for the higher plants chamber (also called C4b compartment). An integral assessment of different MELiSSA loop process designs and control configurations are considered to determine which offers the best performance.

In Fig 6. 1, the latest MPP process design is presented with the liquid phase of C4a and C3 connected (not represented), and the gas phase of C3, C4a, C4b and GM (GM is the acronym for Gas Management). GM unit, which is a membrane-based technology, aims at increasing the partial pressure of oxygen in the gas phase to achieve a high dissolved oxygen concentration in C3. From the GM unit, a concentrated gas flow and a diluted gas flow in oxygen are obtained, being a fraction of the concentrated flow sent towards C3 and the remaining concentrated flow and the residual diluted flow sent back to C5 (see Fig 6. 1b for the GM functionality). Carbon dioxide is also a compound that is concentrated in the GM. The role of C3 is to nitrify the reduced nitrogen of the loop. Nitrogen is mainly present in the form of urea coming from the crew urine. In the present study, a feed of ammonia is introduced in C3 and full nitrification is intended by controlling the dissolved oxygen in C3 at a value of 80%. Eventually, in the MPP, real urine will be fed to C3.

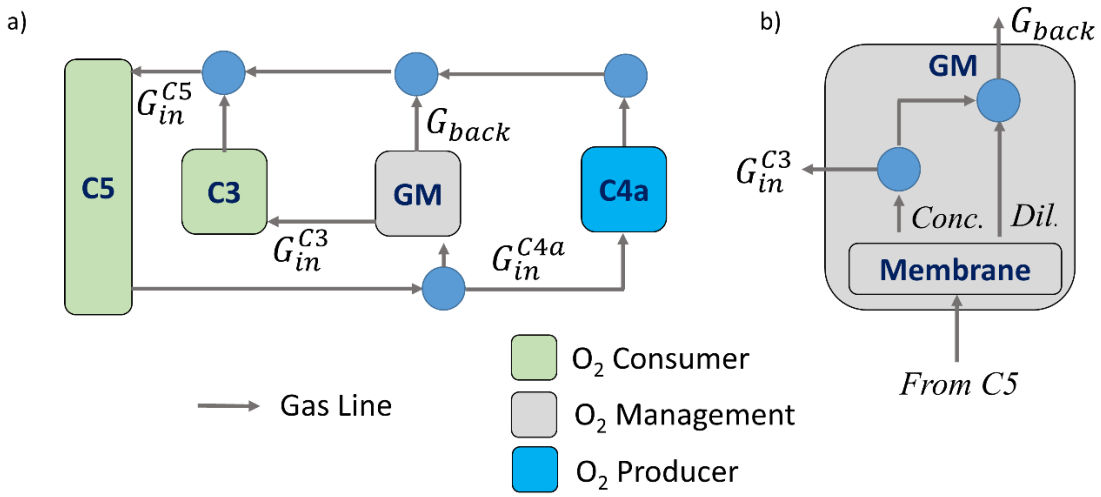

Fig 6. 1. Gas Phase MPP Process Design: a) Current MPP Integration phase; b) Detailed representation of flows within GM

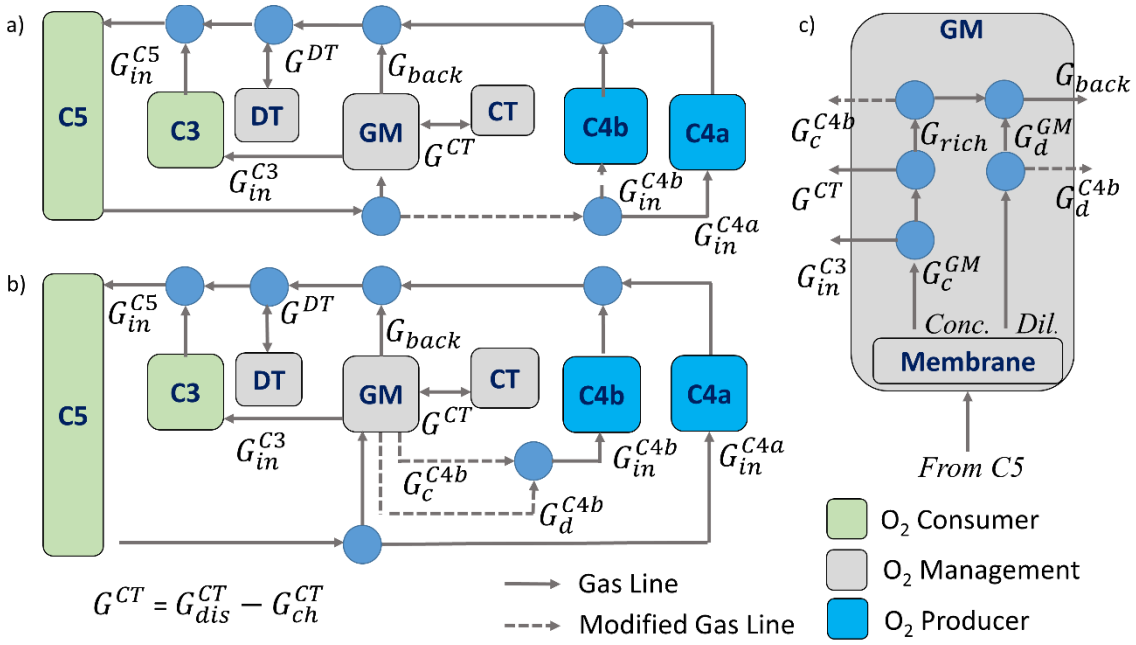

Fig 6. 2. Proposed process designs: a) C4b is fed with C5 outputs; b) C4b is fed with a combination of diluted and concentrated gas; c) Detailed representation of flows within GM. (CT: Concentrated Tank. DT: Diluted Tank)

The challenge addressed in this Chapter and also the challenge to be addressed by the MPP in the near future is the integration of the Higher Plants Chamber. In Fig 6. 2, two options in terms of process flow designs are presented. The first option (Fig 6. 2a) is the simplest in terms of hardware requirements, since the gas outflow of C5 is dispatched in three fractions, being one the input of C4a, another one the input of C4b and a third one being the input of the GM. As mentioned in Chapter 4, an O_2-concentrated gas tank (CT) and a O_2-diluted gas tank (DT) are included to provide buffering capacity to the system for oxygen. Thus, if needed, oxygen can be released from the concentrated gas tank to the system. The second process design (Fig 6. 2b) is more complex in terms of hardware requirements, since it involves more hardware modifications to integrate C4b compared to that presented in Fig 6. 2a. Mainly, in this proposal, C4b is fed with a fraction of the CO_2-rich gas flow and a fraction of the CO_2-poor gas flow obtained in GM. This option would enable having the capacity to control the input oxygen concentration (or carbon dioxide concentration) to be fed to C4b. With this strategy, it is not possible to have the control of both compounds' concentration (oxygen and carbon dioxide) in the input of C4b. As stated, the integration of C4b to the MPP, from a process flow design point of view, can be addressed in multiple ways. The two proposals presented are exemplary cases and the integration possibilities are not limited to these two. Summarizing, in terms of process design, two options are presented:

- *Process Design 1* (see Fig 6. 2a): C4b receives a gas flow coming directly from C5.

- *Process Design 2* (see Fig 6. 2b): C4b receives a combination of a concentrated and a diluted gas fraction from the GM unit.

On top of the process flow design, the control strategy has not a minor impact on the beforementioned performance of the system of interest.

In this regard, three different control configurations are proposed:

- *Control Configuration 1*: Process design 1 is used. The O_2 concentration in C5 is controlled at 21%, which is in turn the O_2 concentration in the inflow of C4b.
- *Control Configuration 2*: Process design 2 is used. The O_2 concentration in C5 is controlled at 21%, which is in turn the O_2 concentration in the inflow of C4b and the CO_2 concentration is controlled at 800 ppm in C4b.
- *Control Configuration 3*: Process design 2 is used. The gas phase of C4b is fed with diluted and concentrated flows from the GM unit. The O_2 concentration in C5 is controlled at 21%, which is in turn the O_2 concentration in the inflow of C4b and the CO_2 concentration is controlled at 800 ppm in C4b.

For all control configurations, the carbon dioxide concentration in C4b can be controlled through the addition of external pure carbon dioxide if 800 ppm cannot be achieved.

It is worth noticing that the main difference between the two configurations is in the gas inflow to C4b. In the first process design option (Fig 6. 2a), gas inflow comes directly from C5, whereas in the second process design option (Fig 6. 2b), the input gas flow is a combination of a concentrated and a diluted gas fraction of the gas management (GM) unit. Consequently, control configuration 3 has one more degree of freedom compared to control configurations 1 and 2. See Table 6. 1 for a summary of the integration strategies assessed and discussed in this Chapter.

Table 6. 1. Summary of the integration strategies assessed.

Strategies	Process Design	Control Configuration	Controlled variables	Manipulated variables
Strategy 1	1	1	O_2 at 21% in C5	O_2 in C4a CT charge/discharge
			Dissolved O_2 at 80% in C3	O_2-rich gas flow fraction
Strategy 2	2	2	O_2 at 21%	O_2 in C4a CT charge/discharge
			Dissolved O_2 at 80% in C3	O_2-rich gas flow fraction from GM
			CO_2 at 800 ppm	Flow from C5

Strategy 3	2	3	O_2 at 21%	O_2 in C4a
			Dissolved O_2 at 80% in C3	CT charge/discharge
			CO_2 at 800 ppm	O_2-rich gas flow fraction
				Combination of CO_2-rich and CO_2-poor gas fraction from GM

6.2.3. C3: Nitrification compartment

See section 4.2.1. in Chapter 4 for a detailed description of the design equations of C3 model

6.2.4. C4a: Cyanobacteria Photobioreactor

See section 4.2.2. in Chapter 4 for a detailed description of the design equations of C4a model.

6.2.5. Higher Plants Compartment

In the MPP, hydroponics technique is used to grow crops given its many advantages over soil-culture. Among others, hydroponics culture is interesting due to an improved water usage, higher carbon yields as well as better contaminant control (Barman & Hasan, 2016). In the MPP, the HPC with a total growing surface of 5 m^2 and a volume of 9.7 m^3 is the main contributor of O_2 production and by extension CO_2 consumption within the current integration phase of the MPP. According to Masot (2007), the contribution of the HPC filled with lettuce *L. sativa* on a daily basis is equal to 55% of the total produced O_2, the rest being supplied by C4a. This data is similar to the results obtained recently in staggered mode of operation carried in the MPP with lettuce (data not published). A detailed description of the HPC configuration can be accessed in Peiro et al., (2020). The model of the HPC is presented in detail in Chapter 5. In this chapter a modification of the model is proposed to include the ratio of colors in the LED-based illumination of the chamber, which include red, far-red, blue and green. In Chapter 5 the modelling approach considers the light electron transport chain and the rubisco carboxylation as the two parameters to compare to calculate the rate of carbon fixation. In the presented model modification, the light irradiance is discretized for the different color spectra. For lettuces, each color has a specific absorption profile as indicated in Fig 6. 3, and a specific quantum yield as reported in Liu and van Iersel (2021) and reproduced in Fig 6. 4. The decay curves in Fig 6. 3 are generated by sensing the decay of light irradiance when passing through a canopy using a LI-180 spectrometer. The size of the canopy is based on the Leaf Area Index (LAI) which is defined as the ratio of leaf area over ground area.

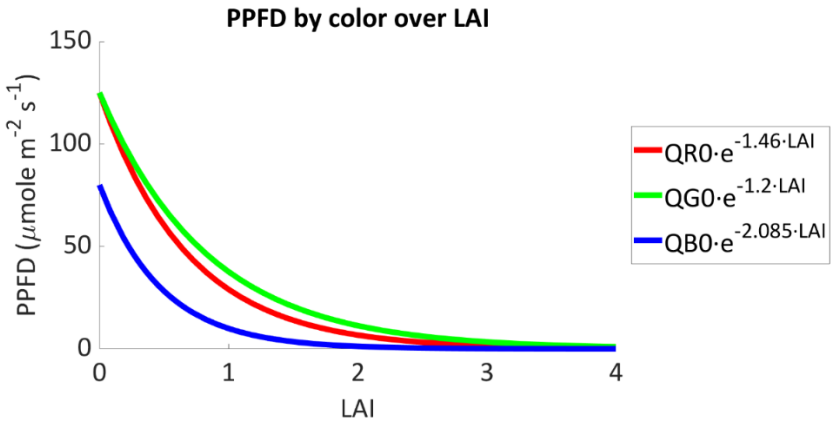

Fig 6. 3. Light intensity at ground level as a function of LAI. Model is fitted to experimental data using *L. sativa* and using LI-190R quantum sensor.

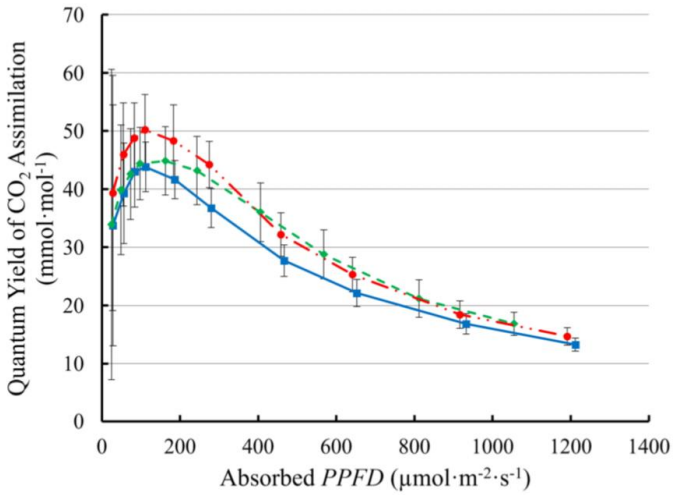

Fig 6. 4. Leaf quantum yield associated to a specific color (red, green blue). Source: van Iersel (2021)

The input of the model is the light intensity discretized in the three different colors. When passing through a leaf or through the whole canopy, light can be reflected, transmitted, or absorbed. One assumption made based on the experimental demonstration of Liu and van Iersel (2021) in lettuces is that absorbance and transmittance, in the spectrum used, are approximately equal. This way it is possible to obtain the reflected, transmitted and absorbed light along the whole canopy.

As a result, and using red color as an example, the calculation for the absorbed light radiation when leaf area index is lower than 1 is the following:

$$I_{abs,R} = I_{C4b,R} LAI - (I_{C4b,R} e^{-k_R}) LAI \cdot 2 \quad (144)$$

The term $(I_{C4b,R} e^{-k_R}) LAI \cdot 2$ represents the number of red photons not captured due to transmittance or reflectance.

When leaf area index is higher than 1, it is considered that only the light reflected by the first layer of leaves is lost and photons reflected by deeper layers are trapped in the canopy and eventually absorbed. Therefore, the reflected red light by the first layer of leaves can be calculated in the following way:

$$I_{ref,R} = I_{C4b,R} e^{-k_R} \tag{145}$$

The transmitted is calculated using the decay constant:

$$I_{tr,R} = I_{C4b,R} e^{-k_{R \cdot LAI}} \tag{146}$$

The absorbed is calculated by solving a simple balance for photons:

$$I_{abs,R} = I_{C4b,R} - I_{tr,R} - I_{ref,R} \tag{147}$$

The total quantity of absorbed photons combining all colors (I_{abs}) is then converted into gross photosynthetic carbon assimilation rate using a polynomial fitting based on the profiles represented in Fig 6. 4. The resulting carbon fixation represents the potential fixation associated to light irradiance, which is compared to the potential carbon fixation associated to the Rubisco carboxylation as similarly presented in Chapter 5:

$$F_g = min\left(I_{abs,RGB} \cdot QY_{RGB}, V_c\right) \cdot LA \tag{148}$$

The resulting gross carbon fixation (F_g) is expressed in moles·s^{-1}.

The net photosynthetic rate (F_n) results from the gross photosynthetic rate (F_g) obtained in (148) through retrieving the respiration fraction (R_n):

$$F_n = F_g(1 - R_n) \tag{149}$$

At this point, it is possible to calculate the carbon consumption rate considering the area of the plants chamber:

$$R_{CO_2}^{C4b} = F_n A^{C4b} \tag{150}$$

Notice in (149), the reaction rate F_n is expressed over the C4b growth surface area.

The resulting dynamic model assumes a perfect homogeneity in the gas phase inside the chamber. For carbon dioxide and oxygen, considering equimolar stoichiometry for the photosynthesis:

$$\frac{dC_{CO_2}^{C4b}|_g}{dt} = G_{in}^{C4b} C_{CO_2}^{C4b}|_g^{in} - G_{out}^{C4b} C_{CO_2}^{C4b}|_g + \frac{R_{CO_2}^{C4b}}{V^{C4b}} \tag{151}$$

$$\frac{dC_{O_2}^{C4b}|_g}{dt} = G_{in}^{C4b} C_{O_2}^{C4b}|_g^{in} - G_{out}^{C4b} C_{O_2}^{C4b}|_g - \frac{R_{O_2}^{C4b}}{V^{C4b}} \tag{152}$$

The validation of the proposed modification of the higher plants chamber model with experimental data is presented in Appendix 6.6.

6.2.6. C5: Crew compartment

The crew compartment is an isolator hosting a mock-up crew consisting of a group of Wistar rats to simulate human respiration activity. C5 has a total volume of 1.6 m^3, the complete specifications of the isolator can be consulted in Alemany et al. (2019). Two fixed production/consumption rates have been assumed in the modeling of the day-night dynamics of the mock-up crew respiration. The resulting dynamic equations are the following:

$$\frac{dC_y^{C5}|_g}{dt} = G_{in}^{C5} C_y^{C5}|_g^{in} - G_{out}^{C5} C_y^{C4b}|_g + \frac{\phi_y^{C5}}{V^{C5}} \tag{153}$$

6.2.7. Gas Management and Storage System

The storage system is not currently present in the MPP, but its effect and suitability in a BLSSs like MELiSSA is also assessed. The gas management and storage system refer to the membrane separation unit (MS) the concentrated and diluted gas tanks (CT and DT respectively) presented as O_2 management units in Fig 6. 2. The proposed storage system in the simulation studies is composed of two 10-Lt tanks with a maximum pressure of 50 bar, one intended to store O_2 concentrated flow (CT) and the other intended to store O_2 diluted flow (DT), both generated in the oxygen concentration membrane.

The state of charge (SOC) of the concentrated tank (CT) is approximated using the ideal gas law to calculate the moles flow rate introduced or removed from the tank during charging and discharging periods as follows (represented in discrete-time):

$$SOC(k+1) = SOC(k) + \frac{(G_{ch}^{CT}(k) - G_{dis}^{CT}(k))P^{CT}(k)}{V^{CT,max}P^{CT,max}} T_s \tag{154}$$

Besides, the updated concentration of gases in the CT is given below:

$$C_y^{CT}|_g(k+1) = \frac{\lambda \cdot SOC(k) \cdot C_y^{CT}|_g(k) + P^{CT}(k) \cdot G_{ch}^{CT}(k) \cdot C_y^c|_g(k) \cdot T_s}{\lambda \cdot SOC(k) + \frac{P^{CT}(k)}{RT} \cdot G_{ch}^{CT}(k) \cdot Ts} \tag{155}$$

$$\lambda = \frac{P^{CT,max}V^{CT,max}}{RT} \tag{156}$$

In these equations, G_{dis}^{CT} and G_{ch}^{CT} refer to the amount of discharging and charging of the CT at time step *k*. In case the CT is discharging, G_{ch}^{CT} will be equal to zero, thereby no change in the CT gas concentration.

It is worth mentioning that the dynamic equations for the diluted tank are similar to the concentrated tank, but when one is charged the other is discharged to keep the pressure in the circulating gas flow. According to Fig 6. 2, the pending gas flow and concentration can be calculated as follows:

$$G_{rich}(k) = G_{dis}^{CT}(k) - G_{ch}^{CT}(k) + G^{cGM}(k) = G^{CT}(k) + G^{cGM}(k) \quad (157)$$

$$C_y^{rich}(k) = \frac{G^{cGM}(k)C_y^{cGM}(k) + G_{dis}^{CT}(k)C_y^{CT}(k)}{G_{dis}^{CT}(k) + G^{cGM}(k)} \quad (158)$$

6.3. Hierarchical Control of the MPP

An improvement of the HCS introduced in Chapters 3 and 4 is proposed for the MPP including oxygen and carbon dioxide as variables to control. The proposed control strategy is organized in three levels in which each control level is associated with a different time scale considering the dynamics it responds to. The detailed description of the proposed control strategy at each level is provided in the following section.

6.3.1. Tertiary control level

The tertiary control level is responsible for finding long-term optimal operating points for different compartments while guaranteeing the O_2 supply to the system. Different operating criteria can be considered by the tertiary controller to optimize the system-level performance. In this case, optimal resource utilization and system reliability are considered as the main objectives of the tertiary controller. The reliability of the system is guaranteed through maintaining the state of charge (SOC) of the concentrated gas tank (CT) around a predefined reference level. Besides, the provision of O_2 by C4a is scheduled considering a nominal light intensity set at 200 W/m^2.

The tertiary control level is focused on solving a mass balance problem to cover the required O_2 in the system, as can be seen in the optimizer module shown in Fig 6. 5. The main difference in relation to Chapter 4 is that the higher plants chamber becomes the main O_2 supplier during light photoperiods, but it becomes a consumer compartment during dark periods. C4a represents the second largest O_2 producer whereas C5 and C3 are the two constant consumers. C4b production capacity is determined based on the plant growth phase. Hence, its total O_2 supply capacity is estimated given the plants age. The CT can absorb or provide O_2 to maintain the mass balance in the system.

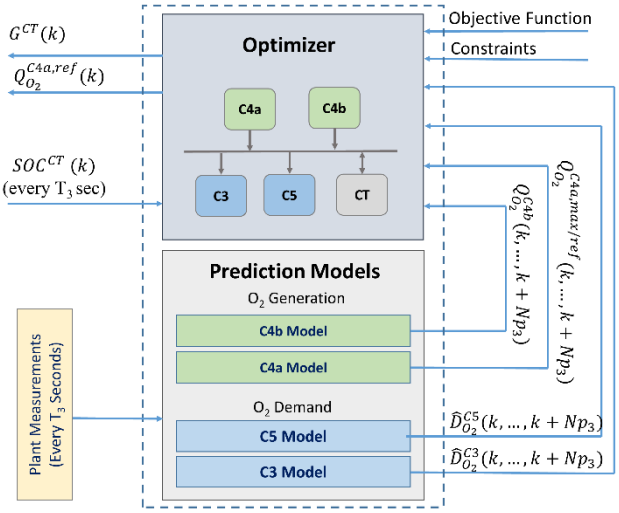

Fig 6. 5. MPC-based tertiary control architecture

6.3.1.1. Prediction models

The tertiary controller deploys the MPC strategy and is equipped with a prediction system to find the approximate O_2 production and consumption rates of the different compartments of the loop. Predictions are updated at a given frequency (T_3 seconds, see Table 6. 4 to check values for HCS parameters) using the most recent information obtained from the system. Predictions are drawn based on the internal model of the different compartments described in this section. The output of the internal models are the expected O_2 consumption rates of C3 and C5 ($\widehat{D}_{O_2}^{C3}$ and $\widehat{D}_{O_2}^{C5}$ respectively) as well as the predicted maximum ($Q_{O_2}^{C4a,max}$) and nominal ($Q_{O_2}^{C4a,ref}$) O_2 production rates of C4a and the predicted O_2 production rate from C4b ($Q_{O_2}^{C4b}$) over the prediction horizon (Fig 6. 5). The approximate maximum and nominal O_2 production rates of C4a are found using its internal model and setting the light intensity to the maximum value technically allowed (364 W/m^2) and the nominal light intensity that is set at a value of 200 W/m^2. The difference between C4a and C4b is that C4a contribution can be adjusted on demand depending on the oxygen needs of C5 and C3, but C4b activity is constant since light intensity in the compartment is not a manipulated variables but fixed.

6.3.1.2. The Tertiary Control Optimizer

At each iteration, the tertiary controller solves the following optimization problem over the prediction horizon (N_{p3}) using the latest measurements, representing the current state of the system and the predicted production and consumption patterns received from the prediction system.

$$J_3(t) = \sum_{j=N_1}^{j=Np_3} \lambda_1 \left[(\widehat{SOC}^{CT}(t+j|t) - (SOC^{CT,ref}(t+j) \right]^2 + \sum_{j=N_1}^{j=Nc_3-1} \lambda_2 \left[(Q_{O_2}^{C4a}(t+j-1|t) - Q_{O_2}^{C4a,ref}(t+j-1) \right]^2 \quad (159)$$

$$U(t) = [Q_{O_2}^{C4a}, G^{CT}]^T \quad (160)$$

Subject to:

$$\sum_{z \in C3,C5} \widehat{D}_{O_2}^{z}(t+j|t) - Q_{O_2}^{C4b}(t+j|t) = Q_{O_2}^{C4a}(t+j|t) + Q_{O_2}^{CT}(t+j|t) \quad (161)$$

$$U^{min} \leq U(t+j|t) \leq U^{max} \quad (162)$$

$$\widehat{SOC}^{CT,min} \leq \widehat{SOC}^{CT}(t+j|t) \leq \widehat{SOC}^{CT,max} \quad (163)$$

$$G^{CT,min} \leq G^{CT}(t+j|t) \leq G^{CT,max} \quad (164)$$

$$Q_{O_2}^{C4a,min} \leq Q_{O_2}^{C4a}(t+j|t) \leq Q_{O_2}^{C4a,max} \quad (165)$$

The two cost terms indicate the penalization on the deviation of the C4a production capacity and CT state of charge from their nominal values ($Q_{O_2}^{C4a,ref}$ and $\widehat{SOC}^{CT,ref}$ respectively). The first constraint forces the system to satisfy a mass balance throughout the whole prediction horizon and the others guarantee that the decision variables collected in matrix *U* as well as the predicted state of charge $\widehat{SOC}^{CT}$ lies within the allowed boundaries.

6.3.2. Secondary Control Level

In the proposed control structure, the secondary controller is responsible for dispatching gas/liquid flow and adjusting the output oxygen concentration in C4a. The goal is to guarantee sustained conditions in the crew compartment by keeping the gas concentrations within the safe boundaries. The sustained conditions are guaranteed by tracking the references received from the tertiary controller, tracking the desired gas concentrations for specific compartments, and favoring a smooth control response. A scheme of the secondary control organization is presented in Fig 6. 6.

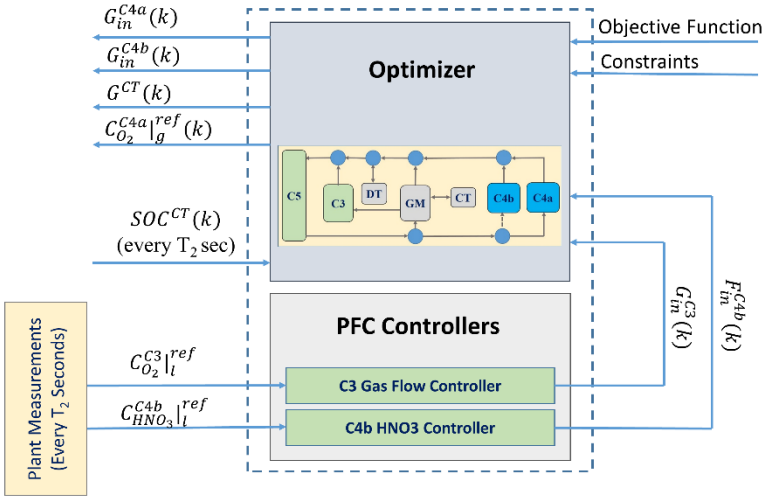

Fig 6. 6. MPC-based secondary control architecture

6.3.2.1. The secondary Controller MPC

The following objective function is considered by the secondary controller at each time step for control configuration 1:

$$J_2(t) = \sum_{j=1}^{j=N_{p2}} \lambda_3(j)\left[(\hat{Y}(t+j|t) - (Y^*(t+j)\right]^2 + \sum_{j=1}^{j=N_{c2}-1} \lambda_4(j)[\Delta U(t+j-1)]^2 \quad (166)$$

$$\hat{Y}(t) = \left[\hat{C}_{O_2}^{C5}|_g(t), G^{CT}(t), Q_{O_2}^{C4a}(t)\right]^T \quad (167)$$

$$Y^*(t) = \left[C_{O_2}^{C5}|_g^{ref}(t), G^{CT,ref}(t), Q_{O_2}^{C4a,ref}(t)\right]^T \quad (168)$$

$$U(t) = \left[G_{in}^{C4b}(t), G^{CT}(t), C_{O_2}^{C4a}|_g(t)\right]^T \quad (169)$$

Where, $G^{CT,ref}$ and $Q_{O_2}^{C4a,ref}$ are the reference values for the CT and C4a respectively, received from the tertiary controller and $C_{O_2}^{C5}|_g^{ref}$ is the O_2 concentration set point for the crew compartment set by the supervisory controller, which in this case is fixed at 21%.

For the control configurations 2 and 3, matrices $\hat{Y}(t)$ and $Y^*(t)$ are modified to include the reference for the CO_2 concentration in C4b ($C_{CO_2}^{C4b}|_g^{ref}(t)$) as a new variable to track. Finally, in control configuration, 3 the matrix of control commands $U(t)$ is modified to include concentrated and diluted gas flow fractions to be used in C4b as new manipulated variables (G_c^{C4b} and G_d^{C4b}):

$$\hat{Y}(t) = \left[\hat{C}_{O_2}^{C5}|_g(t), \hat{C}_{CO_2}^{C4b}|_g(t), G^{CT}(t), Q_{O_2}^{C4a}(t)\right]^T \quad (170)$$

$$Y^*(t) = \left[C_{O_2}^{C5}|_g^{ref}(t), C_{CO_2}^{C4b}|_g^{ref}(t), G^{CT,ref}(t), Q_{O_2}^{C4a,ref}(t)\right]^T \quad (171)$$

$$U(t) = \left[G_c^{C4b}(t), G_d^{C4b}(t), G^{CT}(t), C_{O_2}^{C4a}|_g(t)\right]^T \quad (172)$$

In order to guarantee the safe operation of the system, the operation management problem at the secondary level is also subjected to a set of constraints:

$$C_{O_2}^{C5}|_g^{min} \leq \hat{C}_{O_2}^{C5}|_g(k) \leq C_{O_2}^{C5}|_g^{max} \quad (173)$$

$$C_{CO_2}^{C5}|_g^{min} \leq \hat{C}_{CO_2}^{C5}|_g(k) \leq C_{CO_2}^{C5}|_g^{max} \quad (174)$$

$$S\hat{O}C^{min} \leq S\hat{O}C(k) \leq S\hat{O}C^{max} \quad (175)$$

$$G_{in}^{C5} = G_{in}^{C4a}(k) + G_{in}^{C4b}(k) + G_{in}^{GM}(k) + G_{dis}^{DT}(k) - G_{ch}^{DT}(k) + G_{in}^{C3}(k) \quad (176)$$

The secondary controller is executed at a sample time T_2, which is set lower than that of the tertiary controller. The faster clock of the secondary controller makes it capable of maintaining system safety by quickly responding to unexpected changes in the production or consumption rates of compartments.

At each time step T_2, the measurements system component concentration and the SOC of the storage units are transferred to the secondary controller. The secondary controller then solves the optimization problem over the prediction horizon H_2 to find the optimal control sequence U_2. However, only the first control sample is implemented, and the rest are used for warm start at the next time step.

Even though only one controlled variable ($C_{O_2}^{C5}|_g^{ref}$ for control configuration 1; $C_{O_2}^{C5}|_g^{ref}$ and $C_{CO_2}^{C4b}|_g^{ref}$ for control configurations 2 and 3) differentiates the three control configurations, the control problem is quite different between them.

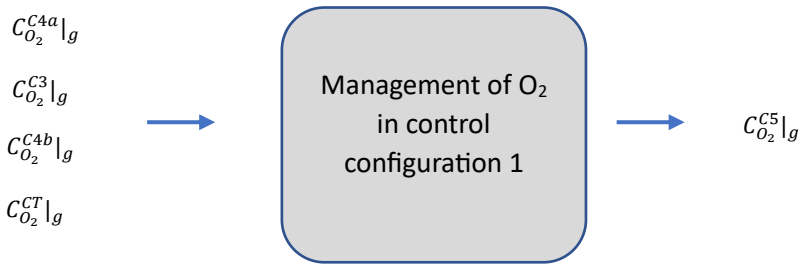

Fig 6. 7. Oxygen management in control configuration 1

The concentration of oxygen in C5 is calculated straightforward based on the concentration of oxygen in the output of the other compartments and considering their flows (Fig 6. 7). Concentration of oxygen in C4a and flows all over the process are the variables to be optimized by the secondary controller. The concentration of oxygen for compartments other than C4a are

not to be optimized, because the operating conditions for these compartments are constant so the consumption/production rates of these compartments will also be constant. Therefore, these compartments operate invariably over time and only the supply of oxygen from C4a and from the buffer tanks are dynamically adjusted.

Since the C4a flow is constrained by the hydrodynamics of the compartment (Alemany et al., 2019) with a value of 2.8 L/min fixing the mixing and gas-liquid mass transfer rate of the bioreactor, the remaining parameters to optimize other than the concentration of oxygen in C4a are the flow to C4b and the charging/discharging of the CT.

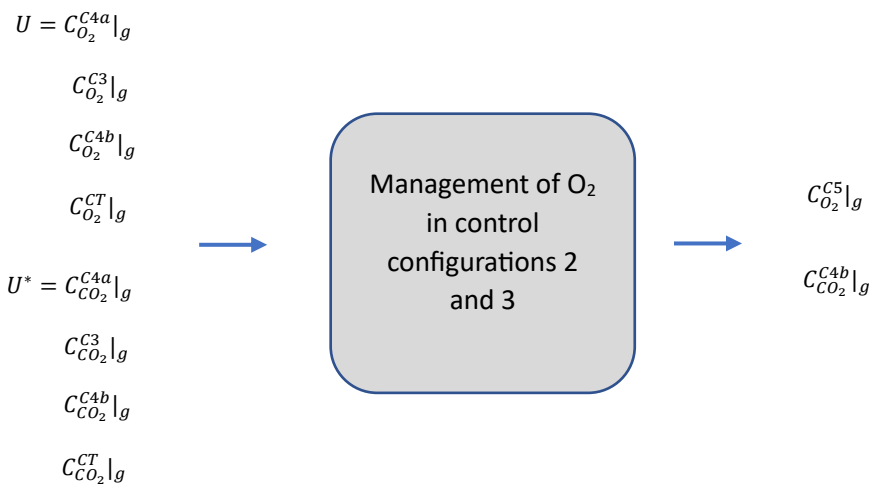

Fig 6. 8. Oxygen and carbon dioxide management in C5 and C4b in control configurations 2 and 3

In control configurations 2 and 3, there is one more controlled variable: the concentration of carbon dioxide in the higher plants chamber (Fig 6. 8). There is also one more manipulated variable: the diluted (G_d^{C4b}) and concentrated (G_c^{C4b}) flows from the gas enriching membrane instead of the input gas flow to C4b (G_{in}^{C4b}) which is the manipulated variable in control configuration 1 and 2. Note that, in order to control the concentration of carbon dioxide in C4b it is also required to calculate or to know the concentration of carbon dioxide at the output of C4a (and also the concentration in the output of C5). But notice that oxygen concentration in the output of C4a is a variable to optimize in the secondary controller to control oxygen in C5. Considering that in C4a the concentration of carbon dioxide and oxygen are linked by the stoichiometry (more specifically by the photosynthetic quotient), it is only possible to optimize the concentration of one of them two, being the concentration of the other constrained by the stoichiometry. The C4a model presented in Chapter 4 and extensively described in Dauchet et al., (2016) stablishes the mathematical relationship between both compound concentrations, but its non-linear nature makes the resolution of the control problem too long to be implemented in a MPC. Instead, a recursive linearization based on a Taylor expansion is carried

each time the MPC is executed. The objective of using such surrogating model strategies for control purposes like the presented linearization of C4a is to obtain a high computation time to resolve the MPC presented in (166)-(172). Besides, other strategies aimed at reducing the computation burden of the internal models of the MPC are also introduced in the following section.

Adaptation of C4a Model: Linearization

Essentially, the model described in Chapter 4 can be generalized with the following expression considering only one state and one input:

$$\frac{dx}{dt} = f(x,u) \tag{177}$$

With the function $f(x,u)$ presenting different non-linearities. This expression can be linearized using the Taylor expansion:

$$\frac{dx}{dt} \approx f(\bar{x},\bar{u}) + \frac{\partial}{\partial x}|_{\bar{x},\bar{u}}(x-\bar{x}) + \frac{\partial}{\partial u}|_{\bar{x},\bar{u}}(u-\bar{u}) \tag{178}$$

The parameters $\bar{x},\bar{u}$ are the state and input values in steady state conditions, which implies that the derivative terms equal 0:

$$\frac{dx}{dt} = 0; \tag{179}$$

To proceed with the linearization, deviation variables from the steady state are defined:

$$x' = x - \overline{x} \tag{180}$$

$$u' = u - \overline{u} \tag{181}$$

The derivative of the deviation variables equals the derivative of the variable as follows for both states and inputs:

$$\frac{dx'}{dt} = \frac{dx}{dt} \tag{182}$$

Hence, the final formulation of (178) is the following:

$$\frac{dx'}{dt} = \frac{\partial}{\partial x}|_{x,u}(x-\bar{x}) + \frac{\partial}{\partial u}|_{x,u}(u-\bar{u}) \tag{183}$$

$$\frac{dx'}{dt} = A\cdot x' + B\cdot \overline{u'} \tag{184}$$

Expression (184) is equivalent to a state space formulation being A and B the states and input matrices respectively. Expanding (178)-(184) from single state and single input model to multiple states and inputs:

$$\frac{dx'}{dt} = \begin{bmatrix} \frac{\partial f_1}{\partial x_1}|_{x,u} & \cdots & \frac{\partial f_1}{\partial x_{14}}|_{x,u} \\ \vdots & \ddots & \vdots \\ \frac{\partial f_{14}}{\partial x_1}|_{x,u} & \cdots & \frac{\partial f_{14}}{\partial x_{14}}|_{x,u} \end{bmatrix} \cdot \begin{bmatrix} {x_1}' \\ \vdots \\ {x_{14}}' \end{bmatrix} + \begin{bmatrix} \frac{\partial f_1}{\partial u_1}|_{x,u} & \cdots & \frac{\partial f_1}{\partial u_8}|_{x,u} \\ \vdots & \ddots & \vdots \\ \frac{\partial f_{14}}{\partial u_1}|_{x,u} & \cdots & \frac{\partial f_{14}}{\partial u_8}|_{x,u} \end{bmatrix} \cdot \begin{bmatrix} {u_1}' \\ \vdots \\ {u_8}' \end{bmatrix} \tag{185}$$

$$\frac{dx'}{dt} = A \cdot x' + B \cdot \overline{u'} \tag{186}$$

State space formulation is represented in (186) and it has several advantages like indicating the relationship between states and inputs and it can also provide information about stability of the controller. In order to linearize the C4a model and formulate it as a state space representation, all the ordinary differential equations and algebraic expressions of the model need to be expressed as a function of states and inputs. This is complex in some parts of the photobioreactor model, especially in the calculation of the illuminated radius and the energy profile.

First, the calculation of the illuminated radius of the bioreactor (R_{il}), where light reaches its compensation point (see equation (21) in Chapter 4), requires the solution of the following expression, which means essentially to isolate R_{il}:

$$\frac{2 \cdot I_o(\delta \cdot R_{ill})}{I_o(\delta \cdot E) + \alpha \cdot I_1(\delta \cdot E)} - \frac{ComPoint}{I_{C4a}} = 0 \tag{187}$$

Illuminated radius is defined as the point in the bioreactor where light is stopped by the shadowing effect of cells. This parameter is a function of the light intensity and the biomass concentration in the photobioreactor. Illuminated radius (R_{ill}) is isolated using Maple 2018 ®, which provides a powerful engine for symbolic calculation.

Having the illuminated radius defined, another part of the model that requires a numeric approximation is the integration of the profile of light radiant energy ($4\pi J_r$), described as a Monod-type law considering light as the limiting substrate, from the illuminated radius (R_{il}) to the total radius of the bioreactor (R_d):

$$\phi_x^{C4a} = C_x^{C4a}|_l \cdot \mu_x^{C4a,max} \cdot \frac{1}{\pi \cdot (R_d)^2} \int_{r=R_{il}}^{r=R_d} 2\pi r \frac{4\pi J_r}{K_j + 4\pi J_r} dr \tag{188}$$

The profile of light radiant energy ($4\pi J_r$) is defined as:

$$4\pi J_r = \frac{2 \cdot I_{C4a} \cdot I_0(\delta \cdot R)}{I_0(\delta \cdot R) + \alpha \cdot I_1(\delta \cdot R)} \tag{189}$$

Given the mathematical complexity of $4\pi J_r$, the Simpson's rule with two partitions has been the chosen method to find a numerical solution of the integral in (188).

After this mathematical treatment of the C4a model, it is possible to proceed with the linearization. Considering that the secondary controller is expected to be executed at a given specific sampling time, model linearization shall be calculated every time with the current operating conditions. Considering the dynamics of C4a bioreactor:

$$\frac{dC_{tic}^{C4a}|_l}{dt} = \frac{F_{in}^{C4a}}{V_l^{C4a}} \cdot \left(C_{tic}^{C4a}|_l^{in} - C_{tic}^{C4a}|_l\right) + \varphi_{CO2}^{C4a} + \phi_{tic}^{C4a} \tag{190}$$

$$\frac{dC_{CO_2}^{C4a}|_l}{dt} = \frac{F_{in}^{C4a}}{V_l^{C4a}} \cdot \left(C_{CO_2}^{C4a}|_l^{in} - C_{CO_2}^{C4a}|_l\right) + \varphi_{CO_2}^{C4a} + \phi_{CO_2}^{C4a} - R_{K1} \tag{191}$$

$$\frac{dC_{HCO_3}^{C4a}|_l}{dt} = \frac{F_{in}^{C4a}}{V_l^{C4a}} \cdot \left(C_{HCO_3}^{C4a}|_l^{in} - C_{HCO_3}^{C4a}|_l\right) + R_{K1} - R_{K2} + \phi_{HCO_3}^{C4a} \tag{192}$$

$$\frac{dC_{CO_3^{2-}}^{C4a}|_l}{dt} = \frac{F_{in}^{C4a}}{V_l^{C4a}} \cdot \left(C_{CO_3^{2-}}^{C4a}|_l^{in} - C_{CO_3^{2-}}^{C4a}|_l\right) + R_{K2} \tag{193}$$

$$\frac{dC_{O_2}^{C4a}|_l}{dt} = \frac{F_{in}^{C4a}}{V_l^{C4a}} \cdot \left(C_{O_2}^{C4a}|_l^{in} - C_{O_2}^{C4a}|_l\right) + \varphi_{O2}^{C4a} + \phi_{O2}^{C4a} \tag{194}$$

$$\frac{dC_X^{C4a}|_l}{dt} = \frac{F_{in}^{C4a}}{V_l^{C4a}} \cdot \left(-C_X^{C4a}|_l\right) + \phi_X^{C4a} \tag{195}$$

$$\frac{dC_{HNO_3}^{C4a}|_l}{dt} = \frac{F_{in}^{C4a}}{V_l^{C4a}} \cdot \left(C_{HNO_3}^{C4a}|_l^{in} - C_{HNO_3}^{C4a}|_l\right) + \phi_{HNO_3}^{C4a} \tag{196}$$

$$\frac{dC_{NH_3}^{C4a}|_l}{dt} = \frac{F_{in}^{C4a}}{V_l^{C4a}} \cdot \left(C_{NH_3}^{C4a}|_l^{in} - C_{NH_3}^{C4a}|_l\right) + \phi_{NH_3}^{C4a} \tag{197}$$

$$\frac{dC_{O_2}^{C4a}|_g}{dt} = \left(\frac{G_{in}^{C4a}}{V_l^{C4a}} \cdot \left(\frac{C_{O_2}^{C4a}|_g^{in}}{100 - C_{O_2}^{C4a}|_g^{in} - C_{CO_2}^{C4a}|_g^{in}} - \frac{C_{O_2}^{C4a}|_g}{100 - C_{O_2}^{C4a}|_g - C_{CO_2}^{C4a}|_g}\right) - \varphi_{O_2}^{C4a} \cdot V_l^{C4a}/MW_{O_2}\right)\frac{24}{V_G^{C4a}} \tag{198}$$

$$\frac{dC_{CO_2}^{C4a}|_g}{dt} = \left(\frac{G_{in}^{C4a}}{V_l^{C4a}} \cdot \left(\frac{C_{CO_2}^{C4a}|_g^{in}}{100 - C_{O_2}^{C4a}|_g^{in} - C_{CO_2}^{C4a}|_g^{in}} - \frac{C_{CO_2}^{C4a}|_g}{100 - C_{O_2}^{C4a}|_g - C_{CO_2}^{C4a}|_g}\right) - \varphi_{CO_2}^{C4a} \cdot V_l^{C4a}/MW_{CO_2}\right)\frac{24}{V_G^{C4a}} \tag{199}$$

From the list of equations (22)-(31), parameters R_{K1} and R_{K2} define the rates of the carbon-species equilibrium and are a function of the carbon-species concentrations themselves, parameters defined by the letter φ define the gas-liquid transfer rate for oxygen, which is a function of oxygen concentration in the liquid and in the gas phase, and for carbon dioxide, which is also a function of the carbon dioxide concentration in both phases. Considering no nitrogen limitation, the differential equations for nitrate and ammonia can be omitted. The list of carbon species, which include total inorganic carbon (TIC), carbon dioxide, bicarbonate and carbonate can also be reduced since some information is redundant. The total inorganic carbon can be omitted if the specific carbon species are used and considering that under the operating pH used in C4a, 8.5, the concentration of carbonate will be zero or very low. So, from the model represented in equations (22)-(31), only the states listed in Table 6. 2 are kept for linearization. The input variables are also represented in Table 6. 2.

Table 6. 2. State and manipulated variables in C4a linearized model

State	Physical Variable	Input	Physical Variable
x_1	$C_{CO_2}^{C4a}\|_l$	u_1	$C_{HNO_3}^{in}\|_l^{C4a}$
x_2	$C_{HCO_3}^{C4a}\|_l$	u_2	$C_{O_2}^{in}\|_g^{C4a}$
x_3	$C_{O_2}^{C4a}\|_l$	u_3	$C_{CO_2}^{in}\|_g^{C4a}$
x_4	$C_X^{C4a}\|_l$	u_4	F_{in}^{C4a}
x_5	$C_{O_2}^{C4a}\|_g$	u_5	G_{in}^{C4a}
x_6	$C_{CO_2}^{C4a}\|_g$	u_6	I_{C4a}

After having selected the model states, with the consequent reduction of the list of ordinary differential equations, it is possible to proceed to the obtention of the state space form of the model prior the calculation of the Jacobian for the states (A) and for the inputs (B) as stated in equations (185) and (186):

$$A = \begin{bmatrix} -1.2e^{-2}u_5 - 1.04e^3 & 0.7 & 0 & A_{1,4} & 0 & 0.16 \\ 1.44e^3 & -1.2e^{-2}u_5 - 1.11 & 0 & 0 & 0 & 0 \\ 0 & 0 & -1.2e^{-2}u_5 - 1.11 & A_{3,4} & 4.49e^{-3} & 0 \\ 0 & 0 & 0 & A_{4,4} & 0 & 0 \\ 0 & 0 & 0 & 0 & A_{5,5} & A_{5,6} \\ 6e^2 & 0 & 0 & 0 & A_{6,5} & A_{6,6} \end{bmatrix} \quad (200)$$

$$B = \begin{bmatrix} 0 & 0 & 0 & 0 & -1.2e^{-2}x_2 & B_{1,6} \\ 0 & 0 & 0 & 0 & -1.2e^{-2}x_3 & 0 \\ 0 & 0 & 0 & 0 & -1.2e^{-2}x_5 & B_{3,6} \\ 0 & 0 & 0 & 0 & -1.2e^{-2}x_6 & B_{4,6} \\ 0 & B_{5,2} & B_{5,3} & B_{5,4} & 0 & 0 \\ 0 & B_{6,2} & B_{6,3} & B_{6,4} & 0 & 0 \end{bmatrix} \quad (201)$$

For clarity, the items of the matrices A and B are expressed as $A_{n,m}$ and $B_{n,m}$ (where n and m refer to the row and column index respectively). Table 6. 3 provides the corresponding expressions of these terms in (200) and (201).

Table 6. 3. Dependency of matrix terms symbolically expressed in (200) and (201)

Matrix	Function
$A_{1,4}$	$f(x_4, u_6)$
$A_{3,4}$	$f(x_4, u_6)$
$A_{4,4}$	$f(x_4, u_5)$
$A_{5,5}$	$f(x_5, x_6, u_2, u_3, u_4)$

$A_{5,6}$	$f(x_5, x_6, u_2, u_3, u_4)$
$A_{6,5}$	$f(x_5, x_6, u_2, u_3, u_4)$
$A_{6,6}$	$f(x_5, x_6, u_2, u_3, u_4)$
$B_{1,6}$	$f(x_4, u_6)$
$B_{3,6}$	$f(x_4, u_6)$
$B_{4,6}$	$f(x_4, u_6)$
$B_{5,2}$	$f(x_5, x_6, u_2, u_3, u_4)$
$B_{5,3}$	$f(x_5, x_6, u_2, u_3, u_4)$
$B_{5,4}$	$f(x_5, x_6, u_2, u_3)$
$B_{6,2}$	$f(x_5, x_6, u_2, u_3, u_4)$
$B_{6,3}$	$f(x_5, x_6, u_2, u_3, u_4)$
$B_{6,4}$	$f(x_5, x_6, u_2, u_3)$

Finally, replacing x and u in A and B for the operating point at a given time as expressed in (200) and (201), it is possible to find the final expression for A and B. The last required step is to convert the continuous linear state space form in (186) to a discrete-time state space form:

$$x_{k+1} = A \cdot x_k + B \cdot u_k \tag{202}$$

To note, all states listed in Table 6. 2 are measurable, the carbon species in both liquid and gas phases by means of sensors and equilibrium calculation, and oxygen and biomass states by sensors. If it is desired to include additional non-measurable states in the state-space form, it is possible, but a state observer or state estimator shall be considered such as a Kalman Filter (statistical approach) or a Luenberger observer (mechanistic-based). This is not the case of the current model. From the list of states and inputs of the discrete-time model in (202), it is of major interest the concentration of oxygen at time k+1, equivalent to the optimal concentration of oxygen in the output of C4a, which combined with the fixed gas flow in C4a with a value of 2.8 L/min allows the calculation of $Q_{O_2}^{C4a,ref}(t)$ in (168). The concentration of oxygen at time k is also important, which is the previously obtained optimal concentration of oxygen in the output of C4a. This information is enough to obtain a unique solution for the system of equations represented by the state space form in (202).

$$\begin{matrix} \boldsymbol{C_{CO_2}^{C4a}|_{l_{k+1}}} - \overline{C_{CO_2}^{C4a}|_l} \\ \boldsymbol{C_{HCO_3}^{C4a}|_{l_{k+1}}} - \overline{C_{HCO_3}^{C4a}|_l} \\ \boldsymbol{C_{O_2}^{C4a}|_{l_{k+1}}} - \overline{C_{O_2}^{C4a}|_l} \\ \boldsymbol{C_X^{C4a}|_{l_{k+1}}} - \overline{C_X^{C4a}|_l} \\ \boldsymbol{C_{CO_2}^{C4a}|_{g_{k+1}}} - \overline{C_{CO_2}^{C4a}|_g} \\ C_{O_2}^{C4a}|_{g_{k+1}} - \overline{C_{O_2}^{C4a}|_g} \end{matrix} = A \cdot \begin{matrix} C_{CO_2}^{C4a}|_{l_k} - \overline{C_{CO_2}^{C4a}|_l} \\ C_{HCO_3}^{C4a}|_{l_k} - \overline{C_{HCO_3}^{C4a}|_l} \\ C_{O_2}^{C4a}|_{l_k} - \overline{C_{O_2}^{C4a}|_l} \\ C_X^{C4a}|_{l_k} - \overline{C_X^{C4a}|_l} \\ C_{CO_2}^{C4a}|_{g_k} - \overline{C_{CO_2}^{C4a}|_g} \\ C_{O_2}^{C4a}|_{g_k} - \overline{C_{O_2}^{C4a}|_g} \end{matrix} + B \cdot \begin{matrix} C_{HNO_3}^{in}|_l^{C4a} - \overline{C_{HNO_3}^{in}|_l^{C4a}} \\ C_{O_2}^{in}|_g^{C4a} - \overline{C_{O_2}^{in}|_g^{C4a}} \\ C_{CO_2}^{in}|_g^{C4a} - \overline{C_{CO_2}^{in}|_g^{C4a}} \\ F_{in}^{C4a} - \overline{F_{in}^{C4a}} \\ G_{in}^{C4a} - \overline{G_{in}^{C4a}} \\ \boldsymbol{I_{C4a}} - \overline{I_{C4a}} \end{matrix} \tag{203}$$

Where, the parameters in bold are those unknown, so there are 6 equations for 6 unknown parameters. Therefore, the system of equations has a unique solution. It should also be noticed that this strategy makes use of the prediction horizon of the MPC defined in (166) to (169) to provide values for the $C_{O_2}^{C4a}|_{g_{k+1}}$. The concentration in the gas phase of CO_2 can be calculated without increasing the number of variables to optimize in the MPC, but by exploiting its linear dependency with oxygen.

Adaptation of C5 Model

The equations for C5 model adapted to the secondary controller are the same as those presented in 0 in discrete form:

$$C_y^{C5}|_g(k+1) = C_y^{C5}|_g(k) + (G_{in}^{C5}(k)C_y^{C5}|_g^{in}(k) - G_{out}^{C5}(k)C_y^{C5}|_g(t) + \phi_y^{C5})T_s \quad (204)$$

Adaptation of C4b Model: Energy Cascade Model

Regarding C4b, an energy cascade modelling approach has been used to predict the production and consumption rates of oxygen and carbon dioxide according to Boscheri et al. (2012). Energy cascade models are empirical models, which, as opposed to mechanistic models, rely on polynomial equations. The presented model by Boscheri et al., (2012) predicts the plant growth (*HCG*) and oxygen and carbon dioxide production and consumption rates as a function of four parameters: the canopy light absorption (A), the canopy quantum yield (CQY), the mean use efficiency (CUE_{24}) and as a function of the photosynthetic photon flux density (I_{C4b}). The expression to find the hourly carbon consumption is the following:

$$HCG = -CUE_{24} \cdot A \cdot CQY \cdot I_{C4b} \cdot I \quad (205)$$

Being I an integer value that can be 1 or 0 for day and night photoperiod activities respectively. From the HCG, it is easy to calculate the hourly oxygen production (HOP) for the photosynthetic activity:

$$HOP = -\frac{HCG}{CUE_{24}} OPF \cdot MW_{O_2} \quad (206)$$

In (206), OPF represents the photosynthetic yield which is set to 1 for lettuce in this case. During dark photoperiods in plants, hourly carbon production (HCP) is quite stable at 34% of HCG, based on data obtained from the MELiSSA Pilot Plant Higher Plants Chamber. Hourly oxygen consumption during dark photoperiod (HOC) is equimolar in relation to dark HCP:

$$HCP = -0.3 \cdot HCG \quad (207)$$

$$HOC = -HCP \quad (208)$$

The discrete-time model of oxygen and carbon dioxide are the following:

$$C_y^{C4b}|_g(k+1) = C_y^{C4b}|_g(k) + (G_{in}^{C4b}(k)C_y^{C4b}|_g^{in}(k) - G_{out}^{C4b}(k)C_y^{C4b}|_g(k) + \frac{\phi_y^{C4b}}{V^{C4b}})T_s \quad (209)$$

For day photoperiod, parameter R_y^{C4b} in equation (211) can take the value HCG or HOP based on what $C_y^{C4b}|_g$ refers to. For night photoperiod, parameter R_y^{C4b} in equation (211) can take the value HCP or HOC based on what $C_y^{C4b}|_g$ refers to.

Adaptation of the Gas Membrane:

The equations for the gas management and storage tanks used in the secondary controller are the same as those presented in section 6.2.7. To avoid the simultaneous charging and discharging of the CT and to keep the charging/discharging flows within the allowed boundaries, the following constraints have been considered:

$$d_{ch}^{CT}(k) + d_{dis}^{CT}(k) = 1 \quad (210)$$

$$0 \leq G_{ch}^{CT}(k) \leq d_{ch}^{CT}(k) \cdot G_{ch}^{CT,max}(k) \quad (211)$$

$$0 \leq G_{dis}^{CT}(k) \leq d_{dis}^{CT}(k) \cdot G_{dis}^{CT,max}(k) \quad (212)$$

$$G^{CT}(k) = G_{ch}^{CT}(k) - G_{dis}^{CT}(k) \quad (213)$$

Where d_{ch}^{CT} (k)and d_{dis}^{CT} (k) are two binary variables.

Adaptation of C3 Model

Since the nitrification reactor is expected, in the current study, to operate at a constant nitrogen load, in the form of ammonium in the input, a simple law can be used to predict the concentration of oxygen in the gas output flow as a function of the input oxygen concentration in the gas flow. This input gas flow concentration corresponds to the concentrated gas flow $C_{O_2}^c|_g(k)$. This law is obtained considering a liquid flow of 32.9 mL/min and an ammonium concentration of 0.32 g/L, adequate to provide nitrate for C4a and C4b demands.

$$C_{O_2}^{C3}|_g(k+1) = C_{O_2}^c|_g(k) - 18.5 \quad (214)$$

6.3.3. Predictive Functional Controllers

Predictive Functional Control (PFC) is used in the secondary and tertiary control level to supply references to the MPC. For basic level controllers, PFC has been shown to be very efficient and complementary to MPC to control complex systems such as BLSS due to its ability to find analytical solutions of optimization problems (Haber et al., 2016). Besides, the combination of

both types of controllers relaxes the computational time if a single centralized MPC is used. Considering a first-order model in discrete-time form:

$$G_m(z) = \frac{\beta_m z^{-1}}{1 - \alpha_m z^{-1}} \tag{215}$$

The system parameters are defined as follows:

$$\alpha_m = \frac{e^{-T_s}}{T_m} \tag{216}$$

$$\beta_m = K_m(1 - \alpha_m) \tag{217}$$

In the coincidence point H, the predicted model output is the following:

$$y_m(k + H|k) = \alpha_m y_m(k|k) + K_m(1 - \alpha_m)u(k|k) \tag{218}$$

The predicted process output ($\hat{y}$) after *n* steps can be deduced considering the predicted error and the desired reference as follows:

$$\hat{y}(k + H|k) = y^{ref} - \hat{e}(k + H|k) \tag{219}$$

It is only necessary to define the expected error after *n* steps:

$$\hat{e}(k + H|k) = \lambda^H e(k|k) \tag{220}$$

$$e(k|k) = y^{ref} - y(k|k) \tag{221}$$

Parameter λ defines the rate of reduction of the error in the trajectory and is a function of the closed loop response time (CLRT), being the shorter CLRT the faster the controller response:

$$\lambda = e^{(-3T_s/CLRT)} \tag{222}$$

The variation on the predicted output is calculated straightforward:

$$\Delta\hat{y}(k + H|k) = (1 - \lambda^H)e(k|k) \tag{223}$$

The control law is obtained considering that the variation on the predicted output should be equal to the variation on the model output:

$$u(k|k) = \frac{(1 - \lambda^H) \cdot \left(y^{ref} - y(k|k)\right) + (1 - \alpha_m^H)y_m(k|k)}{K_m(1 - \alpha_m^H)} \tag{224}$$

In the secondary control level, PFC1 is used to calculate the amount of concentrated gas flow to be sent to C3 to oxidize all the ammonia in the liquid phase. In the primary control level, PFC2 is used to adjust the light intensity in C4a to track the oxygen reference received from the secondary control and PFC3 is used to add external CO_2 to C4b in case a concentration of 800 ppm cannot be guaranteed.

6.3.4. Simulation conditions and controllers' specifications

In Table 6. 4, the MPC controller specifications for Level 3 and Level 2 are defined whereas in Table 6. 5, the specifications of the local controllers are defined.

Table 6. 4. Setpoints and controller specifications for Level 3 and Level 2

Variable	Value
Weights	
λ_1	1
λ_2	10
$\lambda_3 \, for \, C_{O_2}^{C5}\|_g$	10
$\lambda_3 \, for \, C_{CO_2}^{C4b}\|_g$	1
$\lambda_3 \, for \, G^{CT}$	1
$\lambda_3 \, for \, Q_{O_2}^{C4a}$	1
λ_4	1
References	
$C_{O_2}^{C5}\|_g^{ref}$	21%
$C_{CO_2}^{C4b}\|_g^{ref}$	1000 ppm
$C_{O_2}^{C3}\|_l^{ref}$	80%
Horizons	
N_{p3}, N_{c3}	6 hr
N_{p2}, N_{c2}	3 hr
Sample Time	
T_3	1 hr
T_2	0.1 hr
T_1	0.01 hr

Table 6. 5. Specifications for the PFC controllers

Variable	Gain ($\mathbf{K_m}$)	Time constant ($\boldsymbol{\Gamma_m}$)	Coincidence point (H)	Close loop response time (CLRT)	Setpoint
$C_{O_2}^{C4a}\|_g$ based on light	0.007 % O_2/(W/m²)	0.15 h^{-1}	0.01 h^{-1}	$3 \cdot \Gamma_m$	Dynamic
$C_{O_2}^{C3}\|_l$ based on concentrated gas	Dynamic	0.0115 h^{-1}	0.1 h^{-1}	Γ_m	80%
$C_{HNO_3}^{C4b}\|_l$ based on nitrified liquid	10^7 mol-N/m³/(m³/s)	3600 sec^{-1}	1	$3 \cdot \Gamma_m$	11 mol-N/m³*
$C_{CO_2}^{C4b}\|_g$ based on external injection	10.6 ppm CO_2/m³/s	100 sec^{-1}	1	$10 \cdot \Gamma_m$	800 ppm

*NH_4:HNO_3 ratio of 1:1

Fig. 6. 9 shows a summary of all the control levels, the equations that apply for each one of them and how the control structure is related to the process design.

For the presented simulation, a group of 6 rats has been used a surface are of 5 m^2 for the HPC and the photoperiods for the crops and the crew are 16/8 and 12/12 hours respectively

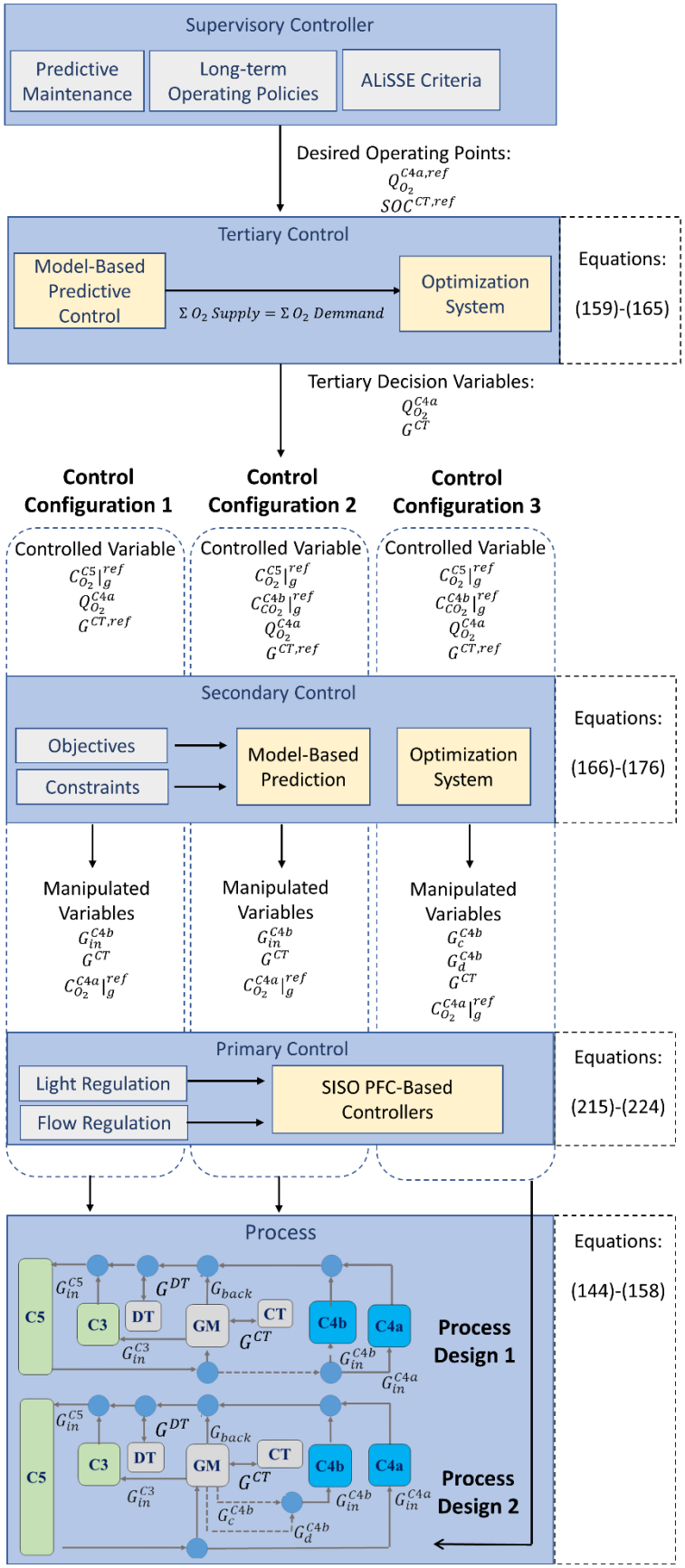

Fig 6. 9. Structure of the control architecture presented in the current chapter with the associated equations

6.4. Results

This section is divided in two parts, the first comparing the performance of the three controllers presented in the previous section and the second analyzing the performance of the hierarchical control structure based on the results of the best controller.

6.4.1. Comparison of controllers

6.4.1.1. Evolution of Controlled Variables

As observed in Fig 6. 10, oxygen concentration is well controlled mainly for control configurations 1 and 3, being worse for control configuration 2. The reasons for the deviation from the reference of 21% O_2 are extensively explored along this section. In all control configurations, a perturbation is observed during the plants' photoperiod switch, when plants start consuming oxygen and releasing carbon dioxide. At that precise moment, a peak of oxygen is detected in the crew compartment as can be observed in Fig 6. 10, but also a peak of oxygen is observed in C4a compartment (Fig 6. 11) and a decrease in the level of the buffer tank (Fig 6. 12).

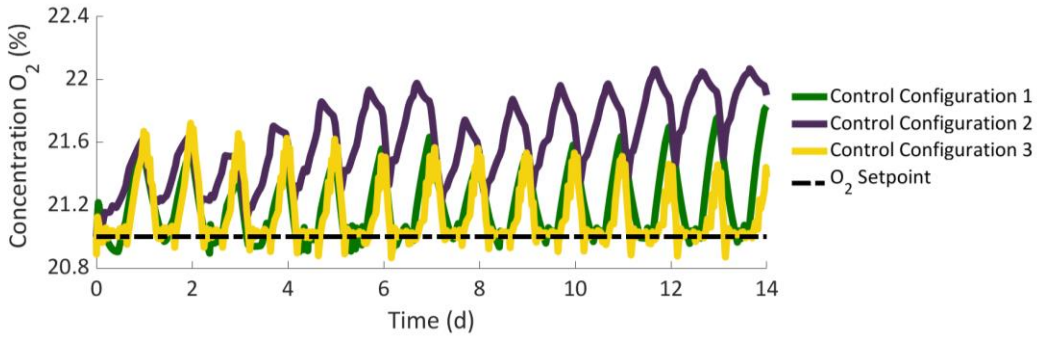

Fig 6. 10. Oxygen concentration in the crew compartment (C5)

This is all driven by the sudden decrease in the C4b oxygen concentration associated to the stop of the photosynthetic activity and the start of the visible decrease in oxygen concentration due to the plants' respiration (see Fig 6. 13). This oscillatory pattern is determined by the sudden changes in the metabolic activities of different compartments. This is quite relevant regarding the crew compartment with two clearly differentiated respiratory rates between photoperiods and hugely relevant regarding the higher plants compartment with a diel metabolism extensively discussed in the previous Chapter.

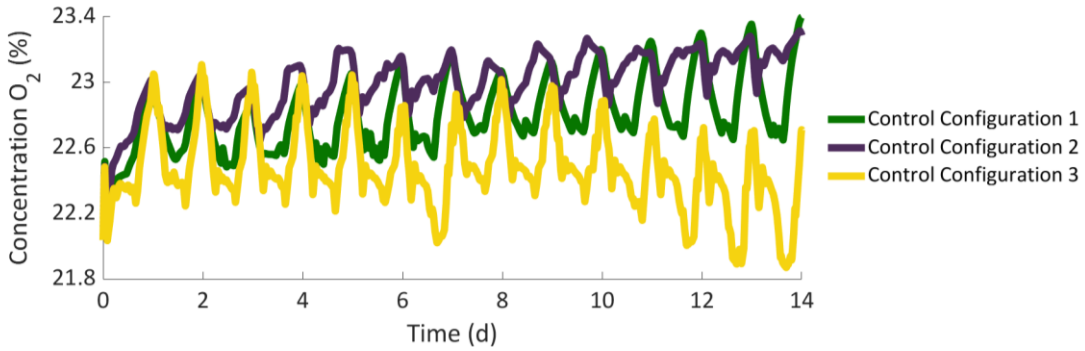

Fig 6. 11. Oxygen concentration in C4a

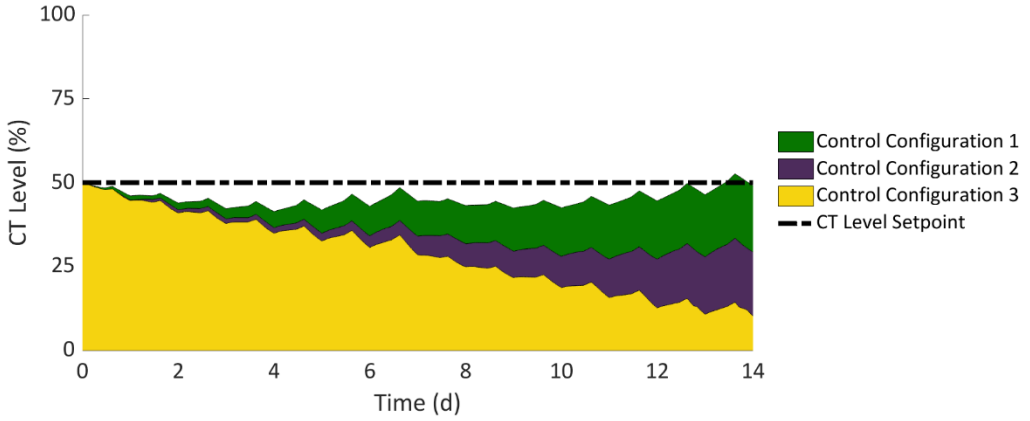

Fig 6. 12. State of charge of Oxygen concentrated tank (CT)

The oxygen concentration in C5 increases when plants start consuming oxygen during dark respirations. It may be a bit counterintuitive since it should be expected oxygen in C5 to be negatively affected by the start of the dark photoperiod in plants. But this behavior is determined by the configuration of the controller. Probably, the prediction horizon for the controller is too short to foresee the change in the plants' consumption pattern, thus the immediate response of the controllers when plants metabolism shifts to the consumption of oxygen during the night is to accumulate oxygen in C5 in excess by releasing the CT and increasing the productivity assigned to C4a. As stated, there is margin for improvement on attenuating the oscillations mainly in C5.

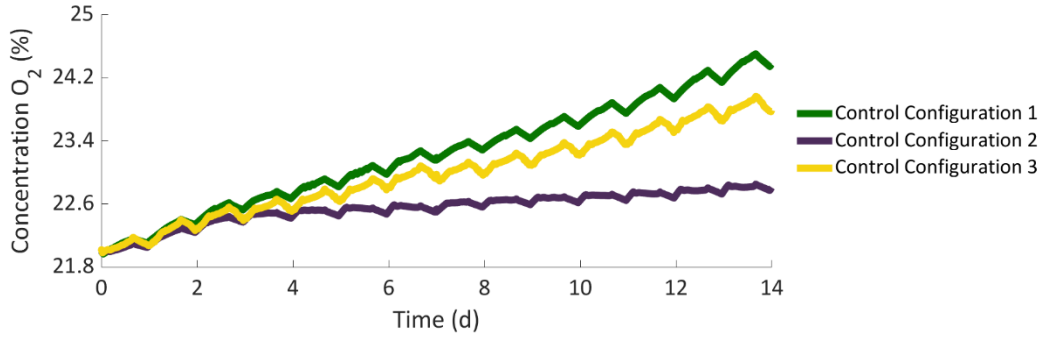

Fig 6. 13. Oxygen concentration in C4b

Regarding the carbon dioxide concentration in C4b, it is interesting to see how the addition of the carbon dioxide tracking in Level 2 improves the efficiency of the carbon usage within the system, considering efficiency as the use of internal resources (carbon dioxide available inside the system) as opposed to the use of external addition of carbon dioxide. The carbon dioxide concentration in C4b has a similar trend in the different control configurations as observed in Fig 6.14a, since in all cases it is controlled, by means of adding external carbon dioxide in the system (Control configuration 1) and by adjusting the gas flows within the compartments (Control configurations 2 and 3). In Fig 6.14b-c, it is demonstrated that in control configuration 1, the use of external CO_2 is much larger than in control configurations 2 and 3. The contribution of carbon dioxide supply from internal resources in control configuration 1 (see Fig 6.14c) does not correspond to a control command aimed at tracking carbon dioxide in C4b, since there is not a control law implemented for this purpose, but only external carbon dioxide addition is used as a control command to track carbon dioxide concentration in C4b. This is not the case for control configuration 2 and 3, whose control law in Level 2 contemplates the use of internal gas flows to control carbon dioxide in C4b as expressed in (170)-(172). The contribution of the carbon dioxide supply is even clearer in Fig 6. 15.

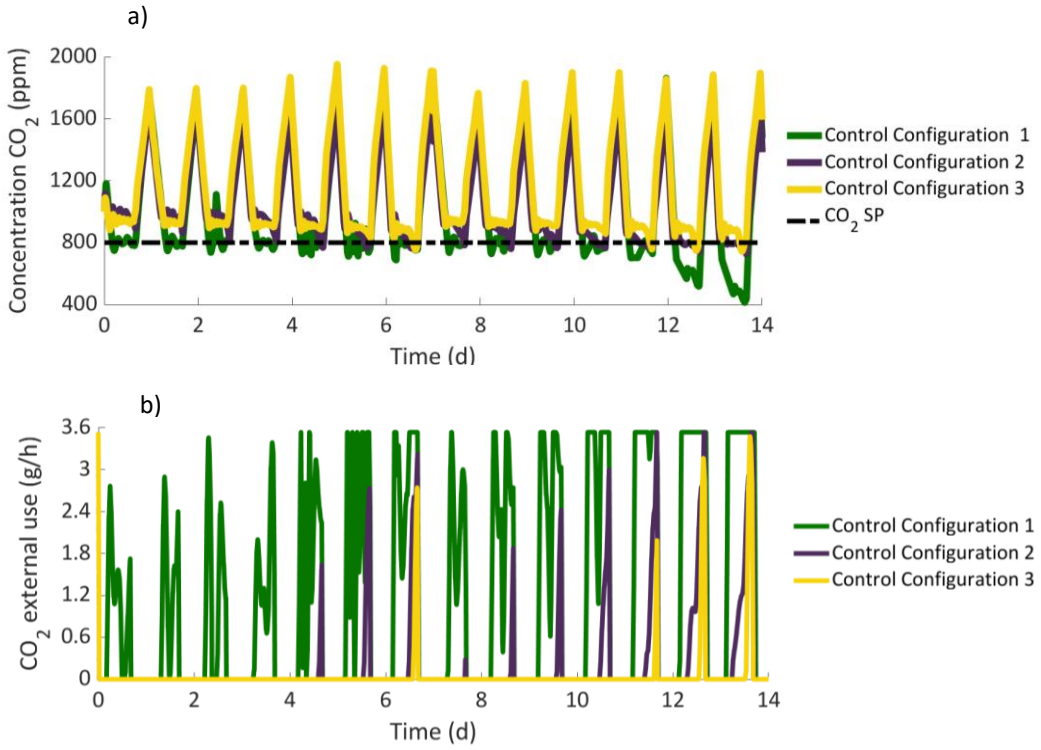

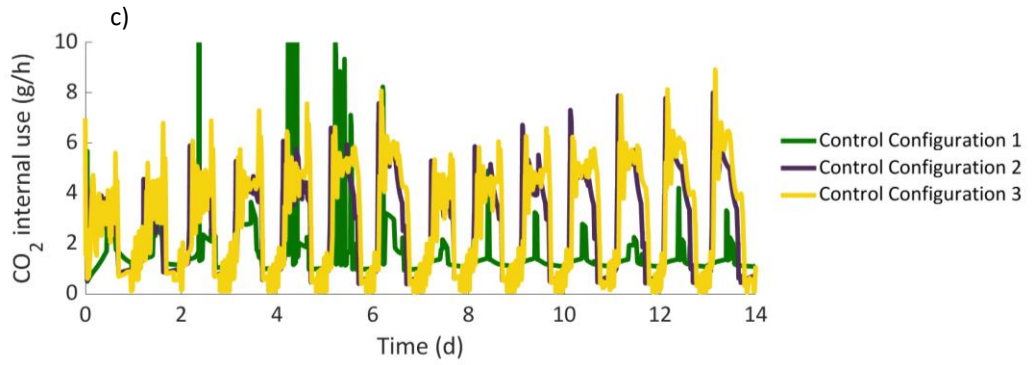

Fig 6. 14. Dynamics of Carbon dioxide in the higher plants compartment. A) Carbon dioxide concentration in C4b; B) External addition of carbon dioxide in C4b expressed as input rate; C) Internal use of carbon dioxide considering the supply of carbon dioxide from the different compartments to C4b and expressed as input rate.

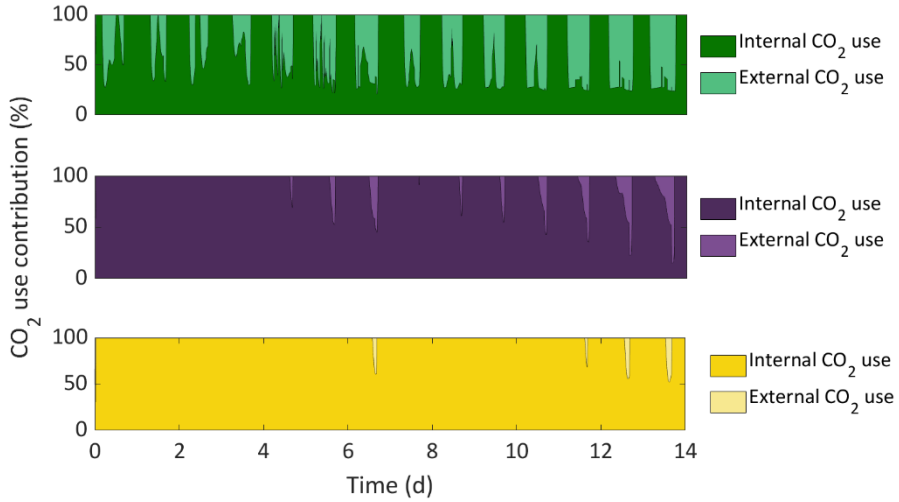

Fig 6. 15. Contribution of CO_2 use in the different control configurations in the following top-down order: Control configuration 1, 2 and 3.

Fig 6. 15 shows that one of the main benefits behind the development of a control architecture is to improve the performance of the system, not only in terms of controllability of compounds (like for the case of CO_2 and O_2), but also in terms of circularity, since the difference regarding the external resource usage is huge in favor of those control configurations promoting the use of such internal resources.

One of the consequences of reducing the carbon dioxide external addition is an overall reduction of the carbon dioxide accumulation in the atmosphere of the different compartments as shown in C4a and C5 results (see Fig 6.16 and Fig 6. 17). This is especially relevant for the crew compartment (C5), which is the most restricted compartment in terms of carbon dioxide accumulation due to its toxicity for the crew. Therefore, a second advantage of enriching the control algorithm with an increased number of controlled variables is the possibility to minimize the concentration of carbon dioxide in the system, which is crucial in BLSS missions.

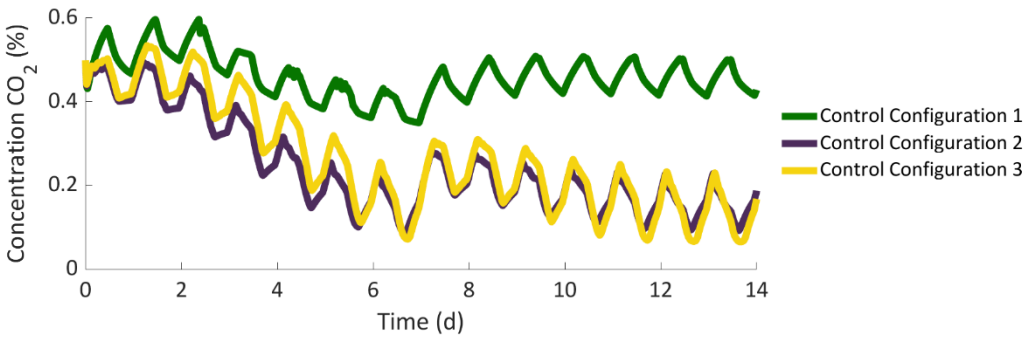

Fig 6. 16. Carbon dioxide concentration in C4a

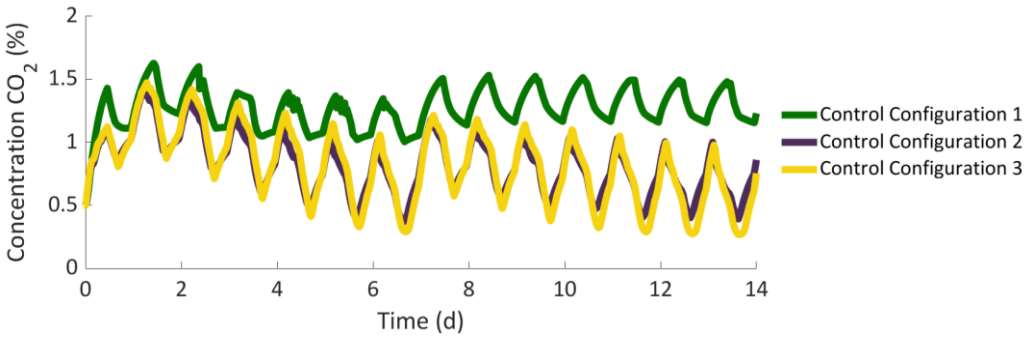

Fig 6. 17. Carbon dioxide concentration in C5

6.4.1.2. Manipulated variables

The two criteria that rule Level 3 of the HCS and, by extension, the operation of the whole process is the storing tank to have a constant state of charge (SOC) of 50% and C4a to operate close to the preferred operating condition of 200 W/m^2. As has been already presented in Fig 6. 12, the criteria to have the concentrated gas tank at 50% is not properly achieved specially for control configuration 3 after 14 days of operation, whereas the performance for control configuration 1 and 2 is better since concentrated gas tank remains closer to 50%. This behavior in control configuration 3 may be explained by either contradictory instructions or even by insufficient instructions. This is further explored in section 6.4.1.4.

On top of the level of the concentrated gas tank and the external carbon dioxide addition, the remaining manipulated variables to discuss are the light intensity in C4a and the internal gas flow dispatches. Regarding C4a light intensity, the control is more precise, and all three strategies remain close to the reference of 200 W/ m^2 (see Fig 6.18).

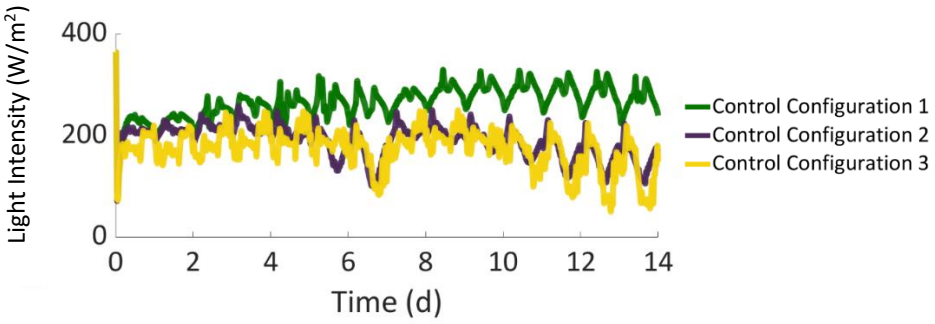

Fig 6. 18. Light intensity in C4a.

The evolution of the light intensity presented in Fig 6. 18 evidences another attribute of HCS which is the capability to include supervision commands. In the presented study this is not fully exploited since constant criteria (50% storage in concentrated gas tank and 200 W/m^2 as nominal light intensity in C4a) are used from higher levels to lower levels in the control hierarchy. In future long-term BLSS missions the use of dynamic supervision criteria definition shall be considered as it would be of high interest for the success of the missions. Such supervision module could be interesting for many cases: The participation of photosynthetic oxygen-producing compartments could be modulated, and different specific weights could be given to one or another. For example, a situation where, due to predictive maintenance tasks, C4a may be switched off temporarily could be anticipated with a maximum illumination period to fill the concentrated gas tank. Similarly, a reduced nitrification may be counteracted with an increased weight for higher plants compartment, which can operate with higher NH_4:NO_3 ratios, compared to C4a which works better with a single Nitrogen-species.

Analyzing more in detail Fig 6. 18, it seems that control configuration 1 remains closer to the desired reference of 200 W/m^2, whereas control configurations 2 and 3 deviate over time from such reference. This is similar to the pattern observed in the other supervision criteria of penalizing deviations from a concentrated tank level of 50% (see Fig 6. 12) in which results are better for control configuration 1 than for control configurations 2 and 3. It can be concluded that control configuration 1 is better to satisfy supervision criteria than control configurations 2 and 3. The reason why this happens is further explored in section 6.4.1.4, but it is likely that controlling both carbon dioxide and oxygen in C4b and C5 respectively may be interfering the capacity to satisfy supervisory objectives.

Finally, gas flows expressed as a fraction from C5 to the rest of the compartments are presented in Fig 6. 19. The main difference between the proposed control proposals is that control configuration 3 has one more degree of freedom compared to control configurations 1 and 2. While control configurations 1 and 2 use the gas outflow from C5 to feed C4b, control

configuration 3 use a combination of the concentrated and diluted gas flows obtained from the membrane separation unit (see Fig 6. 2 for schematic process diagram) to obtain the amount of carbon dioxide required to track the setpoint of carbon dioxide in C4b. This is the reason why in the third plot in Fig 6. 19, corresponding to the control configuration 3, the gas dispatch from C5 to C4b is null. As shown in Fig 6. 2, the fraction of concentrated and diluted flows are obtained after the membrane separation unit. Also, in all plots in Fig 6. 19 the fraction of gas flow to C4a is constant, this is because C4a gas flow is not a decision variable, but it is constraint by the hydrodynamics of the compartment to a value of 2.8 L/min (Alemany et al., 2019). The total flow in and out of C5 is also constraint to a value of 17.14 L/min.

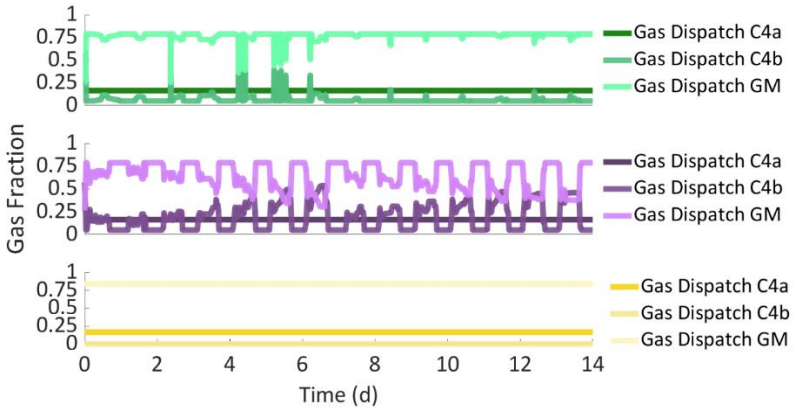

Fig 6. 19. Gas Flows downstream C5. Top-Down order: Control configuration 3, 2 and 1.

A deeper analysis of the use of the concentrated and diluted flows in control configuration 3 (see Fig 6. 20), evidence that the control is a bit aggressive, especially at the moment of photoperiod switch in C4b. This is a pattern already observed in many control commands and controlled variables along this study. For control configuration 3, during the whole testing time, a higher fraction of concentrated gas than diluted gas is used to feed C4b (see Fig 6. 20).

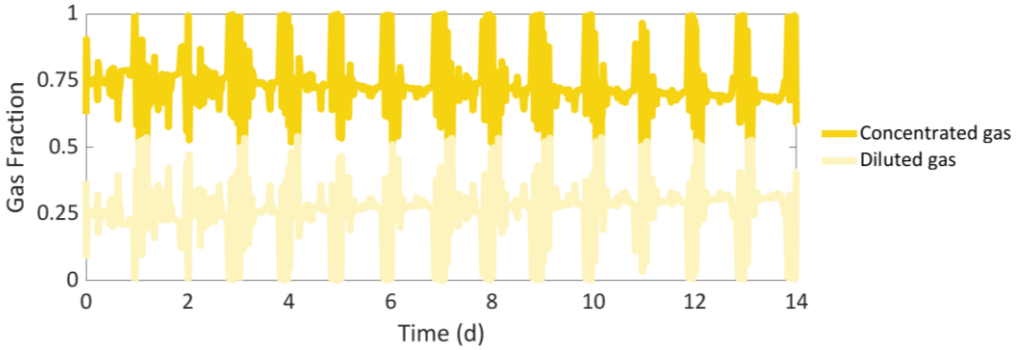

Fig 6. 20. Concentrated and diluted gas flow fractions used to feed C4b in control configuration 3

Notice that the type of membrane used concentrates oxygen as well as carbon dioxide. In Table 6. 6, a summary of concentrations in and out of the gas concentration membrane is presented.

The selected fraction represented in Fig 6. 20 is highly precise since it allows tracking the carbon dioxide setpoint in C4b and reducing the consumption of external carbon dioxide (Fig 6. 14).

Table 6. 6. Summary of concentration in and out of the gas separation membrane

Species	Input (%)	Output (%)	
		Concentrated	Diluted
Oxygen	21.13	44.46	13.73
Carbon Dioxide	0.82	3.07	0.1

6.4.1.3. Assessment of Level 2 controller performance

The differences between the three studied designs are caused by the Level 2 of the hierarchical control structure. More specifically, in terms of controllers' specification, the main differences between the three designs are the amount of variables to optimize in Level 2 and the terms in the cost function. In general, the larger the amount of variables to optimize and terms in the cost function, the longer will it take for the optimization algorithm to converge to a solution. As extensively discussed in this chapter, the main difference between control configuration 1 and the other two is that the first does not include control of CO_2 in Level 2 of the MPC. On the other hand, the main difference between control configuration 1 and 2 and control configuration 3 is that the last one has one more degree of freedom, therefore it has one more variable to be optimized.

Table 6. 7. Number of cost function terms and variables to be optimized at Level 2 for each proposed control configuration

Control configuration	Cost Function Terms	Number of Variables to be optimized
Control configuration 1	5	3
Control configuration 2	6	3
Control configuration 3	6	4

As expected, and as presented in Fig 6. 21, the lower the number of variables to be optimized and the lower the number of terms in the objective function, the smaller the computation time for the MPC to converge to a feasible solution. These results indicate that, while control configuration 1 and control configuration 3 have enough degrees of freedom to properly track their references, control configuration 2 does not. On the contrary, control configuration 2 lacks the required degrees of freedom to track both oxygen in C5 and carbon dioxide in C4b. In fact, in control configuration 2, both setpoints are coupled by the gas flow between C5 and C4b in such a way that a good performance in tracking carbon dioxide in C4b (see Fig 6. 14) and oxygen in C5 (see Fig 6. 10) would not be as good as for control configuration 3. This would explain the

bias in the oxygen concentration observed in C5 in Fig. 6.10. However, the drawback of successfully controlling more parameters by including more manipulated variables as achieved in control configuration 3, is the increase in the computation time as observed in Fig 6. 21.

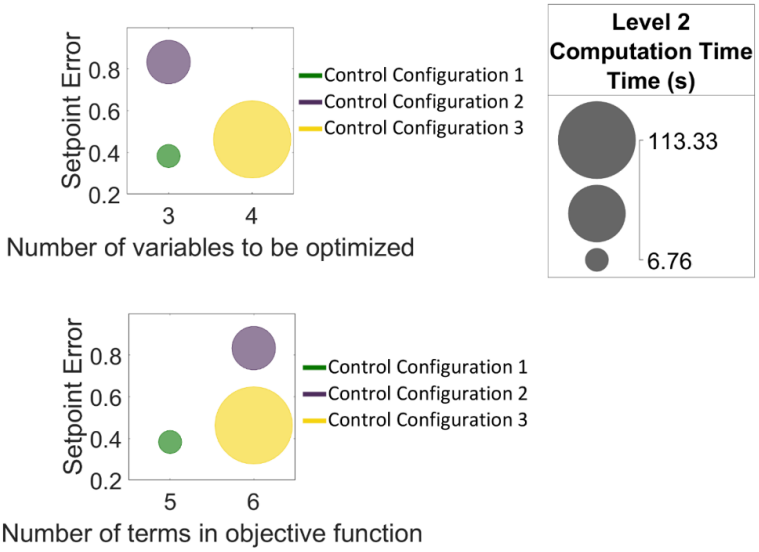

Fig 6. 21. Computation time of Level 2 MPC and setpoint error expressed as a function of the number of variables to be optimized (top) and as a function of the number of terms in the objective function. Setpoint error is expressed as the sum of the difference between the oxygen measurement in C5 and the setpoint at each sampling time.

6.4.1.4. Troubleshooting the results obtained for control configuration 3

As it has been already stated, control configuration 3 has a significant loss of concentrated gas tank (CT) level, which contradicts one of the supervisory commands based on penalizing deviations in CT level from 50%.

The most likely possibility that may be causing this behavior is the precise setpoint tracking requirement of both oxygen and carbon dioxide concentration in C5 and C4b respectively. C4b source of carbon comes mainly from C5, but C5 does not have enough carbon dioxide partial pressure to feed C4b triggering the discharge of the CT. The consequences are: First, discharging CT violating the supervision instruction of keeping a level of 50%; and second, introducing additional oxygen in the system, coming from the CT, that is accumulated in C4b over time (see Fig 6. 13).

- Such malfunction of the system operation of discharging CT and accumulating oxygen in C4b may be resolved by enriching the control problem through penalizing the accumulation of oxygen in C4b (addition of a cost term in the level 2 MPC) or by setting an upper limit not to be violated. Nevertheless, this would, in turn, difficult the resolution of the control problem as has been discussed in section 6.4.1.3. Longer simulations times should also be tested to assess the limits of accumulation of oxygen in

compartments C4a and C4b. Considering the dynamics of oxygen and carbon dioxide concentrations are determined by the PQ of 1.36 of C4a bioreactor (Garcia-Gragera et al., 2021), and the PQ of 1.22 of C4b (see previous Chapter), there exists certain restrictions on the simultaneous controllability of both oxygen and carbon dioxide in the system.

6.4.1.5. Assessment of Hierarchical Control Structure performance: Using control configuration 3 as a case study

Level 3 of the HCS

For this analysis, control configuration 3 is evaluated. This control configuration is chosen because a discussion including the three of the options presented would be redundant. Focusing on oxygen, it is relevant to observe how resources are allocated in Level 3 of the HCS while guaranteeing the soft and hard constraints imposed in the MPC problem are respected: the mass balance to be satisfied for oxygen; the cost function terms such as the deviation of light intensity in C4a and the deviation of the concentrated gas tank level from the reference to be minimized; the technical constraints to be satisfied such as a minimum/maximum level for the concentrated gas tank and a minimum/maximum charge/discharge rate for the concentrated gas tank.

In Fig 6. 22, the results of Level 3 are presented in terms of oxygen production/consumption rate. It can be clearly observed that when C4b starts respiration (dark photoperiod), in order to keep providing oxygen for the consumer compartments (C5 and C3), the concentrated gas tank is discharged, releasing oxygen. On the contrary, when both C4a and C4b contribute to the oxygen production, the concentrated gas tank is charged (expressed as a negative rate). To note as well that C4a and C4b, when carrying photosynthetic activity, contribute almost equally to the oxygen production. The main constraint of Level 3 is to satisfy the oxygen mass balance as expressed in (161). When comparing the overall production rates with the consumption rates (C3 and C5) for oxygen, it is demonstrated that this constraint is satisfied (Fig 6. 23). It should be considered that C4a production can be regulated by light intensity, the concentrated gas tank contribution can also be regulated, but C4b has a fixed light intensity.

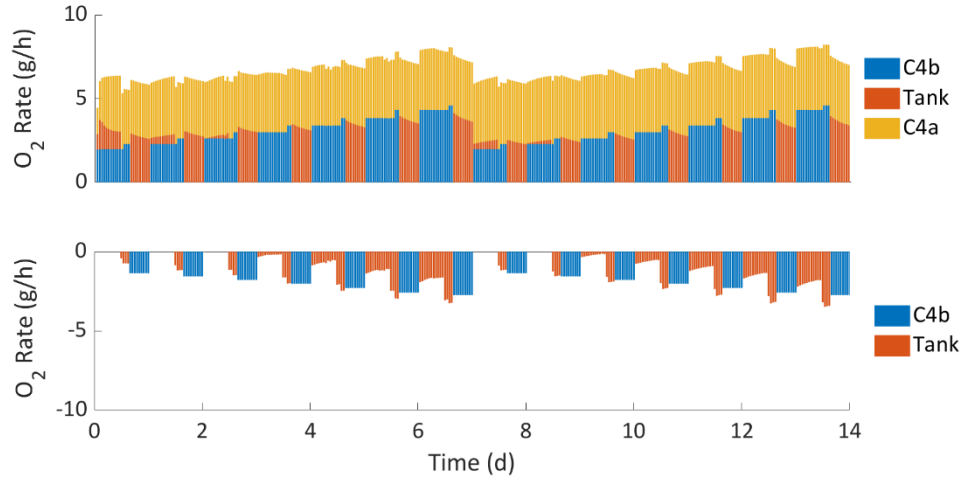

Fig 6. 22. Level 3 predicted oxygen production and consumption rates. Data are reproduced considering the net producing compartments daily (C4b and C4a) and the concentrated gas tank.

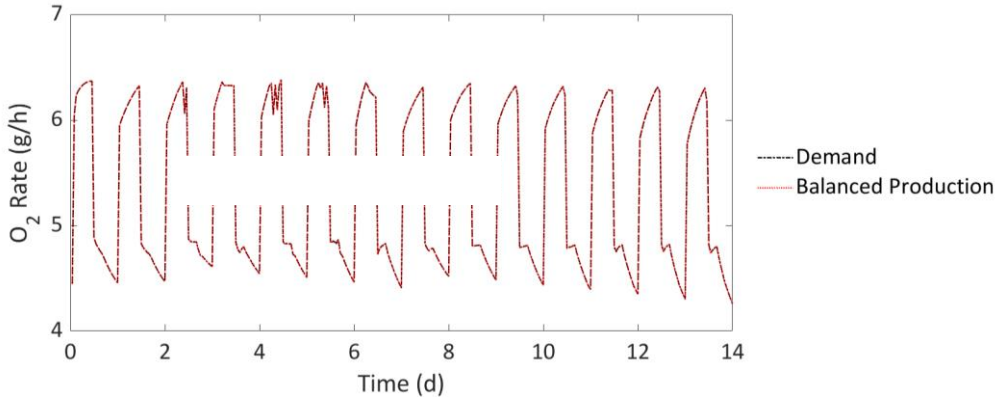

Fig 6. 23. Level 3: Overall Balance. Comparison between expected consumption from the two consumer compartments and the generated production rates for oxygen in C4a, C4b and the concentrated gas tank.

Level 2 of the HCS

The associated production rate assigned to C4a ($Q_{O_2}^{C4a,ref}$ as expressed in Fig 6. 9) and the oxygen supply associated to the gas concentration tank (expressed as resulting CT tank level, $SOC^{CT,ref}$) shall be converted into a control command signal. For C4a, the control command is light intensity and for the concentrated gas tank, it is the charge gas flow. But prior the translation of the references received from level 3 to control commands, such references shall be corrected given level 3 model mismatches, perturbations in the process or any other issues that may generate a deviation between level 3 prediction and the evolution of the process. Level 2 is the responsible to generate these corrected references concerning $Q_{O_2}^{C4a}$ and $SOC^{CT,ref}$. Even though minor corrections are observed in Fig 6. 24, some deviations are visible between the scheduled references by level 3 and the corrections applied by level 2.

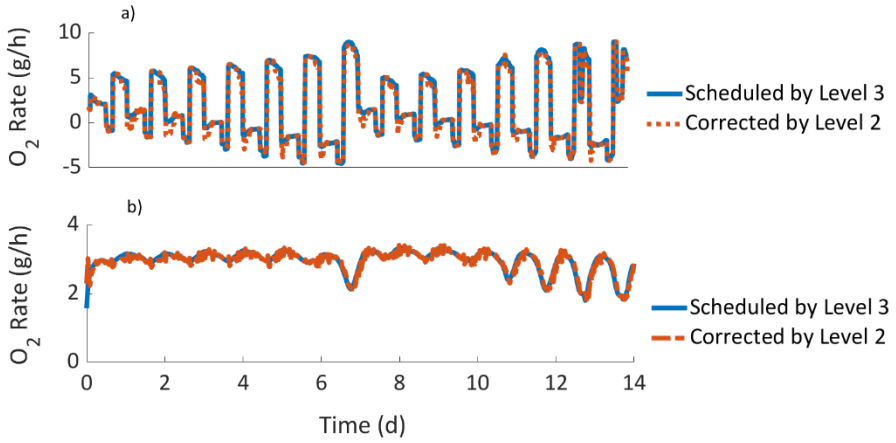

Fig 6. 24. Corrections done by level 2 of the HCS on references received by level 3. a) Level 2 corrections on CT oxygen charge/discharge rate, b) Level 2 corrections on C4a assigned oxygen production rate

From level 2, the resulting oxygen rate $Q_{O_2}^{C4a}$ can be directly converted to an output oxygen concentration reference for C4a and eventually to light intensity considering the flow is fixed at 2.8 L/min. On the other hand, the resulting oxygen charge/discharge rate obtained from the $SOC^{CT,ref}$, can be directly converted to a charging/discharging gas flow knowing the oxygen concentration in the concentrated gas tank and/or in the gas line.

Level 1 of the HCS

In Fig 6.25a-b, the light-based control of oxygen in C4a is represented. It can be observed that light intensity is used to track the oxygen setpoint, which is in turn imposed by Level 2 and Level 3. In the case of control configuration 3, at the end of the simulation the tracking of the setpoint gets unstable. This is likely caused by the situation of the system in this specific moment of time, where, for example, the concentrated gas tank level starts to be limiting and may introduce instabilities in the system.

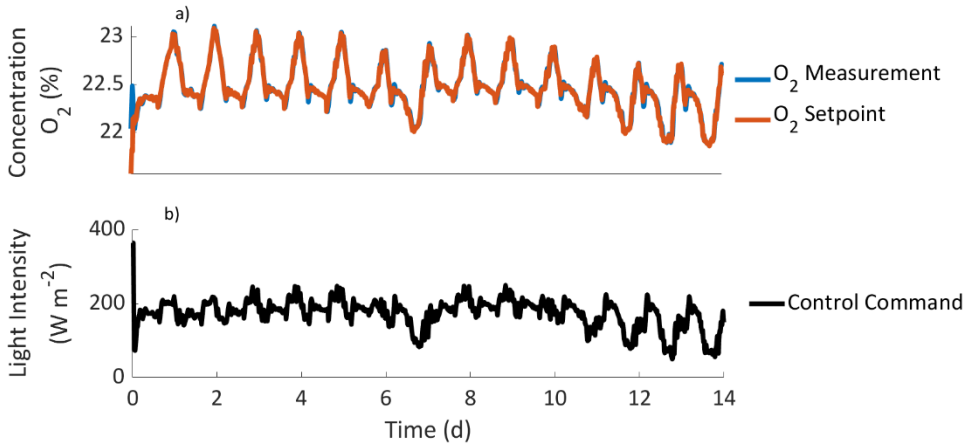

Fig 6. 25. Light-based control of Oxygen in C4a. a) Oxygen control in C4a; b) Light intensity adjustment.

6.5. Conclusions

In this chapter, the capabilities of the HCS presented along the project have been explored using one of the future MELiSSA Pilot Plant integration steps as a case study. With this aim, the controllability of oxygen and carbon dioxide has been assessed together with different configurations of the HCS presented. One of the main conclusions is that the performance of a complex system like a BLSS can sometimes be boosted by improving the control strategy. As demonstrated, with identical or very similar hardware capabilities, resources can be better allocated solely by tuning and enriching the control algorithms. There is a payback though with the control strategy presented, which is the computation time. Indeed, the computation time is proportional to the complexity of the control problem in an MPC-based controller, being such complexity represented by the number of manipulated and controlled variables. There are several possibilities to face this issue: linearizing the models, further simplifying them or using shorter prediction and control horizons, to mention a few. But all these possibilities shall consider their impact on the precision of the MPC solution beyond the computation time. In any case, improved control strategies will be required in the future, considering BLSSs will increase their degree of closure and therefore the control challenges will also get more demanding. It is thus necessary to evolve towards new control strategies to satisfy additional needs of BLSS not addressed in this Chapter nor in the whole study: management of grey and black water, food production, waste processing, energy control, among others.

6.6. Appendix

6.6.1. Appendix 1: Validation of the photosynthesis model based on light color ratio

The HPC in the MPP is a chamber that can host up to 100 lettuce plants divided in 20 trays (5 plants per tray). The gas phase has a volume of 9.7 m^3 when it is empty and a volume of 9.4 m^3 when filled with trays. For the validation of the model-based simulation, the results from day (light phase) carbon fixation have been compared with an experimental test at two modes of operation: batch and staggered mode. For both, simulation and the experimental test, the following operating conditions have been used: nutrients are provided through a hydroponic solution with temperature, pH and electroconductivity values controlled at 22ºC, 5.9 and 1.9 mS/cm respectively; Bulk temperature and relative humidity are controlled at 26ºC and 50% respectively during the day (light) photoperiod, and at 22ºC and 70% during the night (dark) photoperiod; The photoperiod is adjusted to 16 hr of light phase and 8 hr of dark phase; Light intensity is set to 400 µmol m^{-2} s^{-1}; The ratio of red and blue wavelength is set to 4:1; The carbon dioxide concentration is controlled at 1000 ppm; The global leak of the chamber has been reported to be 115 Pa/h, with an equivalent compensation using synthetic air.

Batch Test

The batch test consists on a 25-day test with the chamber full of plants of the same age. A total of 100 9-days age plants are introduced in the chamber and are harvested after 25 days of operation under a controlled environment. The dry biomass of the plants introduced in the chamber are 0.5 mg per plant, with a fresh content of 95%, based on experimental data. Results are represented in Fig 6. 26.

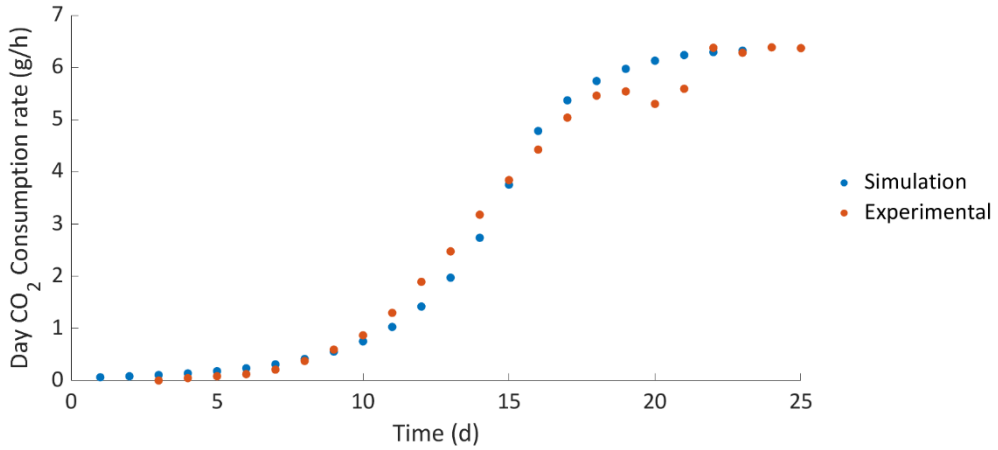

Fig 6. 26. Net CO_2 consumption during light (day) photoperiod

Staggered Test

The staggered test consists on the operation of the HPC with a gradient of crops of different ages. The 25 trays are divided in 4 groups, each group having 5 trays. Every seven days, the five trays with the oldest plants are harvested and 5 new trays are introduced. In this way, it is possible to reduce the variation of the photosynthetic activity over time and the oxygen production in the chamber is maintained constant within a certain variation during continuous operation. Plants are introduced in the HPC when they are 9 days old, and they have a residence time of 28 days within the chamber. Therefore, when harvesting of aged plants and introduction of young plants is done every week, the chamber is filled with plants aged 9 days, 18 days, 27 days and 36 days. The dry biomass of each individual crop for each group is: 0.5 mg, 40 mg, 0.81 g and 5 g. Results are represented in Fig 6. 27.

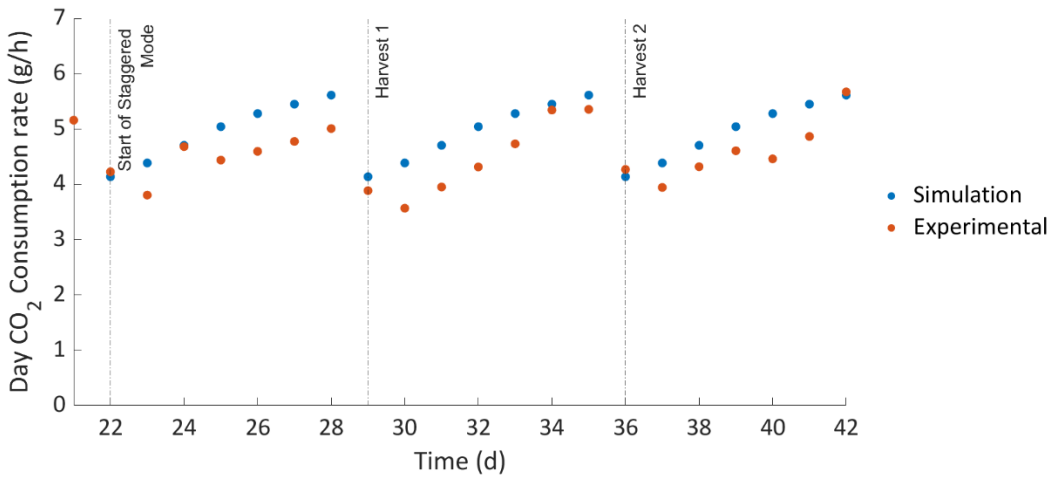

Fig 6. 27. Net CO_2 consumption during light (day) photoperiod

The results presented for the batch and staggered modes of operation in the HPC are very interesting. They demonstrate a very accurate performance of the model-based simulation compared to the experimental data registered in the MPP. This validates the mathematical model presented along this chapter for plants growth and reassures its capability to generate trustful predictions.

7. CONCLUSIONS AND FUTURE WORK

In the presented study, a new control strategy has been elaborated for supervising and operating Life Support Systems for humans in long-term Space missions. This control strategy has a hierarchical organization, with different levels corresponding to different control functions and by extent with different controller specifications, including the execution time and the type of controllers used. This approach aims at providing resilience and reliability to the system, both critical aspects in LSS as widely discussed. A hierarchical control architecture with vertically distributed control functions, with a top-down decision making and a top-down information flow also responds to the process topology of LSS and specially of BLSS, which requires a higher degree of resource optimization which is challenging in terms of control. Therefore, the complexity of BLSS from a control point of view requires a distributed organization of the control functions that can be satisfied with the proposed hierarchical approach, but that would be difficult or would not be satisfactory if only a single layer control architecture would be considered.

The need for a distributed control approach has been proposed considering a reduced BLSS case study, where only the gas phase was analyzed. It is easy to deduce that the control challenge would acquire an additional magnitude if all phases were considered (gas, liquid and solid) and if the control strategy would be extended to control variables other than the process-related ones (i.e., species concentrations, flows) such as energy, crew time or sustainability (summarized in the ALISSE criteria).

In the proposed control architecture, the use of model-based predictive controllers (MPCs) plays a major role and responds precisely to the need to find a reliable control solution to a very complex system, such as BLSS, which in this study has been focused to the MELiSSA loop. It shall be stated that the compartment characterization and modelling efforts carried by the MELiSSA consortium gave to the authors of the presented project a head start, since model availability is a requirement for MPCs. The use of MPCs has been proven to be an interesting option for controlling the MELiSSA loop due to its capacity to deal with complex multiple-input multiple-output control problems, the easiness of handling constraints and also the capacity to deal with different types of models, as discussed in Chapters 5 and 6 (i.e. linear, non-linear, metabolic, mechanistic, first-order models). Although model availability is a requirement for MPCs, the intensive efforts deployed in the MELiSSA project on model development do not only respond to their implementation in the presented control strategy, but on developing a mechanistic understanding of the system of interest. This is in contrast with the most common practice in control applications, where the system of interest is usually approached as a black box, with the relationship between model input and outputs well-known but not the first principles behind

such relationship. In this thesis, new models have been developed for the higher plants compartment covering mass and energy transfers, biochemical conversions including enzyme rates and a constraint-based metabolic flux analysis.

Overall, the presented control architecture is proven to work properly for the two case studies presented in Chapters 4 and 6, but there is margin for improvement. As extensively discussed, the three functions aimed at each control level are well executed; these functions are: in Level 3, the set-point assignment based in supervision and management decisions; in Level 2, the set-point correction based on plant status and in Level 1, the local controller roles covering the control action calculations and signal communication with the physical process. All these functions are well executed, and a stable operation is achieved with the supervisory criteria being satisfied. However, results in Chapter 6, especially for those cases with higher control requirements (combined control of oxygen and carbon dioxide concentration in the crew compartment and in the higher plants chamber respectively) show some signals of computational cost overload. This is mainly attributed to the control architecture itself, which has a hierarchical distribution of functions, but which at the same time is too centralized. Even though all levels of the control structure follow a centralized approach, meaning that each level must find a solution to their assignment control problem for the whole system, this is accentuated in Level 2, which must find corrected set-points for the whole process. As beforementioned, this causes a too high computation cost reaching values in the order of 60 seconds. Such values may not be problematic for the presented case studies, but the MELiSSA loop will demand controllability on more variables over the course of the stepwise integration strategy including oxygen, carbon dioxide, water, food, solid wastes, trace contaminants, energy availability, stored resources, among others. Therefore, it is mandatory to find alternatives to relax the computational cost associated to each level responding to the increasing control complexity of the MELiSSA loop. Another drawback of the presented control architecture is the difficulty to reach convergence while trying to solve the optimization problem embedded in the MPCs of the different control levels. This has not been observed in the presented study but can be expected when the control challenge will increase as MELiSSA works towards higher degrees of circularity. So, using the presented control architecture as a basic platform, control algorithms need to be continuously deployed to face future control challenges. The first aspect to be considered to improve the calculation time is to linearize all models as done in Chapter 6 for the cyanobacteria photobioreactor. This would dramatically decrease the convergence time in the controllers, especially in Level 2. The second improvement would be to use a distributed control approach for each level in the control hierarchy. For the MELiSSA loop and by extension for BLSS

applications, it is of striking interest the use of control solutions developed for the so-called Multi-Agent Systems (MAS). MAS are systems conformed by autonomous agents that coordinate and cooperate individually to satisfy a common goal. From a process point of view MELiSSA is a MAS, but the MELiSSA control approach so far has not considered the MELiSSA loop and its different agents as a MAS, but as a single system. The future work shall include the transition to forms of control where the different agents (compartments) in MELiSSA operate for the common global goal pursued by the loop. For example, in Chapter 6 fixed operating conditions have been imposed to the higher plants compartment from the supervisory level, being the rest produced by the photobioreactor and by the buffer tank. The transit to a distributed multi-agent-based control would involve the negotiation to take place individually between compartment controllers. This would improve the robustness of the control since an error would make one controller to fall and not the whole loop. Also, the computational cost would also be reduced since the control problem would be reduced in smaller sub-problems. The transition to a distributed multi-agent control requires important modifications in the MPC algorithms. One option which has been proven to be very efficient in the use of multi-agent MPC control is the use of the Augmented Lagrange (AL) method. Following this approach, the negotiation between agents (compartments) is formalized as linear constraints. Going back to Chapter 6, the flows and concentrations leaving one compartment to another compartment are formalized as a linear constraint for both compartments. So, there is a linear constraint imposed for the compartment of origin and one constraint for the compartment of destination. Once this overall problem is formalized, an augmented Lagrange is constructed to replace the linear constraints by replacing each interconnecting constraint with an additional linear cost term based on Lagrange multipliers. Other algorithms exploit the idea of converting a constrained MPC to an unconstrained MPC like the popular alternating-direction method of multipliers (ADMM) which has been proved to be very useful in solving decentralized MPC problems like in water networks, logistics, power distribution systems, among others. These complementary methods or adaptations on MPCs are suitable for processes with separate costs but linked by coupled constraints, which is exactly the nature of MELiSSA compartments, and which can, in turn, be parallelized so the convergence time can be speed up.

Summarizing, this study has presented the conceptual basis of a new hierarchical control architecture for BLSS inspired by existing control strategies applied to operate electric microgrids. This control strategy has been mathematically defined, implemented and tested in a virtual environment using the MELiSSA test-bed, the MELiSSA Pilot Plant, as a case study given

the mathematical models available for the different compartments. For the higher plants compartment where there was less model availability, existing models had to be tuned, evolved and extended based on existing literature and available experimental data. This initial lack of model information was considered a chance to propose a structural-functional modelling approach gathering different phenomena taking place in higher plants from mass and energy transfer at macro-scale down to metabolic mechanisms. On top of developing a metabolic model for *L. sativa*, this study is relevant for proposing a methodology for integrating different modelling approaches into a unified framework. This methodology may be of interest to be incorporated into other compartments of MELiSSA. Finally, the hierarchical control structure is proposed for the next big challenge of the MELiSSA Pilot Plant, which is the integration of C3, C4a, C4b and C5. Results demonstrate that the proposed control strategy can successfully control a challenging case study, providing an optimal solution and being modular enough to enrich the control problem without compromising the robustness of the controller itself. However, higher computation times obtained in the resolution of the controllers presented in such challenging case study suggest other controller variants must be considered, especially those tending to the use of a more decentralized approach.

8. REFERENCES

Alemany, L., Peiro, E., Arnau, C., Garcia, D., Poughon, L., Cornet, J. F., Dussap, C. G., Gerbi, O., Lamaze, B., Lasseur, C., & Godia, F. (2019). Continuous controlled long-term operation and modeling of a closed loop connecting an air-lift photobioreactor and an animal compartment for the development of a life support system. *Biochemical Engineering Journal*, *151*. https://doi.org/10.1016/j.bej.2019.107323

Amitrano, C., Chirico, G. B., De Pascale, S., Rouphael, Y., & De Micco, V. (2020). Crop management in controlled environment agriculture (CEA) systems using predictive mathematical models. *Sensors (Switzerland)*, *20*(11). https://doi.org/10.3390/s20113110

Arnold, A., & Nikoloski, Z. (2011). A quantitative comparison of Calvin-Benson cycle models. *Trends in Plant Science*, *16*(12), 676–683. https://doi.org/10.1016/j.tplants.2011.09.004

Barta, D. (2017). Getting Out of Orbit: Water Recycling Requirements and Technology Need for Long Duration Missions Away from Earth. *20th Annual Nanotech 2017 Conference and Expo*, *21*(1), 1–9. https://doi.org/10.1016/j.tmaid.2020.101607%0Ahttps://doi.org/10.1016/j.ijsu.2020.02.034%0Ahttps://onlinelibrary.wiley.com/doi/abs/10.1111/cjag.12228%0Ahttps://doi.org/10.1016/j.ssci.2020.104773%0Ahttps://doi.org/10.1016/j.jinf.2020.04.011%0Ahttps://doi.o

Barta, D., & Henninger, D. (1996). Johnson Space Center's Regenerative Life Support Systems Test Bed. *Advances in Space Research*, *18*(1), 211–222.

Becker, S. A., Feist, A. M., Mo, M. L., Hannum, G., Palsson, B., & Herrgard, M. J. (2007a). Quantitative prediction of cellular metabolism with constraint-based models: The COBRA Toolbox. *Nature Protocols*, *2*(3), 727–738. https://doi.org/10.1038/nprot.2007.99

Becker, S. A., Feist, A. M., Mo, M. L., Hannum, G., Palsson, B., & Herrgard, M. J. (2007b). Quantitative prediction of cellular metabolism with constraint-based models: The COBRA Toolbox. *Nature Protocols*, *2*(3), 727–738. https://doi.org/10.1038/nprot.2007.99

Bemporad, A. (2017). Model Predictive Control Design: New Trends and Tools. *IEEE Conference on Decision and Control*, 6678–6683. http://www.dii.unisi.it/

Bibring, J. P., Rosenbauer, H., Boehnhardt, H., Ulamec, S., Biele, J., Espinasse, S., Feuerbacher, B., Gaudon, P., Hemmerich, P., Kletzkine, P., Moura, D., Mugnuolo, R., Nietner, G., Pätz, B., Roll, R., Scheuerle, H., Szegö, K., & Wittmann, K. (2007). The Rosetta Lander ("Philae") investigations. *Space Science Reviews*, *128*(1–4), 205–220. https://doi.org/10.1007/s11214-006-9138-2

Bidram, A., & Davoudi, A. (2012). Hierarchical Structure of Microgrids Control System. *IEEE Transactions on Smart Grid*, *3*(4), 1963–1976.

Blankenship, R., Tiede, D., & Barber, J. (2011). Comparing photosynthetic and photovoltaic efficiencies and recognizing the potential for improvement. *Science*, *332*, 805–809.

Boscheri, G., Kacira, M., Patterson, L., Giacomelli, G., Sadler, P., & Furfaro, R. (2012). Modified energy cascade model adapted for a multicrop Lunar greenhouse prototype. *Advances in Space Research*, *50*(7), 941–951. https://doi.org/10.1016/j.asr.2012.05.025

Bowman, E., Bowman, D., Cramblit, E., Dunlap, D., Wilson, M., Ghariani, A., Obashe, O., & Van Keuren, S. (2017). Analysis of Chemical and Microbial Components Adsorbed on the Ion Exchange Bed in the Oxygen Generation System Recirculation Loop. In ICES (Ed.), *International Conference on Environmental Systems*.

Brunet, J., Gerbi, O., André, P., Davin, E., Rodriguez, R., Carbonero, F., Perna, G., Suomalainen, E., & Lasseur, C. (2010). Alisse: Advanced Life Support System Evaluator. In COSPAR (Ed.), *38th COSPAR Scientific Assembly 2010* (p. 2010).

Bryds, M., Grochowski, M., Gminski, T., Konarczak, K., & Drewa, M. (2008). Hierarchical predictive control of integrated wastewater treatment systems. *Control Engineering Practice*, *16*(6), 751–767.

Bykova, N. v., Møller, I. M., Gardeström, P., & Igamberdiev, A. U. (2014). The function of glycine decarboxylase complex is optimized to maintain high photorespiratory flux via buffering of its reaction products. *Mitochondrion*, *19*(PB), 357–364. https://doi.org/10.1016/j.mito.2014.01.001

Cagnano, A., Caldarulo, A., & Tuglie, E. (2018). A cooperative control for the reserve management of isolated microgrids. *Applied Energy*, *218*, 256–265.

Chandra Barman, N., & Hasan, M. (2016). A review on present status and future prospective of hydroponics technique. *Plant Environment Development*, *5*(2), 1–7. https://www.researchgate.net/publication/320299106

Chen, X. li, Wang, L. chun, Li, T., Yang, Q. chang, & Guo, W. zhong. (2019a). Sugar accumulation and growth of lettuce exposed to different lighting modes of red and blue LED light. *Scientific Reports*, *9*(1), 1–10. https://doi.org/10.1038/s41598-019-43498-8

Chen, X. li, Wang, L. chun, Li, T., Yang, Q. chang, & Guo, W. zhong. (2019b). Sugar accumulation and growth of lettuce exposed to different lighting modes of red and blue LED light. *Scientific Reports*, *9*(1). https://doi.org/10.1038/s41598-019-43498-8

Cheung, C. Y. M., Williams, T. C. R., Poolman, M. G., Fell, D. A., Ratcliffe, R. G., & Sweetlove, L. J. (2013). A method for accounting for maintenance costs in flux balance analysis improves the prediction of plant cell metabolic phenotypes under stress conditions. *Plant Journal*, *75*(6), 1050–1061. https://doi.org/10.1111/tpj.12252

Ciurans, C., Bazmohammadi, N., Vasquez, J. C., Dussap, G., Guerrero, J. M., & Godia, F. (2021). Hierarchical Control of Space Closed Ecosystems – Expanding Microgrid Concepts to Bioastronautics. *IEEE Industrial Electronics Magazine*, *15*(2), 2–13. https://doi.org/10.1109/MIE.2020.3026828

Cockell, C. S., Rettberg, P., Rabbow, E., & Olsson-Francis, K. (2011). Exposure of phototrophs to 548 days in low Earth orbit: Microbial selection pressures in outer space and on early earth. *ISME Journal*, *5*(10), 1671–1682. https://doi.org/10.1038/ismej.2011.46

Cogdell, R. (2013). Photosynthesis: Earth Life Support System. *New Scientist*, *217*(2902), 2–3.

Conde-Pueyo, N., Vidiella, B., Sardanyés, J., Berdugo, M., Maestre, F. T., Lorenzo, V. de, & Solé, R. (2020). Synthetic biology for terraformation lessons from mars, earth, and the microbiome. *Life*, *10*(2), 1–27. https://doi.org/10.3390/life10020014

Cornet, J F; Dussap, C G; Dubertret, G. (1992). *A Structured Model for Simulation of Cultures of Cyanobacterium Spyrulina platensis in Photobioreactors Coupling Between Light Transfer and Growth Kinetics*.

Cornet, J. F., Dussap, C. G., Gros, J. B., Binois, C., & Lasseur, C. (1995). A simplified monodimensional approach for modeling coupling between radiant light transfer and growth kinetics in photobioreactors. *Chemical Engineering Science*, *50*(9), 1489–1500. https://doi.org/10.1016/0009-2509(95)00022-W

Corpas, F. J., & Barroso, J. B. (2014). NADPH-generating dehydrogenases: Their role in the mechanism of protection against nitro-oxidative stress induced by adverse environmental conditions. *Frontiers in Environmental Science*, *2*(DEC). https://doi.org/10.3389/fenvs.2014.00055

Crusan, J. (2017). *Cislunar Habitation & Environmental Control & Life Support Systems NASA Advisory Council Human Exploration & Operations Committee*.

Cruvellier, N., Poughon, L., Creuly, C., Dussap, C. G., & Lasseur, C. (2017). High ammonium loading and nitrification modelling in a fixed-bed bioreactor. *Journal of Water Process Engineering*, *20*, 90–96. https://doi.org/10.1016/j.jwpe.2017.10.006

Dauchet, J., Cornet, J. F., Gros, F., Roudet, M., & Dussap, C. G. (2016a). Photobioreactor Modeling and Radiative Transfer Analysis for Engineering Purposes. *Advances in Chemical Engineering*, *48*, 1–106. https://doi.org/10.1016/bs.ache.2015.11.003

Dauchet, J., Cornet, J., Gros, F., Roudet, M., & Dussap, C. (2016b). Photobioreactor Modeling and Radiative Transfer Analysis for Engineering Purposes. *Advances in Chemical Engineering*, *48*, 1–106.

Diamant, B. L., & Humphries, W. R. (1990). *Past and Present Environmental Control and Life Support Systems on Manned Spacecraft*.

Dong, C., Fu, Y., Xie, B., Wang, M., & Liu, H. (2017a). Element cycling and energy flux responses in ecosystem simulations conducted at the Chinese Lunar Palace-1. *Astrobiology*, *17*(1), 78–86. https://doi.org/10.1089/ast.2016.1466

Dong, C., Fu, Y., Xie, B., Wang, M., & Liu, H. (2017b). Element cycling and energy flux responses in ecosystem simulations conducted at the Chinese Lunar Palace-1. *Astrobiology*, *17*(1), 78–86. https://doi.org/10.1089/ast.2016.1466

Dunbar, B. (2021). *Moon to Mars*.

Ebrahim, A., Lerman, J. A., Palsson, B. O., & Hyduke, D. R. (2013). COBRApy: COnstraints-Based Reconstruction and Analysis for Python. *BMC Systems Biology*, *7*. https://doi.org/10.1186/1752-0509-7-74

Ellis, W. E., & Willis, N. C. (1968). Design, Development, Fabrication, and Test of an Environmental/Thermal Control and Life Support System in Support of the Apollo Applications Program. *Source: SAE Transactions*, *76*(4), 2529–2553.

ESA. (2022). *Terrae Novae 2030+ Strategy Roadmap*. https://esamultimedia.esa.int/docs/ESA_Agenda_2025_final.pdf

European Comission. (2010). DIRECTIVE 2010/63/EU OF THE EUROPEAN PARLIAMENT AND THE COUNCIL of 22 September 2010 on the protection of animals used for scientific purposes. *Official Journal of the European Union*, 1–162.

Ewert, M., & Stromgren, C. (2019). Astronaut Mass Balance for Long Duration Missions. In ICES (Ed.), *International Conference on Environmental Systems* (pp. 1–8).

Fahrion, J., Mastroleo, F., Dussap, C. G., & Leys, N. (2021). Use of Photobioreactors in Regenerative Life Support Systems for Human Space Exploration. *Frontiers in Microbiology*, *12*. https://doi.org/10.3389/fmicb.2021.699525

Farges, B., Poughon, L., Creuly, C., Cornet, J. F., Dussap, C. G., & Lasseur, C. (2008). Dynamic aspects and controllability of the MELiSSA project: A bioregenerative system to provide life support in space. *Applied Biochemistry and Biotechnology*, *151*(2–3), 686–699. https://doi.org/10.1007/s12010-008-8292-2

Farquhar, G. D., von Caemmerer, S., & Berry, J. A. (1980). A biochemical model of photosynthetic CO<Subscript>2</Subscript> assimilation in leaves of C<Subscript>3</Subscript> species. *Planta*, *149*(1), 78–90. https://link.springer.com/article/10.1007/BF00386231%0Apapers3://publication/doi/10.1007/BF00386231

Frantz, J. M., & Bugbee, B. (2005). Acclimation of plant populations to shade: Photosynthesis, respiration, and carbon use efficiency. *Journal of the American Society for Horticultural Science*, *130*(6), 918–927. https://doi.org/10.21273/jashs.130.6.918

Fulget, N., Poughon, L., Richalet, J., & Lasseur, C. (1999). MELISSA : Global control strategy of the artificial ecosystem by using first principles models of the compartments. *Advances in Space Research*, *24*(3), 397–405. https://doi.org/10.1016/S0273-1177(99)00490-1

Fuller, S., Lehnhardt, E., Zaid, C., & Halloran, K. (2022). Gateway Program Status and Overview. *Journal of Space Safety Engineering*, *9*(4), 625–628.

Gakière, B., Hao, J., de Bont, L., Pétriacq, P., Nunes-Nesi, A., & Fernie, A. R. (2018). NAD + Biosynthesis and Signaling in Plants. *Critical Reviews in Plant Sciences*, *37*(4), 259–307. https://doi.org/10.1080/07352689.2018.1505591

Galston, A. (1992). Photosynthesis as a basis for life support on Earth and in space: photosynthesis and transpiration in enclosed spaces. *Bioscience*, *42*(7), 490–493.

Garcia-Gragera, D., Arnau, C., Peiro, E., Dussap, C. G., Poughon, L., Gerbi, O., Lamaze, B., Lasseur, C., & Godia, F. (2021). Integration of Nitrifying, Photosynthetic and Animal Compartments at the MELiSSA Pilot Plant. *Frontiers in Astronomy and Space Sciences*, *8*. https://doi.org/10.3389/fspas.2021.750616

Gaude, E., Schmidt, C., Gammage, P. A., Dugourd, A., Blacker, T., Chew, S. P., Saez-Rodriguez, J., O'Neill, J. S., Szabadkai, G., Minczuk, M., & Frezza, C. (2018). NADH Shuttling Couples Cytosolic Reductive Carboxylation of Glutamine with Glycolysis in Cells with Mitochondrial Dysfunction. *Molecular Cell*, *69*(4), 581-593.e7. https://doi.org/10.1016/j.molcel.2018.01.034

Gitelson, J., & Lisovsky, G. (2002). *Man-Made Closed Ecological Systems* (CRC Press, Ed.; 1st ed.).

Glaessgen, E. H., & Stargel, D. S. (2012). The digital twin paradigm for future NASA and U.S. Air force vehicles. In American Institue of Aeronautics and Astronautics (Ed.), *53rd Structures, Structural Dynamics, and Materials Conference: Special Session on the Digital Twin* (Issue April). https://doi.org/10.2514/6.2012-1818

Gòdia, F., Albiol, J., Pérez, J., Creus, N., Cabello, F., Montràs, A., Masot, A., & Lasseur, C. (2004). The MELISSA pilot plant facility as an integration test-bed for advanced life support systems. *Advances in Space Research*, *34*(7 SPEC. ISS.), 1483–1493. https://doi.org/10.1016/j.asr.2003.08.038

Gomes, C., Dal'molin, O., Quek, L.-E., Saa, P. A., Nielsen, L. K., Nikoloski, Z., & Toepfer, N. (2015). A multi-tissue genome-scale metabolic modeling framework for the analysis of whole plant systems. *Frontiers in Plant Science*. https://doi.org/10.3389/fpls.2015.00004

Grigoriev, A. I., Sinyak, Yu. E., Samsonov, N. M., Bobe, L. S. , Protasov, N. N. , & Andreychuk, P. O. (2011). Regeneration of water at space stations. *Acta Astronautica*, *68*(9–10), 1567–1573.

Guerrero, J., Chandorkar, M., Lee, T., & Loh, P. (2013). Advanced Control Architectures for Intelligent Microgrids - Part 1: Decentralized and Hierarchical Control. *IEEE Transactions on Industrial Electronics*, *60*(4), 1254–1262.

Guerrero, J., Vasquez, J., Matas, J., de Vicuna, L., & Castilla, M. (2011). Hierarchical Control of Droop-Controlled AC and DC Microgrids—A General Approach Toward Standardization. *IEEE Transactions on Industrial* , *58*(1), 158–172.

Haber, R., Rossiter, J. A., & Zabet, K. (2016). An alternative for PID control: Predictive Functional Control - A tutorial. *Proceedings of the American Control Conference*, *2016-July*, 6935–6940. https://doi.org/10.1109/ACC.2016.7526765

Harley, P. C., Thomas, R. B., Reynolads, J. F., & Strain, B. R. (1992). Modelling photosynthesis of cotton grown in elevated CO2. *Plant, Cell & Environment*, *15*(3), 271–282. https://doi.org/10.1111/j.1365-3040.1992.tb00974.x

Huang, R., Biegler, L. T., & Patwardhan, S. C. (2010). Fast offset-free nonlinear model predictive control based on moving horizon estimation. *Industrial and Engineering Chemistry Research*, *49*(17), 7882–7890. https://doi.org/10.1021/ie901945y

IEEE. (2018). IEEE Standard for the Specification of Microgrid Controllers. *IEEE Std 2030.7-2017*, 1–43.

Igamberdiev, A. U., & Eprintsev, A. T. (2016). Organic acids: The pools of fixed carbon involved in redox regulation and energy balance in higher plants. *Frontiers in Plant Science*, *7*. https://doi.org/10.3389/fpls.2016.01042

ISECG. (2018). *Annual Report 2018*.

ISECG. (2020). *Annual Report 2020*.

Johnson, C. M., Boles, H. O., Spencer, L. S. E., Poulet, L., Romeyn, M., Bunchek, J. M., Fritsche, R., Massa, G. D., O'Rourke, A., & Wheeler, R. M. (2021). Supplemental Food Production With Plants: A Review of NASA Research. In *Frontiers in Astronomy and Space Sciences* (Vol. 8). Frontiers Media S.A. https://doi.org/10.3389/fspas.2021.734343

Junaedi, C., Hawley, K., Walsh, D., Roychoudhury, S., Abney, M. B., & Perry, J. L. (2011). Compact and lightweight sabatier reactor for carbon dioxide reduction. In ICES (Ed.), *41st International Conference on Environmental Systems*. https://doi.org/10.2514/6.2011-5033

Kayatin, M., Carter, D., Schunk, R., & Pruitt, J. (2016). Upgrades to the ISS Water Recovery System. In ICES (Ed.), *International Conference on Environmental Systems* (pp. 10–14).

Kim, J., Kim, H., Choi, S., Jang, J., Jeong, M., & Lee, S. (2017). The importance of the Circadian Clock in Regulating Plant Metabolism. *International Journal on Molecular Science*, *18*(12).

Kirk, A., & Ferry, D. (2018). Photosynthesis versus photovoltaics. *Journal of Computational Electronics*, *17*, 313–318.

Kojima, Y., Koshio, M., Nakamura, S., Maejima, H., Fujioka, Y., & Goda, T. (2007, April 16). A Demonstration Project in Hachinohe: Microgrid with Private Distribution Line. *IEEE International Conference on System of Systems Engineering*.

Kricher, J. (2009). *The Balance of Nature: Ecology's Enduring Myth*. Princeton University Press.

Lasseur, C., & Mergeay, M. (2021). Current and future ways to closed life support systems. *MELiSSA Conference*, *1*, 25–35. https://doi.org/10.32006/eeep.2021.1.2535

Laurini, K., Piedboeuf, K., Schade, B., Matsumoto, K., Spiero, F., & Lorenzoni, A. (2018). The global exploration roadmap. *IAC*.

Law, J., Watkins, S., & Alexander, D. (2010). *In-Flight Carbon Dioxide Exposures and Related Symptoms: Association, Susceptibility, and Operational Implications*. http://www.sti.nasa.gov

Lee, C. P., Elsässer, M., Fuchs, P., Fenske, R., Schwarzländer, M., & Millar, A. H. (2021). The versatility of plant organic acid metabolism in leaves is underpinned by mitochondrial malate-citrate exchange. *Plant Cell*, *33*(12), 3700–3720. https://doi.org/10.1093/plcell/koab223

Liu, J., & van Iersel, M. W. (2021). Photosynthetic Physiology of Blue, Green, and Red Light: Light Intensity Effects and Underlying Mechanisms. *Frontiers in Plant Science*, *12*. https://doi.org/10.3389/fpls.2021.619987

Liu, Y., Jeraldo, P., Herbert, W., McDonough, S., Eckloff, B., de Vera, J.-P., Cockell, C., Leya, T., Baqué, M., Jen, J., Schulze-Makuch, D., & Walther-Antonio, M. (2022). Non-random genetic alterations in the cyanobacterium Nostoc sp. exposed to space conditions. *Nature*, *12*(12580). https://doi.org/10.1038/s41598-022-16789-w

Lopes, J., Moreira, C., & Madureira, A. (2006). Defining control strategies for Microgrids islanded operation. *IEEE Transaction on Power Systems*, *21*(2), 916–924.

Louarn, G., & Song, Y. (2020). Two decades of functional-structural plant modelling: Now addressing fundamental questions in systems biology and predictive ecology. *Annals of Botany*, *126*(4), 501–509. https://doi.org/10.1093/aob/mcaa143

Lovelock, J. (1990). Hands up for the Gaia hypothesis. *Nature*, *344*.

Marchetti, A. G., Ferramosca, A., & González, A. H. (2014). Steady-state target optimization designs for integrating real-time optimization and model predictive control. *Journal of Process Control*, *24*(1), 129–145. https://doi.org/10.1016/j.jprocont.2013.11.004

Marshall-Colon, A., Long, S. P., Allen, D. K., Allen, G., Beard, D. A., Benes, B., von Caemmerer, S., Christensen, A. J., Cox, D. J., Hart, J. C., Hirst, P. M., Kannan, K., Katz, D. S., Lynch, J. P., Millar, A. J., Panneerselvam, B., Price, N. D., Prusinkiewicz, P., Raila, D., … Zhu, X. G. (2017). Crops in silico: Generating virtual crops using an integrative and multi-scale modeling platform. *Frontiers in Plant Science*, *8*. https://doi.org/10.3389/fpls.2017.00786

Masot, M. (2007). *ENGINEERING PHOTOSYNTHETIC SYSTEMS FOR BIOREGENERATIVE LIFE SUPPORT*. Universitat Autonoma de Barcelona.

Massa, G. D., Wheeler, R. M., Morrow, R. C., & Levine, H. G. (2016). Growth chambers on the International Space Station for large plants. *Acta Horticulturae*, *1134*, 215–221. https://doi.org/10.17660/ActaHortic.2016.1134.29

Massa, G., Wheeler, R., Zhang, Y., Romeyn, M., & Smith, T. (2021). Testing of the Veggie Vegetable Production System on the International Space Station. In COSPAR (Ed.), *43rd COSPAR Scientific Assembly*.

Maurice Cheung, C. Y., Poolman, M. G., Fell, D. A., George Ratcliffe, R., & Sweetlove, L. J. (2014). A diel flux balance model captures interactions between light and dark metabolism during day-night cycles in C3 and crassulacean acid metabolism leaves. *Plant Physiology*, *165*(2), 917–929. https://doi.org/10.1104/pp.113.234468

McClain, A. M., & Sharkey, T. D. (2019). Triose phosphate utilization and beyond: From photosynthesis to end product synthesis. *Journal of Experimental Botany*, *70*(6), 1755–1766. https://doi.org/10.1093/jxb/erz058

Mekhalfi, M., Puppo, C., Avilan, L., Lebrun, R., Mansuelle, P., Maberly, S. C., & Gontero, B. (2014). Glyceraldehyde-3-phosphate dehydrogenase is regulated by ferredoxin-NADP reductase in the diatom Asterionella formosa. *New Phytologist*, *203*(2), 414–423. https://doi.org/10.1111/nph.12820

Metcalf, J., Peterson, L., Carrasquillo, R., & Bagdigian, R. (2012). National aeronautics and space administration (nasa) environmental control and life support (ecls) integrated roadmap development. *42nd International Conference on Environmental Systems*.

Michael A.Henson. (1998). Nonlinear model predictive control current states and future directions.pdf. In *Computers and Chemical Engineering* (Vol. 23, pp. 187–202).

Michelet, L., Zaffagnini, M., Morisse, S., Sparla, F., Pérez-Pérez, M. E., Francia, F., Danon, A., Marchand, C. H., Fermani, S., Trost, P., & Lemaire, S. D. (2013). Redox regulation of the Calvin-Benson cycle: Something old, something new. *Frontiers in Plant Science*, *4*. https://doi.org/10.3389/fpls.2013.00470

Miginiac-Maslow, M., & Lancelin, J. M. (2002). Intrasteric inhibition in redox signalling: Light activation of NADP-malate dehydrogenase. In *Photosynthesis Research* (Vol. 72, Issue 1, pp. 1–12). https://doi.org/10.1023/A:1016099228450

Morcuende, R., Krapp, A., Hurry, V., & Stitt, M. (1998). Sucrose-feeding leads to increased rates of nitrate assimilation, increased rates of a-oxoglutarate synthesis, and increased synthesis of a wide spectrum of amino acids in tobacco leaves. *Planta*, 394–409.

Morgan, J. A., & Rhodes, D. (2002). Mathematical modeling of plant metabolic pathways. *Metabolic Engineering*, *4*(1), 80–89. https://doi.org/10.1006/mben.2001.0211

NASA. (2019). *Nasa Spaceflight Human-System Standard. Volume2: Human Factors, Habitability, and Environmental Health*.

Nelson, M., Alling, A., Dempster, W., & Allen, J. P. (1993). Using a closed ecological system to study Earth's biosphere. *BioScience*, *43*(4), 225–236. http://www.jstor.org/stable/1312123

Nelson, M., Burgess, T. L., Alling, A., Alvarez-Romo, N., Dempster, W. F., Walford, R. L., & Allen, J. P. (1993). Using a closed ecological system to study Earth's biosphere: initial results from Biosphere 2. *Bioscience*, *43*(4), 225–236. https://doi.org/10.2307/1312123

Niederwieser, T., Kociolek, P., & Klaus, D. (2018). A review of algal research in space. *Acta Astronautica*, *146*, 359–367.

Nikolov, N. T., Massman, W. J., & Schoettle, A. W. (1995). Coupling biochemical and biophysical processes at the leaf level: an equilibrium photosynthesis model for leaves of C3 plants. *Ecological Modelling*, *80*(2–3), 205–235. https://doi.org/10.1016/0304-3800(94)00072-P

Nobile, M. S., Coelho, V., Pescini, D., & Damiani, C. (2021). Accelerated global sensitivity analysis of genome-wide constraint-based metabolic models. *BMC Bioinformatics*, *22*. https://doi.org/10.1186/s12859-021-04002-0

Ocampo-Martinez, C., Barcelli, D., Puig, V., & Bemporad, A. (2012). Hierarchical and decentralised model predictive control of drinking water networks: Application to Barcelona case study. *IET Control Theory and Applications*, *6*(1), 62–71. https://doi.org/10.1049/iet-cta.2010.0737

Olivares, D. E., Canizares, C. A., & Kazerani, M. (2014). A centralized energy management system for isolated microgrids. *IEEE Transactions on Smart Grid*, *5*(4), 1864–1875. https://doi.org/10.1109/TSG.2013.2294187

Pannocchia, G., & Bemporad, A. (2007). Combined Design of Disturbance Model and Observer for Offset-Free Model Predictive Control. *IEEE Transactions on Automatic Control*, *52*(5), 1109–1113.

Peiro, E., Pannico, A., Colleoni, S., Bucchieri, L., Rouphael, Y., de Pascale, S., Paradiso, R., & Gòdia, F. (2020). Air Distribution in a Fully-Closed Higher Plant Growth Chamber Impacts Crop Performance of Hydroponically-Grown Lettuce. *Frontiers in Plant Science*, *11*. https://doi.org/10.3389/fpls.2020.00537

Pekkanen, S. (2019). Governing the new space race. *American Journal of International Law*, *13*, 92–97.

Peng, B., Guan, K., Tang, J., Ainsworth, E. A., Asseng, S., Bernacchi, C. J., Cooper, M., Delucia, E. H., Elliott, J. W., Ewert, F., Grant, R. F., Gustafson, D. I., Hammer, G. L., Jin, Z., Jones, J. W., Kimm, H., Lawrence, D. M., Li, Y., Lombardozzi, D. L., … Zhou, W. (2020). Towards a multiscale crop modelling framework for climate change adaptation assessment. *Nature Plants*, *6*(4), 338–348. https://doi.org/10.1038/s41477-020-0625-3

Pérez, J., Poughon, L., Dussap, C. G., Montesinos, J. L., & Gòdia, F. (2005a). Dynamics and steady state operation of a nitrifying fixed bed biofilm reactor: Mathematical model based description. *Process Biochemistry*, *40*(7), 2359–2369. https://doi.org/10.1016/j.procbio.2004.09.022

Pérez, J., Poughon, L., Dussap, C. G., Montesinos, J. L., & Gòdia, F. (2005b). Dynamics and steady state operation of a nitrifying fixed bed biofilm reactor: Mathematical model based description. *Process Biochemistry*, *40*(7), 2359–2369. https://doi.org/10.1016/j.procbio.2004.09.022

Popova, T. N., & Pinheiro De Carvalho, M. A. A. (1998). Citrate and isocitrate in plant metabolism. *Biochimica et Biophysica Acta*, *1364*, 307–325.

Poughon, L., Dussap, C. G., & Gros, J. B. (1999). Dynamic model of a nitrifying fixed bed column: Simulation of the biomass distribution of Nitrosomonas and Nitrobacter and of transient behaviour of the column. *Bioprocess Engineering*, *20*(3), 209–221. https://doi.org/10.1007/s004490050583

Poughon, L., Farges, B., Dussap, C. G., Godia, F., & Lasseur, C. (2009). Simulation of the MELiSSA closed loop system as a tool to define its integration strategy. *Advances in Space Research*, *44*(12), 1392–1403. https://doi.org/10.1016/j.asr.2009.07.021

Poughon, L., Laroche, C., Creuly, C., Dussap, C.-G., Paille, C., Lasseur, C., Monsieurs, P., Heylen, W., Coninx, I., Mastroleo, F., & Leys, N. (2020). Limnospira indica PCC8005 growth in photobioreactor: model and simulation of the ISS and ground experiments. *Life Science in Space Research*, *25*, 53–65.

Poulet, L. (2018). *Developpement de modéles physiques pour comprendre la croissance des plantes en environment de gravité réduite pour des applications dans les systémes suuport-vie*. Université Clermont-Auvergne.

Poulet, L., Dussap, C. G., & Fontaine, J. P. (2020). Development of a mechanistic model of leaf surface gas exchange coupling mass and energy balances for life-support systems applications. *Acta Astronautica*, *175*(June), 517–530. https://doi.org/10.1016/j.actaastro.2020.03.048

Poulet, L., Fontaine, J. P., & Dussap, C. G. (2018). A physical modeling approach for higher plant growth in reduced gravity environments. *Astrobiology*, *18*(9), 1093–1100. https://doi.org/10.1089/ast.2017.1804

Pruitt, J. M., Carter, L., Bagdigian, R. M., & Kayatin, M. J. (2015). Upgrades to the ISS Water Recovery System. In ICES (Ed.), *International Conference on Environmental Systems* (pp. 1–20).

Pütz, D., Olthoff, C., Ewert, M. K., & Anderson, M. S. (2016). Assessment of the Impacts of ACLS on the ISS Life Support System using Dynamic Simulations in V-HAB. In ICES (Ed.), *International Conference on Environmental Systems* (pp. 1–16).

Raposo, M., Ribeiro, P., Sério, S., Staiano, A., & Ciaramella, A. (Eds.). (2020). *Computational Intelligence Methods for Bioinformatics and Biostatistics* (Vol. 11925). Springer International Publishing. https://doi.org/10.1007/978-3-030-34585-3

Richalet, J. (1993). *Practique de la Commande Predictive*. Hermes Sciences Publicat.

Salisbury, F. B., Gitelson, J. I., & Lisovsky, G. M. (1997). Bios-3: Siberian Experiments in Bioregenerative Life Support. *BioScience*, *47*(9), 575–585.

Scattolini, R. (2009). Architectures for distributed and hierarchical Model Predictive Control - A review. *Journal of Process Control*, *19*(5), 723–731. https://doi.org/10.1016/j.jprocont.2009.02.003

Schertl, P., & Braun, H. P. (2014a). Respiratory electron transfer pathways in plant mitochondria. *Frontiers in Plant Science*, *5*, 1–11. https://doi.org/10.3389/fpls.2014.00163

Schertl, P., & Braun, H. P. (2014b). Respiratory electron transfer pathways in plant mitochondria. *Frontiers in Plant Science*, *5*. https://doi.org/10.3389/fpls.2014.00163

Schneider, M., Knuesting, J., Birkholz, O., Heinisch, J. J., & Scheibe, R. (2018). Cytosolic GAPDH as a redox-dependent regulator of energy metabolism. *BMC Plant Biology*, *18*(1). https://doi.org/10.1186/s12870-018-1390-6

Severinghaus, J., Broecker, W., Dempster, W., MacCallum, T., & Wahlen, M. (1994). Oxygen loss in biosphere 2. *Transactions American Geophysical Union*, *75*(3), 33–37. https://doi.org/10.1029/94EO00285

Shafto, M., Conroy, M., Doyle, R., Glaessgen, E., Kemp, C., le Moigne, J., & Wang, L. (2010). *Modeling, Simulation, Information Technology & Processing Roadmap*.

Shameer, S., Ratcliffe, R. G., & Sweetlove, L. J. (2019). Leaf energy balance requires mitochondrial respiration and export of chloroplast NADPH in the light. *Plant Physiology*, *180*(4), 1947–1961. https://doi.org/10.1104/pp.19.00624

Siebach, K. (2021). *Roving Mars with Curiosity and Perseverance*. https://www.hgs.org/civicrm/event/info?id=2251

Singh, M., Fuenmayor, E., Hinchy, E., Qiao, Y., Murray, N., & Devine, D. (2021). Digital twin: Origin to future. *Applied System Innovation*, *4*(2). https://doi.org/10.3390/asi4020036

Soussana, J.-F. X., Graux, A.-I., & Tubiello, F. N. (2010). Improving the use of modelling for projections of climate change impacts on crops and pastures. *Journal of Experimental Botany*, *61*(8), 2217–2228. https://doi.org/10.1093/jxb/erq100

Swathy, S. (2012). *Thèse Docteur d'Université systèmes de support-vie : modèle métabolique de la feuille de laitue considérant la conversion d ' énergie et le métabolis me central du carbone*. Université Blaise Pascal.

Tako, Y., Arai, R., Tsuga, S., Komatsubara, O., Masuda, T., Nozoe, S., & Nitta, K. (2010). CEEF: Closed Ecology Experiment Facilities. *Gravitational and Space Biology*, *23*(2), 13–24.

Tan, X. L. J., & Cheung, C. Y. M. (2020). A multiphase flux balance model reveals flexibility of central carbon metabolism in guard cells of C3 plants. *Plant Journal*, *104*(6), 1648–1656. https://doi.org/10.1111/tpj.15027

Taniguchi, M., & Miyake, H. (2012). Redox-shuttling between chloroplast and cytosol: Integration of intra-chloroplast and extra-chloroplast metabolism. *Current Opinion in Plant Biology*, *15*(3), 252–260. https://doi.org/10.1016/j.pbi.2012.01.014

Tatjewski, P. (2017). Offset-free nonlinear model predictive control with state-space process models. *Archives of Control Sciences*, *27*(4), 595–615. https://doi.org/10.1515/acsc-2017-0035

Thornley, J. H. M. (2002). Instantaneous canopy photosynthesis: Analytical expressions for sun and shade leaves based on exponential light decay down the canopy and an acclimated non-

rectangular hyperbola for leaf photosynthesis. *Annals of Botany*, *89*(4), 451–458. https://doi.org/10.1093/aob/mcf071

Thornley, J., Johnson, I. (1980). *Plant and crop modelling: A Mathematical Approach to Plant and Crop Phisiology* (Clarendon, Vol. 1).

Tian, X.; Wang, P.; Huang, D.; Chen, S. ; (2007). Offset-free multistep nonlinear model predictive control under plant-model mismatch. *International Journal of Adaptive Control and Signal Processing*, *21*(February), 731–744. https://doi.org/10.1002/acs

Tsiolkovsky, K. (1926). *Exploration of World Spaces by Reactive Devices*. 1-я Гостип. ГСНХ.

Vasquez, J., Guerrero, J., Miret, J., Castilla, M., & de Vicuña, L. (2010). Hierarchical Control of Intelligent Microgrids. *IEEE Industrial Electronics Magazine*, *4*(4), 23–29.

Verbeelen, T., Leys, N., Ganigué, R., & Mastroleo, F. (2021). Development of Nitrogen Recycling Strategies for Bioregenerative Life Support Systems in Space. In *Frontiers in Microbiology* (Vol. 12). Frontiers Media S.A. https://doi.org/10.3389/fmicb.2021.700810

Vogt, C., Monai, M., Kramer, G., & Weckhuysen, B. (2019). The renaissance of the Sabatier reaction and its applications on Earth and in space. *Nature Catalysis*, *2*(3), 188–197. https://doi.org/10.1038/s41929-019-0244-4

Volpin, F., Badeti, U., Wang, C., Jiang, J., Vogel, J., Freguia, S., Fam, D., Cho, J., Phuntsho, S., & Shon, H. (2020). Urine treatment on the international space station: Current practice and novel approaches. *Membranes*, *10*(11), 1–18. https://doi.org/10.3390/membranes10110327

Vu, T., Nguyen, B., Cheng, Z., Chow, M., & Zhang, B. (2020). Cyber-Physical Microgrids: Toward Future Resilient Communities. *IEEE Industrial Electronics Magazine*, *14*(3), 4–17.

Wheeler, R. (2010). Plants for human life support in space from myers to mars. *Gravitational and Space Biology 23(2)*, *23*(2).

Xiao, Y., Chang, T., Song, Q., Wang, S., Tholen, D., Wang, Y., Xin, C., Zheng, G., Zhao, H., & Zhu, X. G. (2017). ePlant for quantitative and predictive plant science research in the big data era—Lay the foundation for the future model guided crop breeding, engineering and agronomy. *Quantitative Biology*, *5*(3), 260–271. https://doi.org/10.1007/s40484-017-0110-9

Yu, C., Liang, Z., & Huang, A. H. C. (1984). Glyoxylate Transamination in Intact Leaf Peroxisomes. *Plant Physiology*, *75*(1), 7–12. https://about.jstor.org/terms

Zabel, P., Bamsey, M., Schubert, D., & Tajmar, M. (2016). Review and analysis of over 40 years of space plant growth systems. *Life Science in Space Research*, *10*, 1–6.

Zheng, Y. C. (2020). Mars Exploration in 2020. *The Innovation*, *1*(2). https://doi.org/10.1016/j.xinn.2020.100036

Zhou, J., Wang, J. Z., Hang, T., & Li, P. P. (2020). Photosynthetic characteristics and growth performance of lettuce (Lactuca sativa L.) under different light/dark cycles in mini plant factories. *Photosynthetica*, *58*(3), 740–747. https://doi.org/10.32615/ps.2020.013

Zhou, W., Liang, X., Li, K., Dai, P., Li, J., Liang, B., Sun, C., & Lin, X. (2021). Metabolomics analysis reveals potential mechanisms of phenolic accumulation in lettuce (Lactuca sativa L.) induced by low nitrogen supply. *Plant Physiology and Biochemistry*, *158*, 446–453. https://doi.org/10.1016/j.plaphy.2020.11.027